2015

# COMPUTATIONAL FLUID DYNAMICS (CFD) MODELING AND VALIDATION OF DUST CAPTURE BY A NOVEL FLOODED BED DUST SCRUBBER INCORPORATED INTO A LONGWALL SHEARER OPERATING IN A US COAL SEAM

Ashish R. Kumar
*University of Kentucky*, ashi.ismd@gmail.com

STUDENT AGREEMENT:

I represent that my thesis or dissertation and abstract are my original work. Proper attribution has been given to all outside sources. I understand that I am solely responsible for obtaining any needed copyright permissions. I have obtained needed written permission statement(s) from the owner(s) of each third-party copyrighted matter to be included in my work, allowing electronic distribution (if such use is not permitted by the fair use doctrine) which will be submitted to UKnowledge as Additional File.

I hereby grant to The University of Kentucky and its agents the irrevocable, non-exclusive, and royalty-free license to archive and make accessible my work in whole or in part in all forms of media, now or hereafter known. I agree that the document mentioned above may be made available immediately for worldwide access unless an embargo applies.

I retain all other ownership rights to the copyright of my work. I also retain the right to use in future works (such as articles or books) all or part of my work. I understand that I am free to register the copyright to my work.

REVIEW, APPROVAL AND ACCEPTANCE

The document mentioned above has been reviewed and accepted by the student's advisor, on behalf of the advisory committee, and by the Director of Graduate Studies (DGS), on behalf of the program; we verify that this is the final, approved version of the student's thesis including all changes required by the advisory committee. The undersigned agree to abide by the statements above.

Ashish R. Kumar, Student

Dr. Thomas Novak, Major Professor

Dr. Braden Lusk, Director of Graduate Studies

# COMPUTATIONAL FLUID DYNAMICS (CFD) MODELING AND VALIDATION OF DUST CAPTURE BY A NOVEL FLOODED BED DUST SCRUBBER INCORPORATED INTO A LONGWALL SHEARER OPERATING IN A US COAL SEAM

THESIS

A thesis submitted in partial fulfillment of the
requirements for the degree of Master of Science in
Mining Engineering in the College of Engineering
at the University of Kentucky

By
Ashish Ranjan Kumar
Lexington, Kentucky

Director: Dr. Thomas Novak
Professor of Mining Engineering
Lexington, Kentucky

December 2015

ABSTRACT OF THESIS

# COMPUTATIONAL FLUID DYNAMICS (CFD) MODELING AND VALIDATION OF DUST CAPTURE BY A NOVEL FLOODED BED DUST SCRUBBER INCORPORATED INTO A LONGWALL SHEARER OPERATING IN A US COAL SEAM

Dust is a detrimental, but unavoidable, consequence of any mining process. It is particularly problematic in underground coal mining, where respirable coal dust poses the potential health risk of coal workers' pneumoconiosis (CWP). Float dust, if not adequately diluted with rock dust, also creates the potential for a dust explosion initiated by a methane ignition. Furthermore, recently promulgated dust regulations for lowering a miner's exposure to respirable coal dust will soon call for dramatic improvements in dust suppression and capture.

Computational fluid dynamics (CFD) results are presented for a research project with the primary goal of applying a flooded-bed dust scrubber, with high capture and cleaning efficiencies, to a Joy 7LS longwall shearer operating in a 7-ft (2.1 m) coal seam. CFD software, Cradle is used to analyze and evaluate airflow patterns and dust concentrations, under various arrangements and conditions, around the active mining zone of the shearer for maximizing the capture efficiency of the scrubber.

KEYWORDS: Longwall Mining, Dust Control, CFD Modeling, Flooded-Bed Dust Scrubber, Scale-Modeling.

Ashish Ranjan Kumar
Student's Signature

December 11th, 2015
Date

# COMPUTATIONAL FLUID DYNAMICS (CFD) MODELING AND VALIDATION OF DUST CAPTURE BY A NOVEL FLOODED BED DUST SCRUBBER INCORPORATED INTO A LONGWALL SHEARER OPERATING IN A US COAL SEAM

By

Ashish Ranjan Kumar

Dr. Thomas Novak

Director of Thesis

Dr. Braden Lusk

Director of Graduate Studies

Dec 11th, 2015

(Date)

# DEDICATION

This thesis is dedicated to my grandmother and aunt.

I have been extremely fortunate to have been brought up by them, who set a wonderful example before me to follow.

# ACKNOWLEDGEMENTS

I would take this opportunity to acknowledge the supports of all individuals who supported me throughout the course of this project and in my life.

I am thankful to Dr. Rick Honaker who gave me the opportunity to join the research group at the Department of Mining Engineering, University of Kentucky, and be a part of the Big Blue Nation.

I am grateful to Dr. Thomas Novak, who was my thesis advisor and mentor and helped me out at all stages of the project. He gave me immense freedom to decide everything on myself and was quick to come up with helpful suggestions throughout.

I would also wish the acknowledge the vital inputs of Dr. Joseph Sottile during the course of computer modeling as well as while building the 1:1 scaled model of the shearer. Invaluable help of Edward Thompson in the laboratory is also acknowledged.

I am thankful to Dr. William Chad Wedding who helped me all the way until I started working on the high performance computing facilities. He was always eager to provide useful inputs, should I have slightest of issues with designing or computer modeling.

I would also like to thank Dr. Braden Lusk, Dr. Andrez Wala, Dr. Kyle Perry, Dr. Jose Grana Otero, Dr. Zachary Agiuotantis and Dr. Kozo Saito for their encouragement.

I acknowledge Ms. Megan Doyle, Ms. Lesley Brenner, Ms. Kathy Kotora and Ms. Geaunita Caylor. It would not have been be possible for me to come anywhere close to writing the thesis without their help.

I am thankful to Ms. Kathy Ice Wedding who made my journey to the United States look very easy. I am also thankful to Dr. Emily Dotson, whose suggestions were of utmost importance during preparation of the thesis.

I am thankful to Alpha Foundation for having funded the research. Thanks are due to the Centre of Disease Control, National Institute for Occupational Safety and Health (CDC, NIOSH). I am thankful to the management at the Tunnel Ridge mine for hosting the

research team involved in the project and helped gather vital data for the CFD simulations and to Joy Global for having us tour their facility and get important design considerations.

I am thankful to my friends at the Indian School of Mines and colleagues at Reliance Power with whom I share some of the most memorable memories of my life. I was fortunate enough to have got a wonderful group of graduate students. They have made my stay at the department truly memorable.

Lastly, I would like to thank my siblings and family who have supported me throughout. I thank Ulupi for her resolute support since last 18 years. I also thank her family for supporting all my decisions throughout.

**TABLE OF CONTENTS**

## LIST OF TABLES

**LIST OF FIGURES**

# 1 Introduction

## 1.1 Background

Dust is an unwanted, but inevitable, element of nearly every operation in a coal mine. Dust is generated primarily from cutting and loading operations, but dust can be entrained in the air during other mining operations, e.g., coal haulage. Of particular concern to miner health is exposure to respirable dust, i.e., mineral dusts of 10 μm or less. Prolonged exposure to high levels of respirable dust can lead to coal workers' pneumoconiosis (CWP), also referred to as black lung, a debilitating respiratory illness. The Mine Safety and Health Administration (MSHA) has estimated that there have been 76,000 deaths attributed to CWP since 1968, and the coal mining industry has paid nearly $45 billion USD as compensation to mine workers with CWP (MSHA, 2015). Although there have been products developed to protect miners from respirable dust, e.g., airstream helmets, the only viable approach to reducing CWP is to reduce a mine worker's exposure to respirable dust.

In addition to being a health hazard, fine coal dust can also be a serious safety hazard. Methane is liberated during coal extraction and is generally considered to be explosive in concentrations between 5% - 15% in air. And, although mines are ventilated to prevent methane from reaching an explosive concentration, a methane ignition can occur due to a gas outburst or improper ventilation in the presence of a sufficient source of energy, such as a spark. If the total quantity of methane is relatively low, the ignition will be limited to a small portion of the mine. However, if there is a significant amount of coal dust accumulated on mine surfaces, the force of the methane ignition can entrain the dust in the air, providing fuel to the explosion, causing the explosion to propagate throughout a large portion of the mine.

Rock dust (crushed limestone) is used to render the coal/rock dust mixture inert; however, inadequate amounts of rock dust or improper application of rock dust may not render the rock/coal dust mixture inert. Under these conditions, a relatively small methane ignition can become a very powerful and deadly dust explosion. It is believed that coal dust was largely responsible for the explosion at the Upper Big Branch Mine in April 2010 that killed 29 miners (MSHA, 2014). Other such explosions include the disasters at

Senghenydd in South Wales of 1913, Courrières mine in 1906, Luisenthal in 1962, and the Benxihu Colliery in 1942. (The world's worst coal mining disasters, 2015).

It is clear that fine coal dust in a mine presents both health and safety hazards to miners. And, although there have been many improvements in coping with dust, the most effective approach for dealing with dust is to capture it as closely as possible to cutting and loading operations.

### 1.2 Problem statement

In 2014, 47 longwall faces accounted for nearly one-half of the total U.S. underground coal production (Energy Information Agency, April 2015). Considering that there are approximately 400 underground coal mines in the US (Energy Information Agency, April 2015), it is clear that longwall installations are very high production set ups compared with continuous miner sections. For example, the average longwall section currently produces approximately 3.5 M short tons of clean coal per year.

Unfortunately, a consequence of the high production of a longwall installation is the large amount of dust generated and methane liberated from a relatively small portion of an underground mine. The shearer is responsible for a high percentage of dust generation on a longwall (Jankowski and Orgasniscak, 1983). The armored face conveyor (AFC), self-advancing powered supports, crusher, and stage loader also contribute to the dust in and around the active longwall face. In addition, longwall faces are generally ventilated with high quantities of air, primarily to dilute methane concentration, but also to reduce the gravimetric concentration of respirable dust.

Beginning in 1970s, flooded bed scrubbers were being developed for continuous miners to capture and remove respirable dust at the point of dust generation on continuous miner sections. Dust laden air is sucked into the scrubber, driven by a fan. The air passes through an impingement screen wet by water sprays which arrest the dust particles. A demister downstream forces the air to shed the moisture before being discharged into the mine atmosphere. The scrubber has been extremely successful and, dust scrubbers are now standard on continuous miners.

However, dust control for continuous miners, which are used in room-and-pillar mining and for developing the gate entries for longwalls, is much easier than that for longwall shearers because the required quantity of air at the continuous miner face is generally much less than the required quantity of air at the longwall face. Consequently, the dust produced by a continuous miner can removed from the air by modern-day scrubbing systems because the scrubbers can be sized to match the airflow quantities at the face. However, the high flow rates and large quantities of air at a longwall face quickly disperses the dust, making it difficult to capture. Because it is impractical to attempt to capture all of the air at the longwall face, a longwall scrubber must be designed so as to quickly capture the dust close to the point of generation, before it is dispersed in the airstream.

As longwall panels have grown in size, so has the associated dust generated. The longwall operators need to investigate each possible source and adopt suitable remedial measures to reduce the generation or arrest the migration of dust. MSHA has also recently circulated the final respirable dust rule which lowers the permissible dust standards from 2.0 mg/$m^3$ to 1.5 mg/$m^3$ and from 1.0 mg/$m^3$ to 0.5 mg/$m^3$ in the intake airway effective at the end of a two year transition period in an underground coal mine. The rules have also redefined the normal production shift and have called for a full-shift sampling. This further requires the longwall operators to revisit their current methodology to maintain compliance.

### 1.3 Scope of Work

The major objective of this research project is to demonstrate the feasibility of applying an efficient flooded bed scrubber to a longwall shearer. Rather than attempting to scrub all of the generated dust, the scope of the work is limited to the investigation of a scrubber for the dust generated by the headgate cutting drum only.

The research effort involves computational fluid dynamics (CFD) modeling with experimental validation for the application of a headgate-drum dust scrubber. (Because this research is part of a project involving a team of researchers from the University of Kentucky, Department of Mining Engineering, it was conducted as part of that effort. Consequently, some aspects of this research is integrated with the work of other members of the research team. The thesis will clearly identify those situations.)

The research involves visits to a cooperating mine to obtain dimensions of the face (length, width, and height) as well as face equipment dimensions. Other information collected includes operational parameters such as cutting rates, position and flowrate of water sprays, airflow quantities and velocities, position of mine personnel in the airway, and so forth. These parameters are used to construct the CFD model. (It is noted that comparisons between the model and mine cannot be made because the construction and installation of an MSHA approved scrubber on an operating shearer is impractical at this time.)

CFD modeling is carried out on SC/Tetra software which includes a preprocessor, a solver, and a post processor, integrated into a single package. The strength of this software lies in its ability to generate unstructured meshes automatically. The high performance computing (UKY-HPC) facility at the University of Kentucky is used to run the SC/Tetra solvers because of the very large number of elements used in the model. Steady state modeling is first conducted to establish the definite flow field under a given set of conditions. This is followed by transient state modeling of dust particles to compute the capture efficiency of the scrubber for the same conditions. Modeling of capture is carried out for two distinct face airflows as well as six different scrubber airflows.

Experimental validation is an essential part of any software modeling effort. Consequently, a 1:20 scale model of the longwall panel, identical in geometry to the flow domain of the CFD models is used to validate the CFD software model. Carbon dioxide is used to mimic the dust particles on the scale model because of its convenience, both in its production and measurement.

Finally, the performance of a dust scrubber involves many design parameters, including the type of scrubber mesh material, number of mesh layers, etc. However, because of the success of the flooded-bed dust scrubber used in continuous miners, this research includes no effort in redesign of the scrubber, other than to change its dimensions to fit into available space inside the shearer. Consequently, this research effort concentrates on inlet location and dimensions, flow rates, pressures, etc., to maximize capture efficiency.

## 1.4 Organization of the Thesis

The thesis is organized into six chapters. Chapter 1 discusses the purpose of the project. Chapter 2 is focused on the prevailing longwall technology and the accompanying dust control methods presently used. Chapter 3 focuses on the design aspects of the dust scrubber proposed by the researchers at the Department of Mining Engineering, University of Kentucky. Chapter 4 discusses the computational fluid dynamics modeling and includes the steady-state as well as transient state results. Chapter 5 discusses the full-scale replica of a longwall shearer as well as a 3-D printed, 1:20 scaled model constructed at the University of Kentucky as well as the associated experiments. Finally, chapter 6 summarizes the results and makes recommendations for future work.

# 2 Prevailing Technologies and Literature Review

## 2.1 Longwall Mining Method

Coal fuels numerous thermal power plants in the United States and accounts for almost 39 % of nation's electricity generation (US Energy Information Administration, 2015). United States produced almost 1120 million tons of coal in the year 2011 (Marc Humphries, 2013). Almost 33.7 % of coal production comes from underground coal mines and more than 50% of the underground production is accounted for by longwall panels (Most requested statistics- NMA, 2014).

Longwall is a highly mechanized form of underground mining. The main production face on a longwall often exceed 300 m (1000 feet) in width and is bound by parallel roadways at the ends. The gate-roads may be miles long depending on the dimensions of the property. The longwall shearer is the production machine and moves back and forth along a relatively flat coal seam beneath the canopies of a series of self-advancing powered supports. Modern shearers like the one shown in Figure 2.1 are often rated in excess of 2,000 kW (2,982 hp). The cutting drums have grown beyond 1.52 m (5 feet) in diameter and are able to extract a wide range of seam thickness. Double-drum shearers are almost exclusively used and have capabilities to produce more than 5000 tons of coal per hour. The width of cut is normally referred to as a 'webb'.


Figure 2.1.: A CAT EL 1000 shearer. (Source: https://mining.cat.com/products/underground-mining/longwall/shearers)

Modern day supports with advanced hydraulics are designed to operate at different heights and may last up to several million cycles. The supports are designed to 'yield' under load and therefore are able to withstand tremendous overlying strata pressure. As the face advances, the overlying strata undergoes a controlled fall behind it as shown in Figures 2.2 and 2.3.

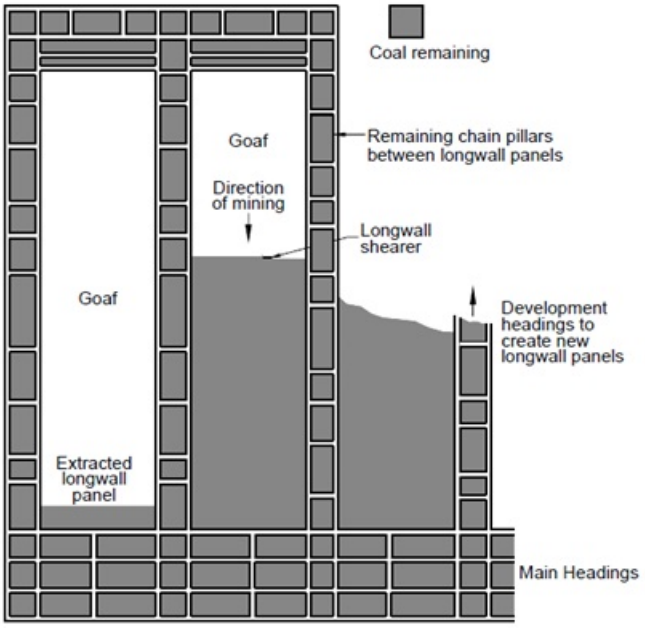


Figure 2.2: A typical layout of the longwall panel. (Source: National Mission Project on Education through ICT, IIT Kharagpur).

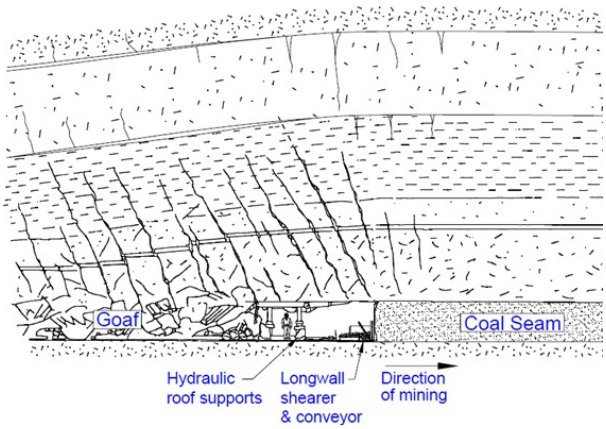


Figure 2.3: Cross sectional view of the longwall face under extraction (Source: National Mission Project on Education through ICT. IIT Kharagpur).

Coal is hauled along the face using a high capacity chain conveyor, referred to as an armored face conveyor (AFC), which is powered by large drives at the headgate and tailgate. The AFC also serves as a guide track for the shearer to tram and has the flexibility to snake towards the face by being pushed by hydraulic jacks attached to the base of the shields. Figure 2.4 shows a representative longwall set up. Power cables, as well as hoses, are laced and protected along the AFC.

Figure 2.4: Shearer EL 3000 (Source: CAT product brochure, www.cat.com/products/underground-mining/longwall/shearers).

Remotely controlled continuous miners are used for developing the gate entries before longwall mining can occur. Accompanied by shuttle cars, continuous miners work in 'room-and-pillar' fashion to create the gate entries.

Longwall mining requires a large air quantity to be delivered to the face area. Not only does the ventilation air keep has to keep the dust hazards at bay, but it must also dilute methane liberations to a safe level. Longwalls on an average pump in 31.64 $m^3/s$ (67,000 cfm) of air to their operations, which is a 65 % rise (Rider and Colinet, 2007) compared to 1995 data.

## 2.2 Dust Sources on a Longwall

The physical dimensions of longwall panels have grown and production has risen with introduction of new technology. While the longwall method has been found to be most productive of all coal mining methods, it is also considered notorious for producing highest dust concentrations (Watts and Parker, 1986). Coal dust exposure has contributed to the death of 69,377 underground miners between 1970 and 2004 and operators have paid

compensation to the tune of USD 39 billion during the period of 1980-2005 (Longwall – Beckley workshop, CDC, NIOSH).

High dust concentrations on a longwall panel can be attributed to the following sources:

(i) Shearer, because of fine extraction and further fanning action of drums.
(ii) Self-advancing powered supports, mainly because of crushing of coal underneath them.
(iii) Stage-loader where the coal transfer from AFC takes pace and due to generation of fines.
(iv) Armored face conveyors, generating dust while transportation.
(v) Intake air, carrying dust generated from "outby" sources.
(vi) Caving and roof falls within the gob.

On a typical longwall panel, shearer has the biggest share of dust contribution as shown in Table 2-1. Dust generation varies between 1000-5000 mg/Ton of coal production (R.L. Mundell, 1977). So, a panel producing 20,000 Ton/day would generate dust of the order of 20-100 kg/day. Further research shows that less than 1 % of the respirable dust actually becomes airborne (Cheng and Zukovich ,1973).

Dust concentration studies (Bhaskar, 1987) have also indicated that the dust concentration decreases rapidly beyond 100 m of the source.

Table 2.1 Sources of dust generation on a longwall face (Source: Jankowski and Orgasniscak, 1983).

| Source | Mine A % | Mine B % | Mine C % | Mine D % | Mine E % | Mine E % |
|---|---|---|---|---|---|---|
| Intake | 1.0 | 5.0 | 5.0 | 5.0 | 9.0 | 8.0 |
| Stage Loader | 25.0 | 57.0 | 19.0 | 20.5 | 64.0 | 13.0 |
| Supports | 10.0 | 31.0 | 1.0 | 1.0 | 0.0 | 29.0 |
| Shearer | 60.0 | 10.0 | 28.0 | 53.0 | 15.0 | 50.0 |
| Shearer-Cleaning | 4.0 | 7.0 | 47.0 | 20.5 | 12.0 | 0.0 |

An analysis of the dust sources also suggests that a dust control method should primarily focus to achieve the following goals (Ruggieri and Jankowski, 1983):

(i) Confining the dust close to the face and not let it spread in the walkways.

(ii) Arresting the dust, probably by using a medium like water.

(iii) Shielding the operator from dust which might have escaped from arrangements indicated above.

### 2.3 MSHA Dust Standards

Mine Safety and Health Administration (MSHA) initiative to end the black lung disease has led to a new set of rules with a two year phase-in period by which all the coal mine operators need to comply with the new dust standards. Some of the salient features of the proposed rules (United States Department of Labor, 2014) are:

(i) Compliance is now based on a single full-shift sampling. The mine will get a citation if the sample exceeds the dust levels for any shift, instead of averaging out to a lower value using a mean of all samples.

(ii) Dust standards are now lowered from 2.0 $mg/m^3$ to 1.5 $mg/m^3$ in the active coal production areas of the mine. Mine intake entries are required to have the dust levels under 0.5 $mg/m^3$, reduced by 50 % from existing 1.0 $mg/m^3$.

(iii) The full shift sampling also ensures that dust measurements are logged on for the entire 12 hour shifts, compared to the earlier 8 hour long sampling requirements.

(iv) MSHA has come with a new definition of a normal production shift. Samples are to be obtained when the production is at least 80 % of the running average of last 30 production shifts.

(v) The rule requires the coal miners to immediately act to lower the dust concentrations in the areas which show signs of excess dust concentration.

(vi) More frequent sampling is required in the areas which have shown to have high dust levels.

(vii) MSHA also requires sampling using high-technology devices, like a continuous personal dust sampler (CPDM), which provides real time sampling results.

(viii) Ventilation plans are now required to be updated to specify the individual dust controls technology used to each mechanized mining unit.

(ix) Periodic scans of lungs has been made available to all miners, to detect on setting of the disease at an early stage, rather than at a later stage which might result in fatalities.

(x) MSHA also needs the sampling done by a qualified person, who has been through MSHA course of instruction, passed an examination as well as renewal of his certificate done every three years.

The aforesaid dust standards decrease further if quartz is present in the mine atmosphere.

## 2.4 Dust Control Methods

Underground coal mine operators have always strived to devise various methods to alleviate the harmful and irreversible effects of the coal dust. Modern day scrubbers installed on continuous miners can efficiently handle an air quantity much higher than 3,000 cfm, mandated by MSHA and cleanse the air. Isolation of continuous miner operators can also be carried out in an efficient fashion. But unlike room and pillar panels, it is not practical to treat all the air reaching the main production face and render it less harmful for personnel. The dust level could be very high under highly turbulent airflow on a longwall face in the immediate vicinity of the cutter drums before it gets diluted by the ventilating air to varying extents. The longwall therefore has to adopt some combination of the following remedial measures to keep the dust under control and comply with the regulations:

### 2.4.1 Ventilation

Ventilation is the primary method to adequately dilute the dust concentration to an extent to render it harmless. Dilution increases with increasing airflow because of more turbulent mixing. However, if the airflow velocity exceeds a certain threshold value, the air begins to act as another sources of dust instead. In addition to this, the intense airflow begins to cause discomfort to the operators. Studies (T.F.Tomb, 1992) have also shown that dust concentration along the face decreases when the airflow velocity increases beyond 5.10 m/sec (1004 fpm).

Most of longwalls in the United States use ventilation airflows exceeding 31.6 $m^3/s$ (67,000 cfm) with an average velocity of 3.4 m/sec (665 fpm) (Rider and Colinet, 2007). High airflow volumes also confine the dust close to the active face and does not let it spread onto the walkway, thereby shielding the personnel.

Further, the mine ventilation system should be designed to supply sufficient airflow quantity to dilute methane liberations which have resulted in severe explosions underground (Wedding, 2014).

### 2.4.2 Shearer Drum Water Sprays

Modern underground machinery, whether working against hard rock or a coal face are equipped with water sprays. Shearer drum water sprays as shown in Figure 2.5 are designed to point directly at the tip of the bit. Many of the water sprays (B.K.Belle, 2000) working underground operate at pressures of 552-827 kPa (80-120 psi). Not only do they cool the bits extending their useful lives, they also make the immediate area wet and arrest the fine dust. Solid cone and hollow cone are the preferred sprays. Water reaching the sprays often exceed 4.1 lit/sec (65 gpm).

Figure 2.5. Water sprays in action (Source: Andrez Drum, Mining Tribune, Poland

### 2.4.3 Low RPM of Cutting Drums

Most of the longwalls have their shearer drums rotating at 40-70 rotations per minute. This alleviates the fanning action of the shearer drum rotating at higher speeds. This also lowers the power requirements of the shearer. Overall reductions are often to the tune of 40 % for

dust and 15 % for power to the shearer. Deeper cuts produce larger chunks of coal and therefore are better when it comes to reduction in dust generated.

Further works (W.W. Roepke, 1976) has also suggested that the operators "cut at maximum depth at all times, at minimum RPM and with the lowest possible number of bits, which have the lowest possible tip angle." However, an optimization study should be carried out for the shearer in question because a low number of bits would lead each bit to experience higher torque and increased vibration.

### 2.4.4 Shearer Clearer

Shearer clearer is an arrangement with a splitter arm installed on a shearer with a number of sprays mounted on it and facing the coal face (Jayaraman, Jankowsk, & Kissell, 1985). The sprays on the splitter arm usually operate at pressures exceeding 1034.21 kPa (150 psi). An arm similar to the one shown in Figure 2.6 uses the air moving capabilities of the sprays and keeps the dust laden air confined to the face and prevents it from migrating towards the walkways.

Figure 2.6. Shearer clearer on a shearer (Source: Connexa product brochure, www.connexa.com.au)

The arm itself needs to be extended as far as possible ahead of the headgate drum to be effective. A large sprays mounted close to the tip of the shearer clearer also may be designed to knock down the dust.

### 2.4.5 Sprays on Powered Supports

Self-advancing powered supports have water sprays embedded into the canopy and pointing downwards as shown in Figure 2.7. As the shearer advances, (Organiscak, Listak, & Jankowski, 1985) the armored face conveyor is snaked and water sprays are triggered periodically arresting the fine dust in the vicinity of the shearer. Similar to other sprays, periodic maintenance is important for proper functioning and keeping them clog free and effective.

Figure 2.7. Water sprays located on the underside of the canopy of the powered supports (Organiscak, Listak, & Jankowski, 1985).

### 2.4.6 Belt Conveyors

Belt scrappers similar to the one shown in Figure 2.8 at the head and tail ends prevent the accumulation of dust on belt conveyors. Further, periodic maintenance prevents any misalignment which might lead to spillage. Water sprays rendering the coal wet while transportation also reduces the dust.

Figure 2.8 A typical coal cleaner installed underneath the belt (Source: Luoyang Ruita Rubber Co. Ltd).

Full or flat cone sprays arranged as shown in Figure 2.9, running 0.06-0.25 lit/sec (1-4 gpm) of water at around 344.74 KPa (50 psi) have been found to be effective (Longwall – Beckley workshop, CDC, NIOSH).

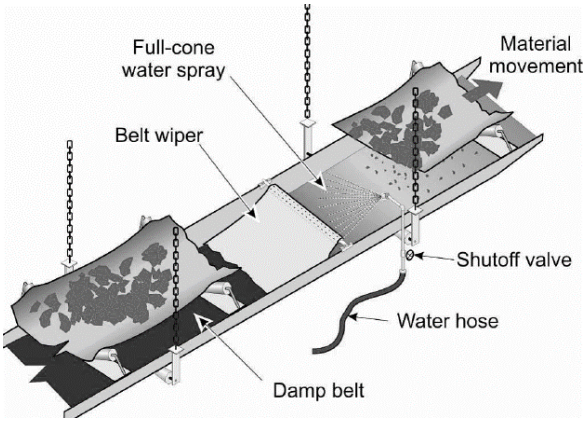


Figure 2.9 Water sprinklers and wipers to control the dust coming from the belt entry (Source: Longwall-Beckley workshop, CDC, NIOSH).

### 2.4.7 Water Sprays on the Stage Loaders

Stage loaders as well as crusher systems add significant quantity of dust to the longwall system. (Jayaraman, Jankowski, & Organiscak, 1992). A high pressure water powered scrubber is also put on the top of crusher. Crusher sprays as shown in Figure 2.10 arrest the fines generated.

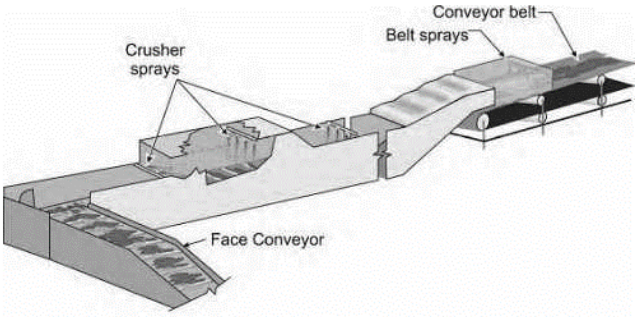


Figure 2.10 Sprays mounted close to the crusher, belt sprays also shown. (Source: AAPgate: Clean Development & Climate).

### 2.4.8 Upwind Positioning of Shearer Operator

Keeping the shearer operator upwind of the shearer provides protection from direct dust laden air. On longwall faces following a bi-directional sequence, the shearer operators and jack setters need to reverse directions and remain upwind. Clearly, one of many simple

change in methodology, may have a pronounced effect over the lives of miners. A modified cutting sequence (Balasu, Chaudari, Harvey & Ren, 2005) where the leading drum will produce most of the coal and the trailing drum will cut a minimal amount of coal has also proved useful towards reducing the exposure limits.

### 2.4.9 Gob-curtains and Wing Curtains

Leakage into the gob is high at the headgate entry. Since the air has to turn at right angles, the shock loses are also on the higher side (A.B.Cecala & J.A.Organiscak, 1986). Figure 2.11 shows the placement of a gob curtain which helps air make a smooth transition and hence keeps it moving at a high speed. Underground experiments showed 35 % higher airflow velocity when compared to a set up without a curtain.

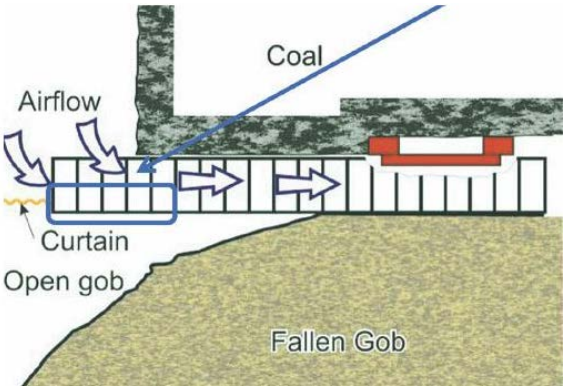


Figure 2.11 Gob curtains installation to prevent invaluable air to leak into the gob. Source: Thimons, December 2011.

Wing-curtain is useful especially when the shearer breaks into headgate entry and generates a lot of dust (Jankowski, Kissel, & Daniel, 1986). Figure 2.12 shows the set up.

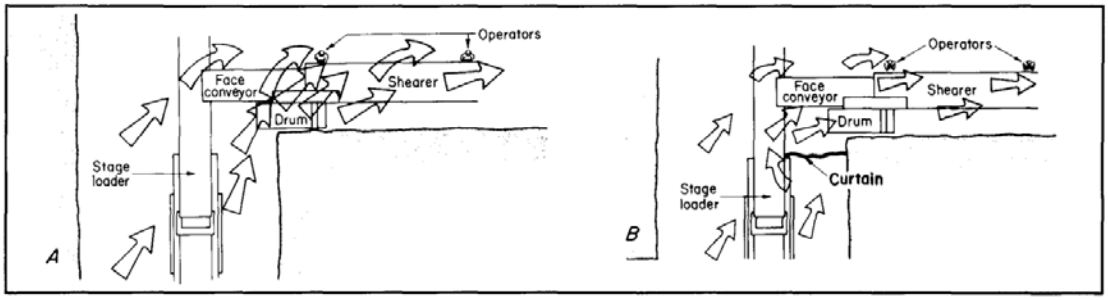


Figure 2.12 Positioning of wing curtain to demonstrate the entrainment of dust, after Janskowski et.al 1986.

### 2.4.10 Bit-Design

Sharp bits generate less dust when compared to rather dull or worn out bits. Bit replacement whenever it begins to show signs of appreciable wear is also one of the standard practices addressing the dust control.

## 2.5 Previous Attempts at Dust Scrubbers

The active production area of a longwall panel presents an extremely hostile environment. The already existing highly turbulent airflow at high volumes is also affected by moving machinery. As such any mechanical remedy to cut down on the dust should be able to withstand the harsh environment including vibrations and coal hits.

The Federal Coal Mine Health and Safety Act, 1969 laid down stringent regulations with respect to dust and the mine operators found it extremely difficult to comply with them. Operators also resorted to unidirectional cutting amongst host of other steps, but only to report decline in production to the tune of 30 % (Foster-Miller, Inc., 1987).

The industry has experimented with various designs of dust scrubbers with varying degrees of success. Operational ease, ease of maintenance and cost-benefit analyses have always been the driving factors. As the underground mining machines grew in size, power and became increasingly capable of more coal production, newer and innovative ways of combatting dust were required.

One of the earliest designs called for intakes close to either drum as shown in Figure 2.13 below. The idea was to capture dust laden air, let it move past a flooded bed filter and mist eliminator.

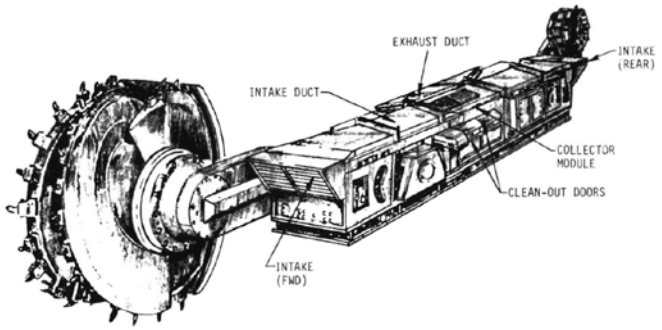


Figure 2.13 A design of one of the earliest dust scrubbers (Source: Foster-Miller Inc, 1987).

Tests were run in a full scale model of a longwall face. However, even at airflows close to 4.72 $m^3/s$ (10,000 cfm), dust reductions recorded were negligible (Steve Wirch, 1995).

The Mining Research and Development Establishment (MRDE) of the National Coal Board in Britain meanwhile was experimenting with two novel designs. The shearer drum and the cowl were the two promising areas which could be exploited to extract dust before it escapes into the mine atmosphere, rendering it too difficult to be captured. Figures 2.14 and 2.15 show the design.

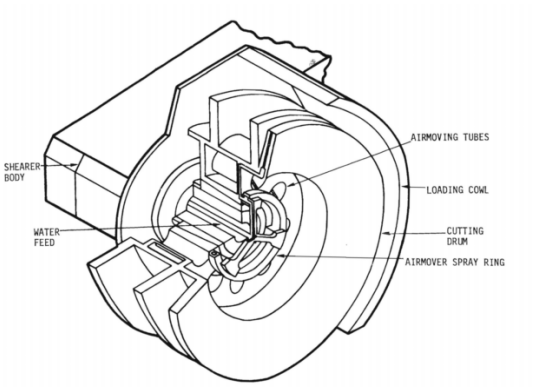


Figure 2.14 Extraction drum conceived by the Mine Research and Development Establishment.

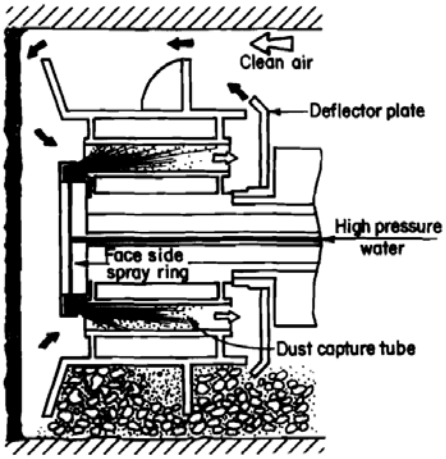


Figure 2.15 Ventilated drum with high pressure sprays to capture the dust from close to the coal face, Source: Foster-Miller Inc, 1987.

Ventilated drums (Foster-Miller, Inc., 1987) were experimented with in early 1980s, where dust laden air was redirected towards the axis of the shearer drum using a series of high

pressure shrouded sprays operating at 10342 kPa (1500 psi) and 1 lit/sec (16 gpm) as shown in Figure 2.16.

The underlying idea was to wet the dust particles and let the entire air move around a deflector plate to arrest the dust. The deflector plate also served as an arrangement to make the air recirculate, which in turned was aimed to improve the capture and cleaning efficiencies. A dust reduction of approximately 50 % was often reported at a face airflow volume of approximately 13.2 $m^3$/s (28,000 cfm) at 14.80 m/sec (350 fpm) and through the drum flow of around 1.60 $m^3$/s (3,500 cfm).

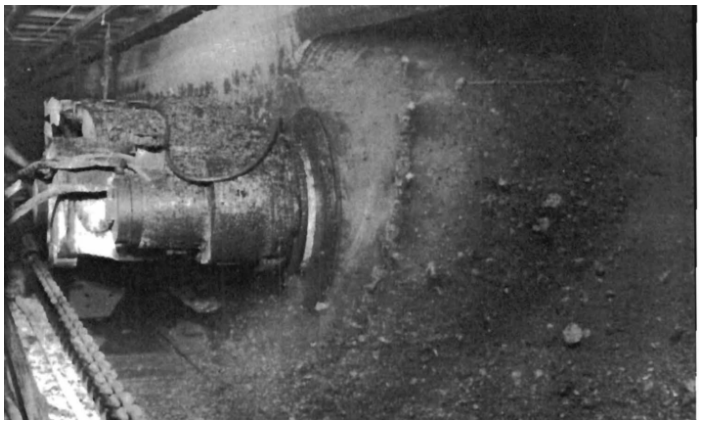

Figure 2.16 Laboratory testing of the ventilated drum (Foster-Miller, Inc., 1987).

The design however, required excessive engineering (Foster-Miller Inc., 1987) as well as great deal of maintenance and could not make it to be a standard package on all shearers. The arrangement would call for impeccable water distribution arrangements using manifolds which was not the best of ideas considering the space around the rotating drum. Failure of rotary seals as well as frequent plugging of tubes and wear of nozzles were other factors that posed serious concerns which required immediate attention.

The pressure of water coming out of the sprays always had a critical role to play in the efficiency of cleaning. However, maintaining high pressures throughout would require an onboard pressure pump which has its own difficulties. Clogging was a frequent problem on because of location of the inlet very close to the coal face. Moreover, this set up was more successful when the cutting drum had a diameter in excess of 1.70 m (67 inches).

Ventilated Cowl as shown in Figure 2.17 was conceived for its ease of assembly when compared to the ventilated drum. It, however had similar issues with high maintenance. The capacity of the drum extracting coal is kept higher than the conveying system, and as such the drums would often get buried inside the freshly cut coal limiting the airflow to the cowl. This would render the system ineffective. However, in cases of bi-directional cutting, which is mostly always preferred now, the direction of the entire set up was required to be reversed which was clumsy. Cowls are always subjected to heavy wear and this further restricted the overall reduction in dust (Foster-Miller, Inc., 1987).

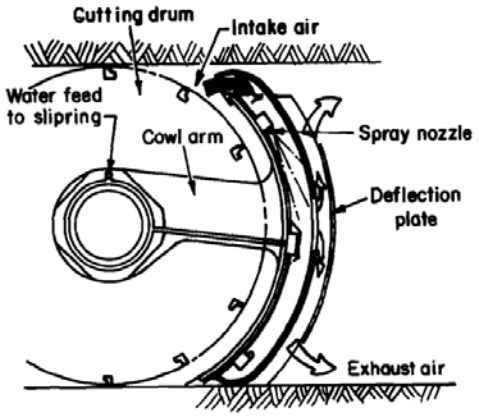


Figure 2.17 A ventilated cowl with the deflection plate, spray nozzle and the water feed slip-ring, Source: Foster-Miller Inc, 1987.

Water powered 'spot' scrubbers were next developed by the US Bureau of Mines and would often have four sprays contained in a box (Steve Wirch, 1995). This was versatile when it came to mounting. A series of experiments fixed the best position to be somewhere close to the center of the control panel. Most of these requited the scrubber airflow to be at least 20 % of the face airflow to be effective. The spot scrubbers working at 1.9 $m^3/s$ (4,000 cfm) with a face airflow of 9.4 $m^3/s$ (20,000 cfm) showed capture efficiencies in excess of 80 %. A decrease up to 25 % was observed on tests during the pass from headgate to tailgate. Figures 2.18 and 2.19 show the set up.

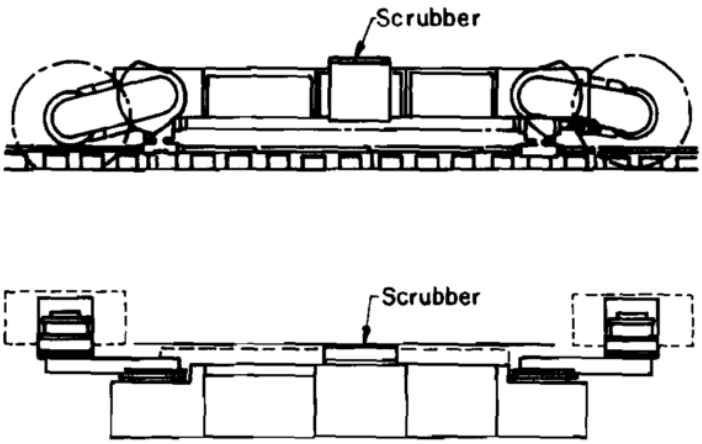


Figure 2.18 A schematic showing the location of a spot scrubber on a shearer.

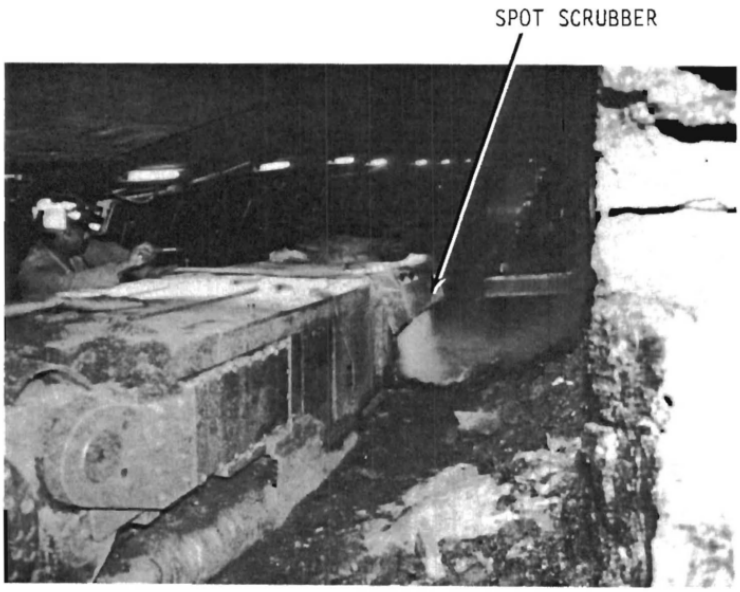


Figure 2.19 A spot scrubber installed on the shearer.

However, a lot of other factors came into play and the deployment on an actual longwall panel was not found to be very promising. With the increase in face airflow, the airflow through the scrubber had to increase proportionally and this is where the design was limited by fan capacities. Further, the inlets required precisely engineered designs. Being located in a shadow area as far as the airflow is considered, the capture efficiency was never expected to be on a higher side.

Donaldson Company in 1980 also experimented with putting a dust collector driven by fan and using water sprays and mist eliminators on a Eickhoff EDW 340L shearer (Donaldson

Company, 1980) as shown in Figure 2.20. The primary objective of the project was to look for a reduction in respirable dust up to 75 % without affecting its safety and productivity. The set up was tested at the Eastern Associated Coal Corporation's Keystone # 1 mine in Keystone, West Virginia. Field testing showed a dust level reduction exceeding 60 % along the face. However, multiple breakdowns were encountered owing to rocky seam conditions and another shearer had to be put in its place. Initial results reiterated the importance of location of collector inlets as well as ratio of scrubber airflow to the face airflow.

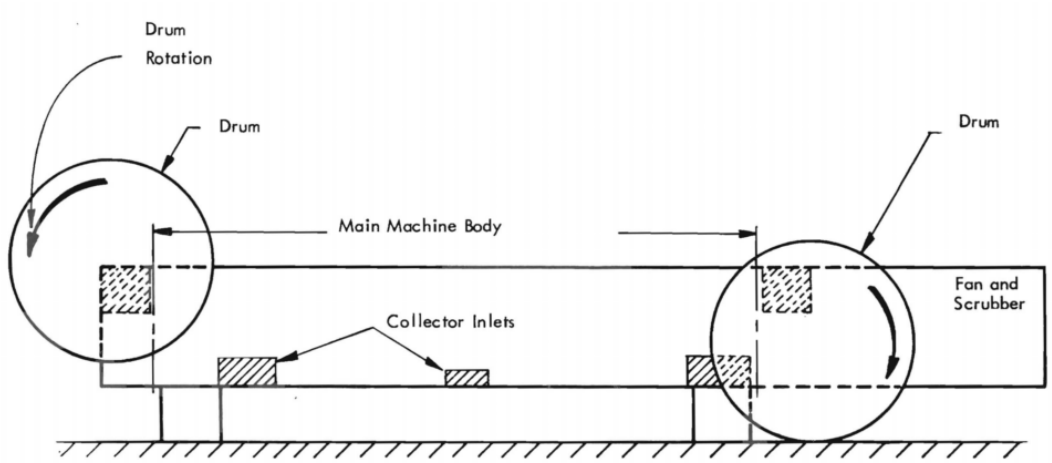


Figure 2.20 Front view of Eickhoff shearer, experimented upon for dust collector (Natesa I. Jayaraman).

Testing showed a high capture efficiency when the airflow through the scrubber was in excess of 40 % compared to the face airflow. Since the longwall panel was also leaking a lot of air into the gob, varying reductions were observed along the length of the face.

This attempt provided a good head start to work on other shearers as well. Success of the project also prompted installation of similar set ups on shearers in other mines including the ones operated by Clinchfield Coal Company, Kaiser Steel Company- York Canyon Mine and Sunnyside Mine, Eastern Associated Coal Company and Consolidation Coal Company among others. Figure 2.21 shows a set up for the Consolidation Coal Company.

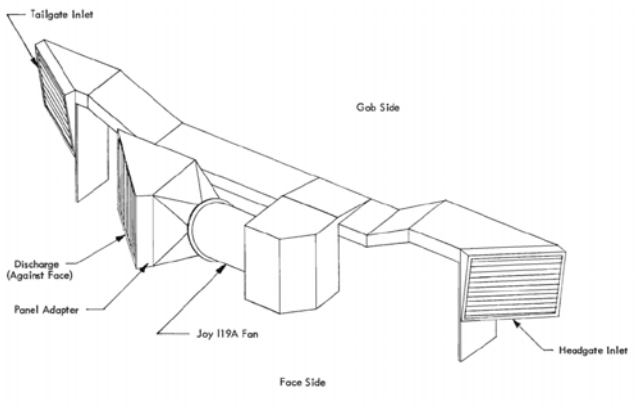


Figure 2.21 Scrubber set up on EDW 300 mine operated by the Consolidation Coal Company.

A research project was undertaken by CSIRO, Australia under the Australian Coal Association Research Program (ACARP) to develop a dust control technology for thick seam coal mines. Envirocon came on board to develop and fabricate a shearer scrubber system that would be efficient and sturdy to withstand the punishing environment of the longwall. Scope of the work included development of the shearer scrubber system and demonstrate the effectiveness with field trials. CFD modeling of the new scrubber was also planned to arrive at the best possible location, orientation and flows through it.

The 3-dimensional CFD model extends 110m x 60m x 4.5m and includes the shearer (Tin X Ren, 2007) along with the main gate and used over 2 million mesh elements as shown in Figures 2.22 and 2.23.

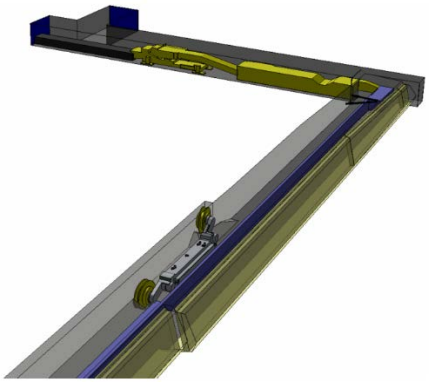

Figure 2.22 The 3-dimensional geometry of the panel for the CFD simulations (Tin X Ren, 2007).

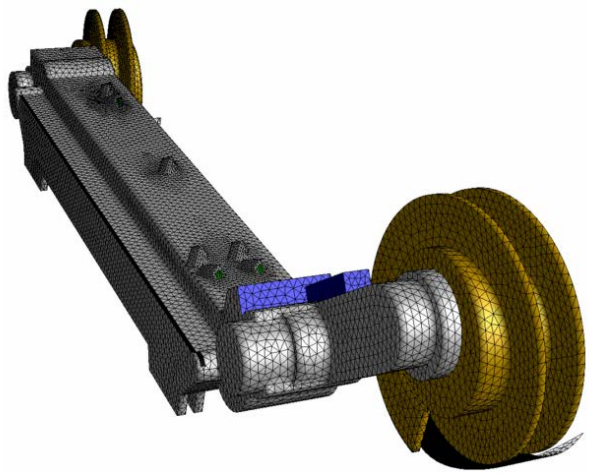

Figure 2.23 The mesh around the shearer (Tin X Ren, 2007).

Simulations were run with face airflow volumes from 30.0 $m^3$/s to 110.0 $m^3$/s. Drums were assumed to rotate at 35 rpm and porous media modeling was done for shearer curtains as well as spill plates. “Respirable dust particles” were modelled as a single phase flow. Simulations were also run for different layouts of the dust scrubber as shown in Figure 2.24.

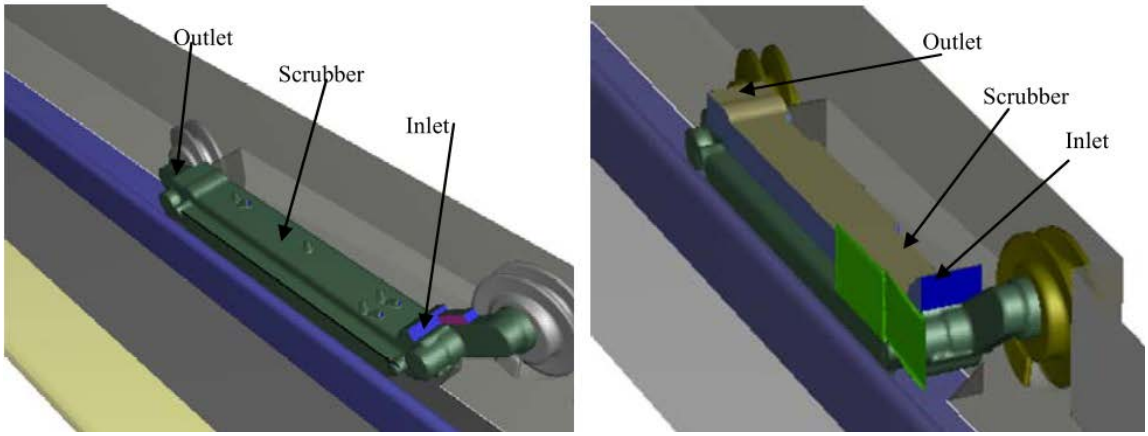


Figure 2.24 The mesh around the shearer (Tin X Ren, 2007).

CFD simulations were run to arrive at good capture efficiencies with varying flows (4.0 $m^3$/s- 10.0 $m^3$/s) through the scrubber and the face. Dust particles were assumed to follow a Rosin Rammler distribution and varied in sizes 1-10 µm. Post processing yielded path lines showing dust propagation as shown in Figure 2.25.

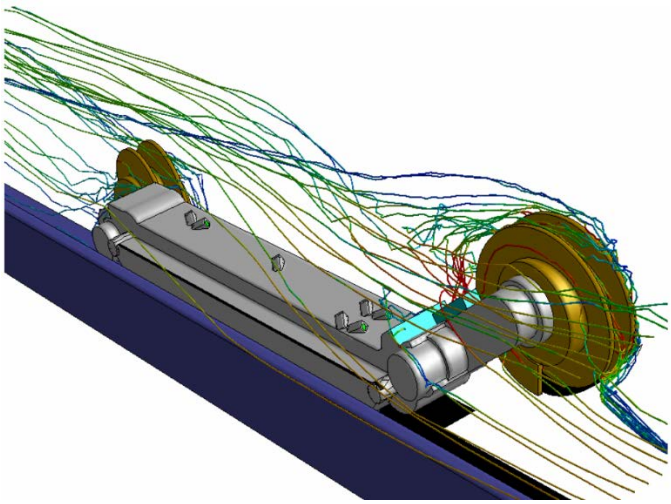

Figure 2.25 Path lines of the dust particles generated on post processing (Tin X Ren, 2007).

Results were also correlated with the data obtained from the mines and CFD models were further calibrated. The CFD models showed excellent agreement with the data gathered, other than the areas close to the boundaries and walls. Figure 2.26 shows the velocity contours.

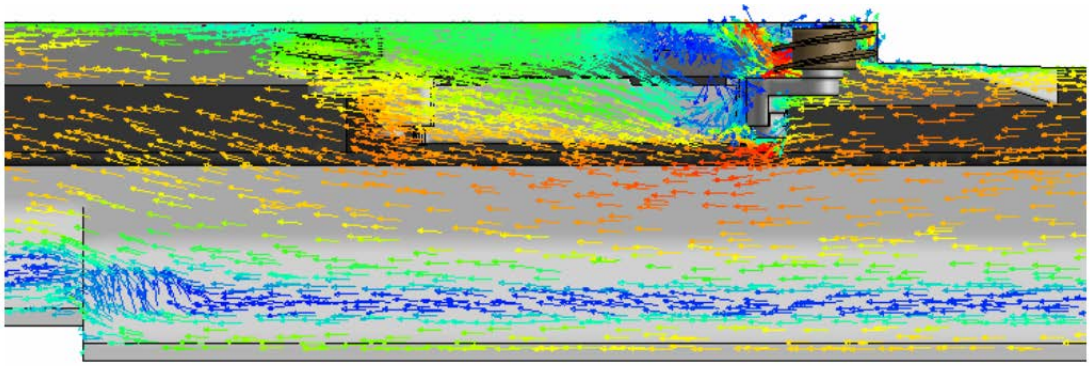

Figure 2.26 Velocity vectors near the shearer (range: 0-3.5 m/sec).

It was also established that the inlet directed opposite to the ventilation airflow direction at the face improves the efficiency of capture. Further, discharging the air from the scrubber and keeping it parallel to the coal floor with an inclination of no more than 15 degree also helps the dust get confined at the coal face. It was again established that the scrubber flow should be an appreciable fraction of the face flows. Scrubbers working at least 8.0 $m^3/s$

were simulated to be efficient at a face airflow of 80.0 $m^3/s$ which was considered as a moderate flow on the thick coal seam.

Simulations also indicated that the positioning of the inlets and the discharge should be of utmost importance. Airflows should be incapable of acting as a new source of dust instead. However, results also show that the dust scrubber won't be effective in capturing all the dust generated on the longwall panel.

These have been some of the most important efforts towards designing an effective scrubbing system to be installed on the shearer.

## 3 Design Considerations for the Scrubber

Most approaches for tackling longwall dust problems work to dilute the dust concentration to harmless levels or to shield the miners. This research project aims to capture a large percent of dust generated by the leading drum of the shearer by means of a flooded bed scrubber. The scrubber is designed to maximize dust capture. It should capture dust laden air close to the headgate drum and discharge the clean air into the air stream near the face.

In order to effectively capture dust generated at the face, numerous features were included in the design. Previous attempts at using dust scrubbers on a longwall shearer were examined for their pros and cons. The following points were emphasized through the course of the design phase of the scrubber.

An effective scrubber largely depends on a high percentage of the air at the face flowing into the scrubber inlet. A visit to an assembly facility of JOY Global yielded useful information with respect to the design. Importance of a good inlet design was always the key. This led the UK researchers to extend the inlet leading into the flooded bed to be as close as possible to the leading shearer drum and where maximum dust generation occurs. The underlying idea is to capture as much dust as possible before it is dispersed by the intense airflow at the longwall face.

The scrubber inlet and its ductwork extend along the upper portion of the ranging arm to locate the inlet close to, but without interfering with, the cutter drum of the shearer. This ensures that the inlet is no more than 5 cm (2 in.) above the ranging arm when the drum is fully lowered. The inclusion of an articulated joint, hinged at the same point of the ranging arm. This ensures the continuity of airflow with the ranging arm in any position.

The ranging arm with the inlet of the proposed scrubber needs to be lowered to clear shields. The maximum distance that any newly designed component could rise above the main shearer body is restricted to 0.25 m (10 in.). Any engineering module that could deliver an air quantity comparable with modern day scrubbing systems could not have been accommodated on top of the shearer body. Therefore the addition of two distinct compartments – one for the scrubber and demister, and the other for the fan and drive motor to the existing shearer body. These compartments were inserted between the main control

module and the drive modules on either side of the shearer. Figure 3.1 shows the proposed design of scrubber installed on the longwall shearer. The flowing paragraphs describe the scrubber elements.

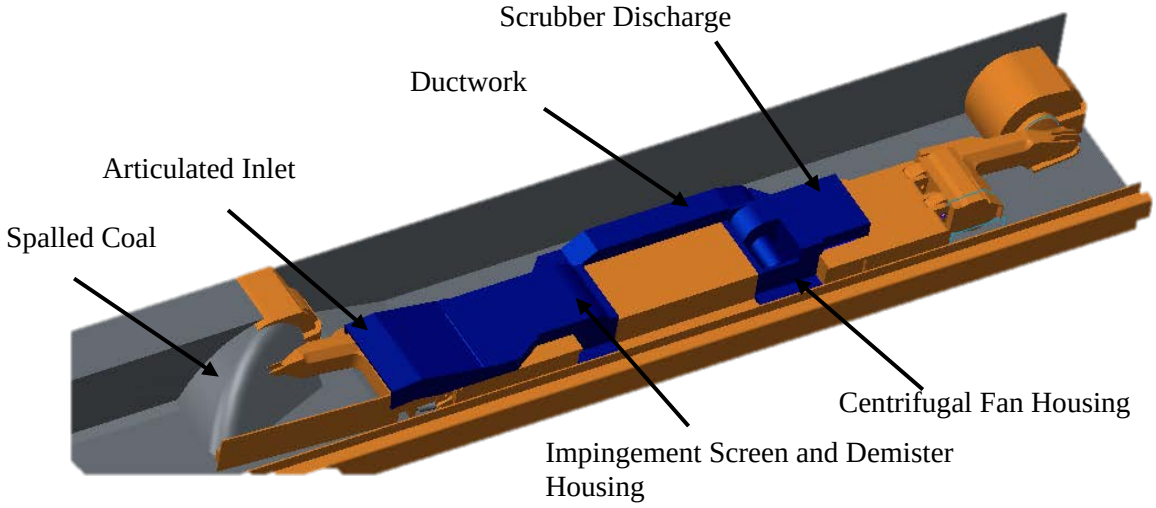


As previously stated, the height of the inlet above the top surface of the ranging arm is

Figure 3.1 Proposed design of a flooded bed dust scrubber installed on the shearer.

transition from the widest part of the inlet to the impingement screen has been designed to be smooth, keeping the shock losses to a minimum as shown in figure 3.2.

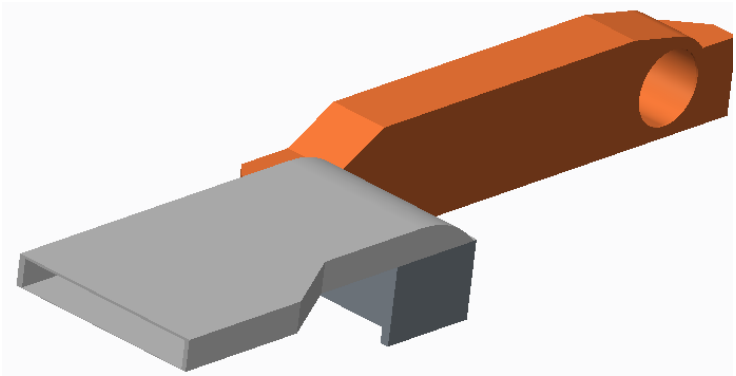

Figure 3.2 The inlet leading to the impingement screen and demister housing, showing the gradual transition to a narrow section.

The dust laden air flows through ductwork over the drive module and into the compartment containing the flooded bed and demister components. A set of water sprays working at 0.41 lit/sec (6.5 gpm) each floods the bed, which consists of 20 mesh layers of closely woven

wire threads. (The number of layers may change depending on the application.) Past research shows that the bed is able to capture more than 90% of the dust particles entering the scrubber (National Institute for Occupational Safety and Health, 1997). Figure 3.3 shows the arrangement of the flooded bed installed at a 45º angle to the direction of airflow. The screen, similar to the one shown in figure 3.4, is kept inclined to provide a larger surface area for the dust particles to contact.

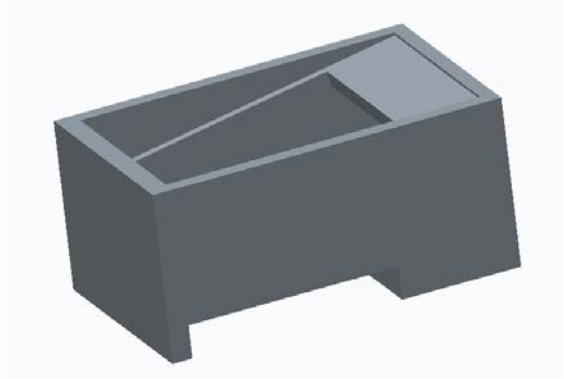

Figure 3.3 The housing for the impingement screen.

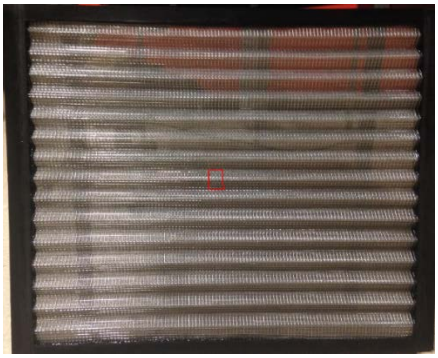

Figure 3.4 The impingement screen.

The sprayed water droplets on the impingement screen encapsulate the majority of the dust particles. These water droplets with the entrapped dust particles then drain into a 95 liter (25 gal) black water sump located beneath the demister. The cleaned, but saturated air, continues its flow through ductwork, which is connected between the scrubber housing and the fan housing. This ductwork would require being made of thick steel to withstand the harsh environment between the shearer and the longwall face. The area behind the main

control panel does not provide access to enclosed components for maintenance; therefore, ductwork can be run behind the shearer without creating problems.

Design of the ductwork and housings have a pronounced effect on the performance of the fan. Frictional pressure losses, associated with cross-sectional areas, lengths, and surface roughness, along with shock losses due to ductwork turns, contractions, and expansions, dictate the operating point (pressure and quantity) of the fan at a specified speed. Efforts were made to minimize these losses; nonetheless, practical limitations for the placement of components makes the reduction of these losses difficult. As a result, the fan (50 hp) is sized to overcome these losses by providing a sufficient pressure to allow an air quantity in excess of 10 kcfm.

The air having exited the impingement screen is predominantly free of dust, while the majority of dust particles are encased by water droplets. The ductwork directs this dense mist towards the demister which is located directly behind the flooded bed in the same compartment. As its name implies, the demister is a device that removes the water droplets from the mist. Its functional elements are a parallel set of sinuous fins with protruding notches. The water droplets have higher momentum than that of air because of their mass. Unlike air, the droplets cannot change direction quickly and frequently while passing through the demister. As a result, the droplets impact the wavy surface of the demister as well as at the hook extrusions. Figure 3.5 shows the demister used for the scrubber.

Figure 3.5 The demister to arrest the water droplets from the air.

In order to quickly handle the water flow measuring up to 25 gallons per minute being sprayed onto the bed, a 95 liter (25 gallon) black-water sump is installed beneath the

demister. The sump is drained using an electric sump pump. The pump will drain the dirt laden water and discharge it either onto the coal on the armored face conveyor.

A variable frequency drive centrifugal controls the speed of the fan. A 50-hp motor drives a centrifugal fan. Because of the space available in the fan compartment, the physical configuration of a centrifugal fan is more appropriate than that of a vane axial fan for this application. The fan housing shown in figure 3.6 was designed for installation of the fan.

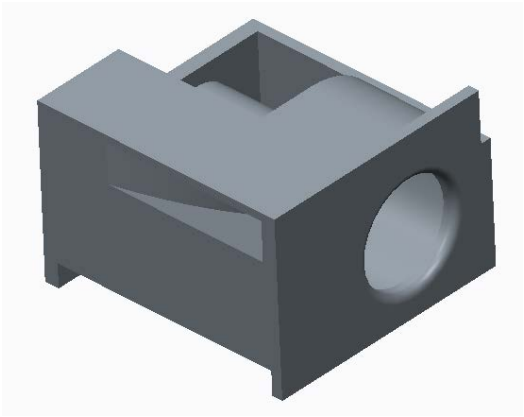

Figure 3.6 The fan housing for the centrifugal fan.

The specifications of the fan motor is shown on table 3.1.

Table 3.1 Configuration of the fan motor.

| Parameter | Values |
|---|---|
| Make | Toshiba |
| Model number | 0502SDSR41B-P |
| Power | 37 kW (50 hp) |
| Voltage (Volt) | 230/480 |
| Current ratings (Ampere) | 116/58 |
| Power factor | 87.5 % |
| Maximum RPM | 3600 |

Table 3-2 shows the specifications for the centrifugal fan, model SQBI-200.

Table 3.2 Configuration of the centrifugal fan.

| Parameter | Values |
|---|---|
| Volumetric flow rate | 7.08 $m^3/s$ (15,000 cfm ) |
| Operating static pressure range | 2.00 kPa (8.0 in. wg) |
| Optimum operating temperature | 21° C (70° F) |
| Density of air | 1.20 $kg/m^3$ (0.075 $lb/f^{t3}$) |
| Fan RPM | 3550 |
| Brake horse power | 34.53 kW (46.3 BHP) |
| Wheel description | SQ backward bladed |
| Static efficiency | 40.4 % |

A centrifugal fan working at airflows required for this project will discharge air at a speeds around 25-30 m/sec for the airflows of 3-6 $m^3/s$ (6,350-12,700 cfm) through the scrubber. However, the discharge parallel to the mine floor lowers the possibility of the discharged air acting as another source of dust. Also, a portion of the shock losses caused by the sudden air discharge into the mine atmosphere can be recovered using a well-designed évase which rests on the top surface of the trail drive compartment and lets the air velocity gradually decrease before being discharged. The addition of the évase increases the height of the shearer by approximately 25 cm as shown in the figures 3.7 and 3.8.

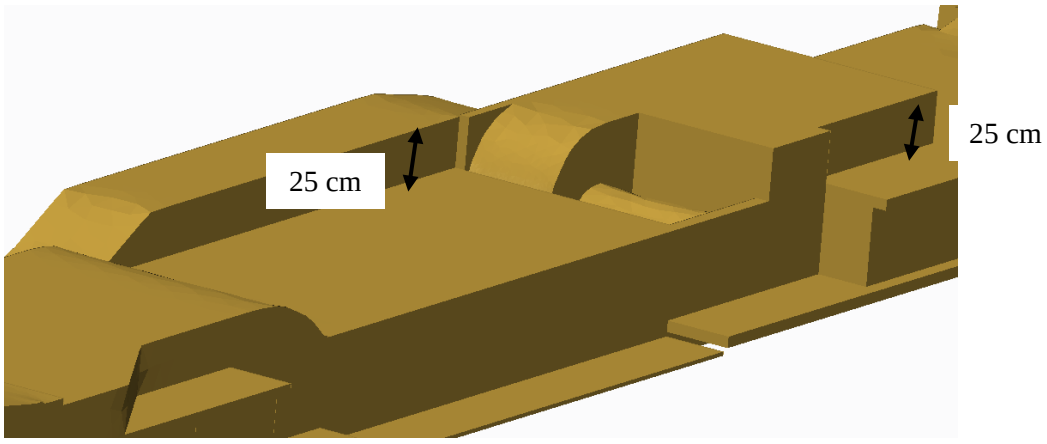


Figure 3.7 An isometric view of the shearer with the proposed scrubber, showing the increase in height.

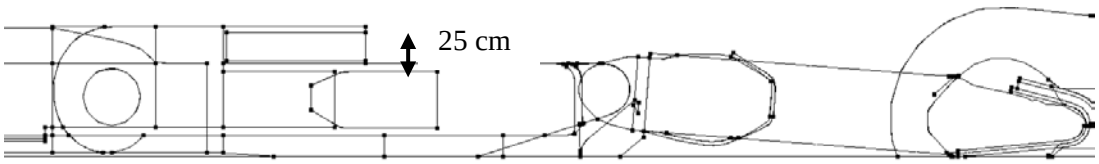


Figure 3.8 Front view showing the increase in height after installation of the ductwork and discharge.

Figure 3.9 shows the increase in width of the shearer due to addition of ductworks, towards the coal face.

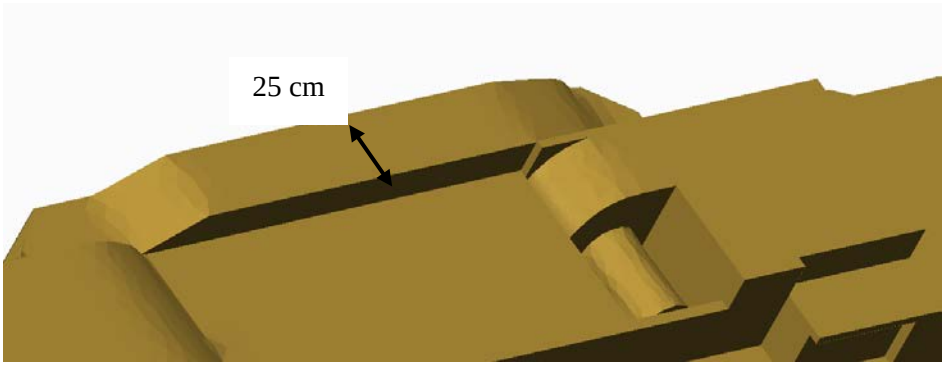


Figure 3.9 The duct work protruding out of the shearer body towards the coal face.

The impingement screen housing (0.98m, 38.5 in) as well as the fan housing (1.32 m, 52 in) together cause an increase in the existing length of the shearer by approximately 2.30 m (7 ft 6 in) as shown in the figure 3.9. This represents an approximately 12.5 % increase in length of the shearer, which now stands at 18.9 m (62 ft). No problems in navigation on account of an increase in length are expected to occur since the coal seam is relatively flat at the cooperating mine. This arrangement, however, may not provide a general solution for all longwall panels, since each seam has specific characteristics.

# 4 Computational Fluid Dynamics Modeling

Fluid flow can be expressed by a set of Euler's equations which are based on conservation of mass, momentum, and energy. These are conveniently represented as partial differential equations. Computational fluid dynamics (CFD) is the branch of fluid dynamics where these partial differential equations are replaced by numerical approximations and algebraic equations. The equations with numerical values can be then be solved by modern day computers.

CFD modeling yields qualitative as well numerical predictions of a fluid flow. CFD has proved itself to be a useful tool for scientists and engineers in a variety of areas. CFD modeling has been used extensively in the aerospace industry to model the flow around airfoils, aircrafts, re-entry vehicles, etc. The defense and military sectors use CFD to model the motion of projectiles, supersonic and hypersonic flows, and many other applications. CFD is now being used to model the dispersion of heat in CPUs and other computing components. Meteorologists use it to predict weather based on existing and ever changing conditions. Modeling of smoke plumes is another application. The oil and gas industry uses CFD to model and predict flows and maximize recovery of hydrocarbons from reservoirs. Chemical and processing industries widely use this technique to model flows for mixing and maximizing the yields from their equipment.

Numerical modeling has proved itself to be a powerful tool for numerous engineering applications. This is especially true in cases where experiments are difficult and expensive to set up. Small scale experiments can be used to validate and calibrate the models. Numerical models also help researchers by providing good approximations beforehand. Often, this is one of the approaches used in applications like designing bridges, buildings, etc.

CFD modeling has been established as a good numerical method (A.M.Wala, J.C.Yingling, & Zhang, 1998) for analyzing airflow in underground mines. Since, the success of the UK research project depends on the percent reduction in dust in a mine environment, certain experiments can be designed to validate the performance of a CFD model. To be successful, the research should have a judicious involvement of modeling as well as

laboratory experiments. Table 4.1 shows a comparison between the processes of running laboratory experiments and CFD modeling.

Table 4.1 A comparison between experimental procedure and CFD modeling.

| Parameter | Laboratory experiments | CFD modeling |
|---|---|---|
| Size | Limited to laboratory settings or a limited flow domain. | Can handle actual size models, easy to shape to suit the computations. |
| Nature of parameters handled | Usually keep a certain parameter constant and vary others. | Can vary multiple parameters at the same time and monitor the changes. |
| Transient State Phenomenon | Number of data points obtained depends on process under study and equipment. | Any number of points in space and time can be monitored easily |
| Cost | Can be cheap or expensive depending on the set up. | Calls for software, computing facilities and a subject matter expert as the investment. |
| Accuracy and Reliability | Could be higher since actual phenomenon is replicated. | Accuracy as good as the CFD models. |
| Sources of Error | Set up errors, measurement errors. | Modeling errors, meshing and discretization errors. |

### 4.1 Process of CFD Modeling

The usefulness of prediction by a CFD model is directly dependent on the accuracy of models themselves. Therefore, a sequence of steps is usually executed to generate an accurate CFD model.

The problem statement is clearly put forward as the first step. The available inputs and expected output parameters are defined. Geometry of the flow domain is generated in CAD software as a 3D drawing. This drawing is then exported to CFD modeling software in a suitable format amenable for CFD modeling. The *.stl, *.stp and *.x-t files usually preserve the features of the geometry during the entire transformation process.

The presence of symmetry usually helps reduce the computational domain to a large extent by reducing the resources utilized in the given set of simulations. The computational time is often reduced significantly, without affecting the results.

The flow domain is then identified. It is usually kept to a size small enough to be able to capture the relevant phenomenon, thereby letting the user study the relevant portion of the domain. The volumes and surfaces are then registered in the CFD modeling software. Fluid inlets, outlets, restraining walls and other important elements with their classifications are encountered most frequently and are registered. A computational mesh is generated, usually having millions of discrete elements depending on the complexity of the geometry. Each of these mesh elements represents a discretized computational volume. Better results can be expected with a finer mesh at the cost of more time and resources.

A suitable turbulence model is then selected which can encompass all or most of the expected processes and phenomenon with the model. The model should be in accordance with the kind of flow and obstacles encountered. The K-ε model is usually considered to be a fairly robust model for a majority of applications; however, a comparison must be made with other more specific models for any difference in results.

The boundary conditions are established and convergence criteria fixed for the problem. The simulations are run until the convergence occurs or the number of cycles or set time criterion is met. Post processing is carried out thereafter. The CFD model may be further recalibrated with experimental results, and model validated to explore other parameters.

## 4.2 Preprocessing

### 4.1.1 Drawings and Geometry Generation

Preprocessing, as previously discussed, involves the following steps to make the model conformable to run simulations:

(i) Generating the initial geometry in a CAD software.

(ii) Importing the geometry to the CFD software.

(iii) Cleaning the geometry in terms of removal of intersecting and isolated elements, fins and other geometrical features not amenable to meshing.

(iv) Generating an initial octree.

(v) Inserting prism layers and hence the volume and surface mesh generation.

An initial drawing, as shown in figure 4.1, had minute details of all the features present on the JOY 7LS shearer, thus making it very complicated. This *.stl file was therefore not conducive to CFD simulations. Addition of other machinery, including powered supports and armored face conveyer, would have made handling the set up too cumbersome. Furthermore, unnecessary amounts of time and cost would have gone into generating the simulations.

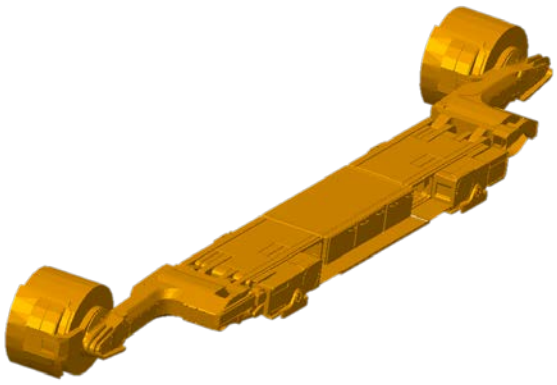

Figure 4.1 JOY 7LS shearer, similar to the one being used at the coal mine, the drawing shows all the structural details of the shearer.

It was decided to eliminate minute details which would not have made any appreciable difference to the CFD models. Original geometry (*.stl) files were used to redraw a simpler

version of all the machinery at the face without discarding any relevant details. Figure 4.2 shows the simplified structure of the shearer.

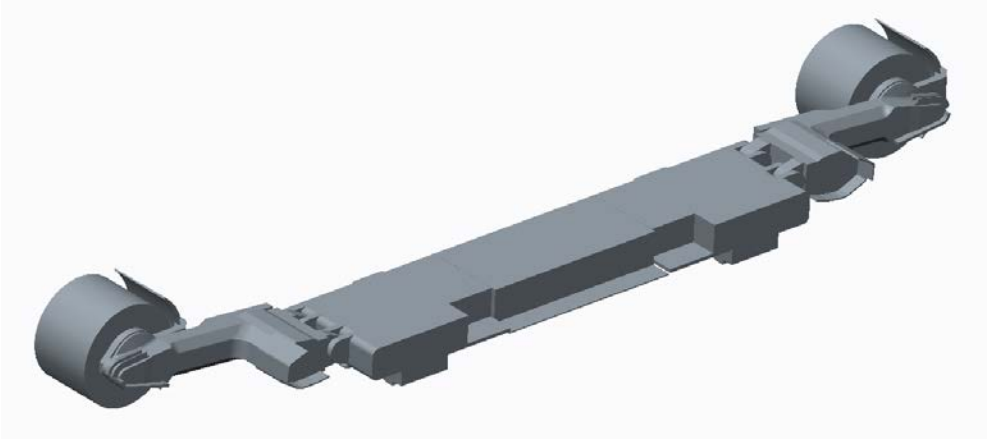

Figure 4.2 The simplified structure of the shearer (JOY 7LS).

A concave structure concentric with the leading drum was first conceived to represent the coal face under extraction at the panel. However, a visit to the mine and a careful observation of the muck profile of the extracted coal close to the shearer soon led to modifications in the drawing.

Coal chunks were also observed to fly off tangentially ahead of the shearer drum. The pile kept on growing before being restricted by the intense airflow at the coal face. This resulted in a distorted convex shaped pile which was carried along the face by the shearer. Figure 4.3 shows the coal pile. Furthermore, this was considered to be the primary source of dust on the longwall face.

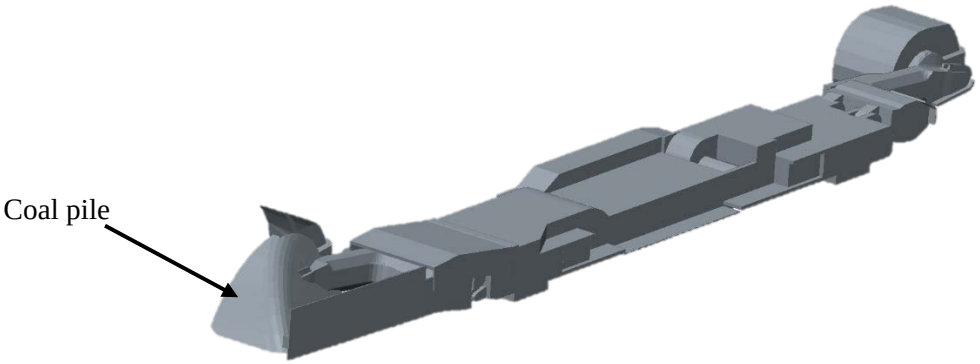


Figure 4.3 Shaded view of shearer with the scrubber mounted on it, coal piled up close to the leading drum can be seen.

Powered supports were removed from the CFD model for reasons discussed later in this section. Figure 4.4 shows the entire layout of the zone close to the shearer. This would be exported into a format (*.stp or *.x-t, conducive to CFD modeling on SC-Tetra.

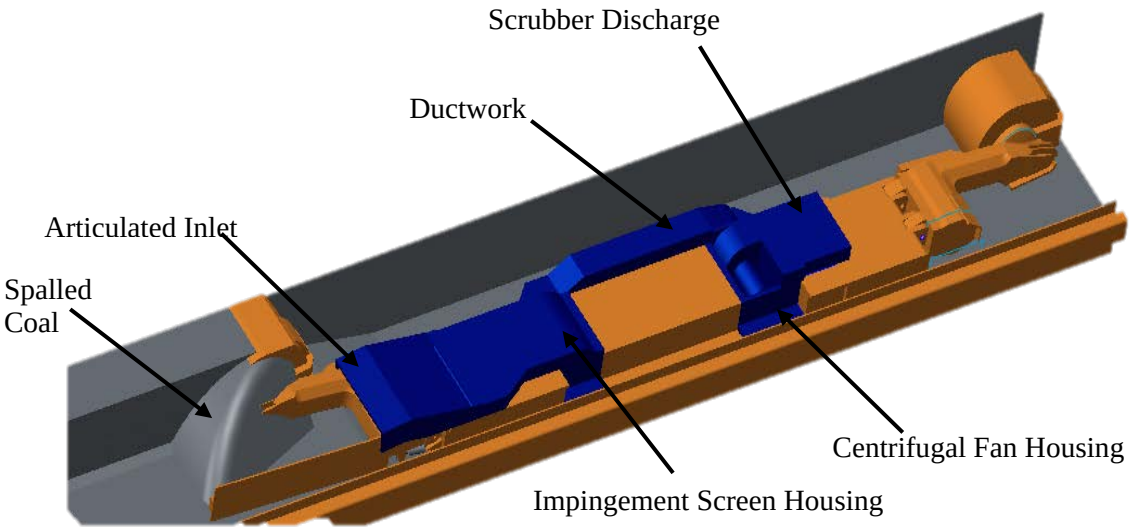


Figure 4.4 A 3D computer aided drawing of the longwall face close to the active mining zone, flooded bed dust scrubber components are shown in blue color.

The geometry imported in SC-Tetra required no further scaling with respect to size. It, however had some issues with surfaces and so an initial cleaning was done on prime mode of the software. Figure 4.5 shows the imported geometry ready for further pre-processing.

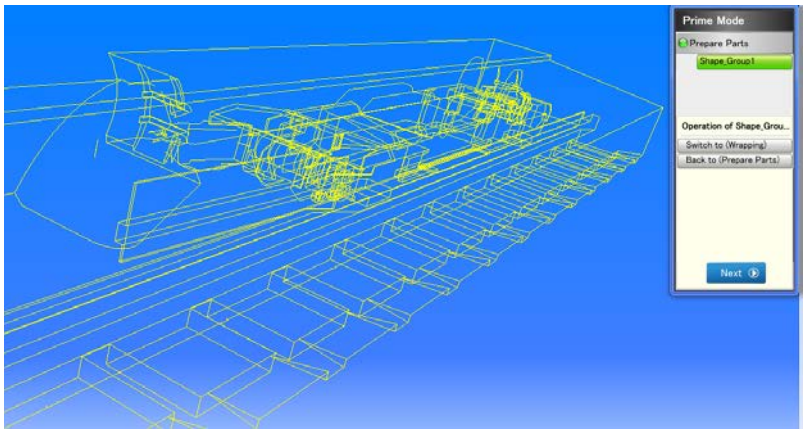


Figure 4.5 Importing the geometry into prime mode.

Intersecting faces were identified and cleaning was carried out to remove all facets with sizes smaller than the identified minimum dimensions of the features. These steps were repeated multiple times until the geometry was free of errors.

To render the geometry free of any errors, the following steps are executed:

(i) Removal of overlapping facets.
(ii) Boundary creation.
(iii) Sheet sewing.
(iv) Detection of non-manifold shapes.
(v) Detection of contact edges and virtual solids.

With the region recognition carried out, the geometry can now be moved to the model mode. The relevant volumes as well as faces were then registered. Some of the important elements for this set up are *Flow_Volume*, *Face_Inlet*, *Face_Outlet*, *Scrubber_Inlet*, *Scrubber_Outlet*, *Coal*, *Shearer*, *Conveyor Belt*, *Walls* and *Shearer_Clearer*.

As discussed earlier, the powered supports do not have their canopies and other components included in the CFD model because of two reasons:

(i) Most of the capture occurs close to the leading drum of the shearer and therefore this zone is of utmost interest for the CFD simulations.
(ii) Volume going into final CFD models is reduced which greatly reduces the number of mesh elements required and hence the computational time. Computational time becomes substantial during the course of transient state simulations since the complex simulations can easily run into hours.

### 4.1.2 Octree Generation

Octree elements act as the spots to place the mesh elements. These are also used to conveniently partition a three dimensional space into discrete elements. These have a regular cubic shaped structure. Figure 4.6 shows a course octree for the set up.

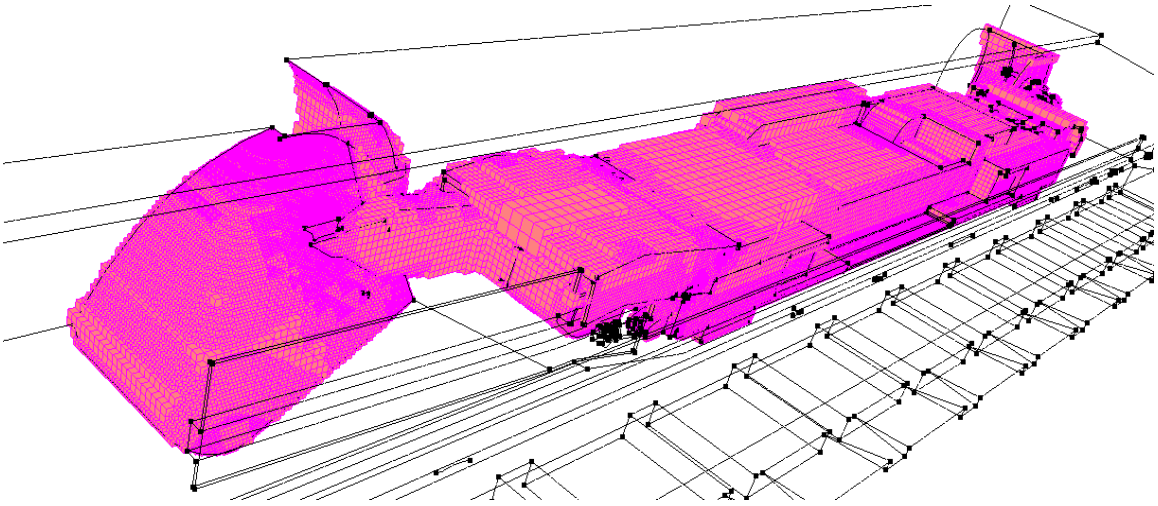

Figure 4.6 An initial octree for surface mesh generation; octree elements act as cells to place the mesh elements.

SC/Tetra offers three distinct ways to generate an octree. An octree can be generated by keying in the size of the minimum octant size based on the physical dimensions of the flow domain. Octree can also be generated by keying in parameters like the size ratio of the root octant as well as the refinement levels. Octree can also be generated automatically by the SC/Tetra where it uses the target number of elements and arranges the stipulated number of cells based on the geometry and analysis conditions. This feature is especially useful when the geometry is simple or doesn't have complex features and steep gradients. Multiple local refinements are often required to control the gradient of the octree and hence the mesh in a better way. It also helps capture the large changes in a physical parameter more precisely and with better accuracy.

### 4.1.3 Volume and Surface Mesh Generation

Mesh generation is an integral part of any CFD analysis. CFD software runs by applying Euler's equations to all the mesh cells. These partial differential equations are solved by discretization of the flow domain and a numerical integration carried out.

Meshing can be described as the procedure of discretizing the entire flow domain into elements of numerous shapes such as tetrahedron, pyramid, prism, hexahedron, etc., depending on the geometry, to represent the variation of physical quantities in space and time. The governing equations of fluid flow are then applied to all these cells individually

using the finite volume method and numerically integrating them. Each of these elements or cells is called a mesh element and an organized group of cells is referred to as a grid. Traditionally, meshing has been the most sophisticated, time consuming and costly exercise as with respect to CFD modeling. 'Structured' meshes are used whenever the flow domain has a regular geometry or possesses multiple symmetries where the transition from one grid element to the next is uniform. 'Unstructured' meshes are used whenever the flow domain is characterized by complexities and steep gradients. Modeling a domain as complicated as a longwall panel utilizes unstructured meshes. It possesses irregular connectivity. A 'hybrid' mesh contains structured as well as unstructured portions. These meshes however boast of capabilities to represent the geometries better. A good mesh, preferably, should have over 99 % of the surface covered by the prism layers.

**Boundary layer capture and prism layer insertion**

External flows around real life bodies always offer viscous forces (shear and no-slip effects) close to the surfaces resulting in turbulences. Figure 4.7 shows the profile of boundary layer close to an airfoil. SC Tetra offers prism layers, to represent this zone of flow, governed by shear. Thickness of first layer, variation rate of thickness and number of layers together define the prims layers. Thickness of first layer is very important and is based on judicious understanding of the boundary layer phenomenon. Usually, one-quarter of the thickness of the adjacent cell thickness is a good approximation to begin with.

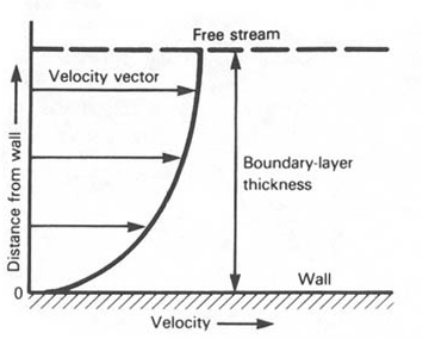


Figure 4.7 Profile of a boundary layer (NASA EP -89, 1971, p.68).

**No slip walls**

The velocity of the fluid in this scenario is considered to have the same velocity as that of the wall.

Stress $\sigma_x$ , acting in the +X direction can be represented by:

$$\sigma_x = \mu\, \delta(u-u_B)/\delta y$$

where, u = Velocity of fluid in X direction [m/sec]

$u_B$= Velocity of wall in X direction [m/sec]

μ= Coefficient of viscosity of the fluid [Pa.s]

**Log law walls**

Usually, airflow on a longwall is highly turbulent and has a Reynold's number on the order of hundreds of thousands. Experiments have established that for turbulent boundary layers in a homogenous flow parallel to a flat plate:

$$\frac{u}{u^*} = \frac{1}{\kappa} \ln \frac{u^* y}{\nu} + A$$

Where, κ = Karman constant (=0.4)

A = A constant (=5.5)

y = Distance from the wall surface [m]

u = Flow velocity at a distance y [m/sec]

u* = Friction velocity, $(\Gamma 0/\rho)^{1/2}$ [m/sec]

ρ = Density of the fluid [$kg/m^3$]

Γ0 = Shear stress [$kg/(m/sec^2)$]

V = Kinematic viscosity,μ/ρ [$m^2/sec$]

Figures 4.8 and 4.9 demonstrate the condition where log-law is applied on the walls.

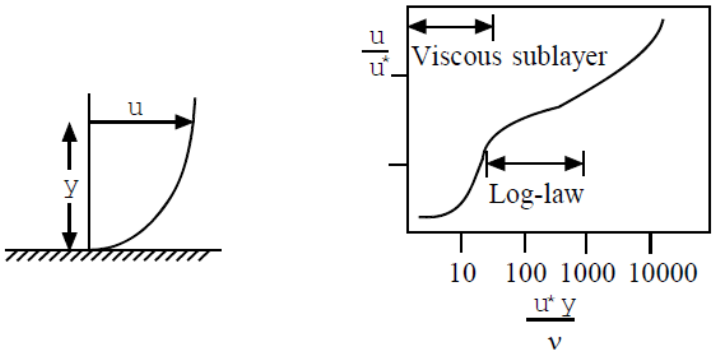


Figure 4.8 Profile of a log law wall (Source: Cradle CFD manuals).

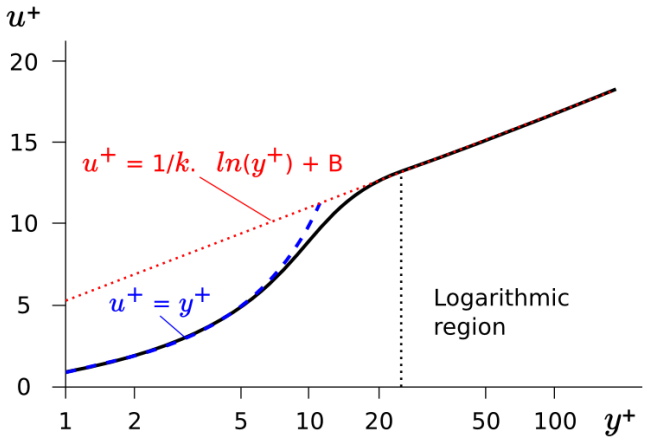


Figure 4.9 Profile of a log law wall, two curves meet at Y+=11.6 (Source: Cradle CFD manuals).

When the value of y+<30, the equation can be approximated as,

$$\frac{u}{u^*} = \frac{u^* y}{\nu}$$

where the symbols have usual meanings.

At y+=11.6, stress obtained from both the equations have similar values. Since the flow occurring on a longwall panel is highly turbulent, log-law is applied to the walls. The walls are further considered to be rough and suitable constants applied for simulations to account for roughness. Table 4.2 summarizes the most common range of velocities encountered on the general longwall face.

Table 4.2 : Estimation of values of Y+ at 300 K for air.

| Velocity [m/sec] | Y+=30 | Y+=100 | Y+=300 |
|---|---|---|---|
| 0.70 | 0.0090 | 0.0380 | 0.1340 |
| 1.00 | 0.0066 | 0.0269 | 0.0937 |
| 3.00 | 0.0022 | 0.0089 | 0.0312 |
| 5.00 | 0.0013 | 0.0054 | 0.0187 |
| 7.00 | 0.0009 | 0.0038 | 0.0134 |

The following table 4.3 shows the summary of boundary conditions.

Table 4.3 Summary of general analysis conditions for CFD simulations.

| Parameter | Values |
|---|---|
| Analysis type | Turbulent flow |
| Turbulent flow model | RANS (Reynold's average Naviers Stokes) |
| Turbulence model | Standard k-EPS model |
| Method | Steady state analysis , transient state analysis |
| Material properties | Air (incompressible/ 20° C) |
| Undefined (fluid stress) | Stationary wall |
| Boundary conditions | Face inlet: flow rate specified<br>Face outlet: static pressure (0 Pa)<br>Scrubber inlet/ outlet : flow rate specified<br>Coal/ shearer/ belt/ walls/ shearer clearer: moving/ stationary wall (log law) |
| Output control | Fld cycle : 200<br>R File : 500 |
| Solver settings | Courant number: 10 or low.<br>Relaxation factor: 0.9 for incompressible fluid<br>Convergence criterion : average residual being 10e-4 (exit iteration)<br>Accuracy of time derivative terms: first order implicit scheme |

The prism layers are inserted to capture as much of the surfaces as possible. Lowering the insertion percent affects the boundary layer capture severely. Usually, 99.0 % or more of the surfaces of the model should have prism layers inserted on it. The percent can be relaxed to some extent if the geometry is very complex. Using the octree file (*.oct), the boundary condition file (*.s) and suitable parameters for prism layers depending on the dimensions of the flow domain and expected velocities, meshes are generated. The volume mesh (*.pre_tetra) is generated first, followed by the surface mesh file (*.pre). Figure 4.10 shows the mesh of the shearer surface, the coal face and the shearer clearer. Similarly, figure 4.11 and 4.12 show the fine mesh close to the inlet of the scrubber and on the walls.

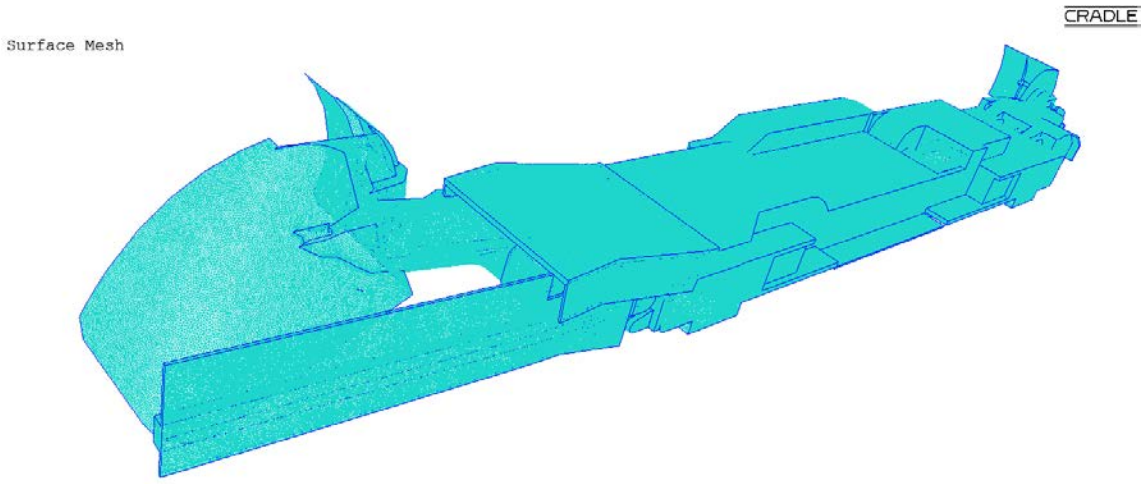


Figure 4.10 Surface mesh on the model representing the active mining zone with the shearer; the mesh close to the coal pile has been refined to capture the motion of dust particles precisely.

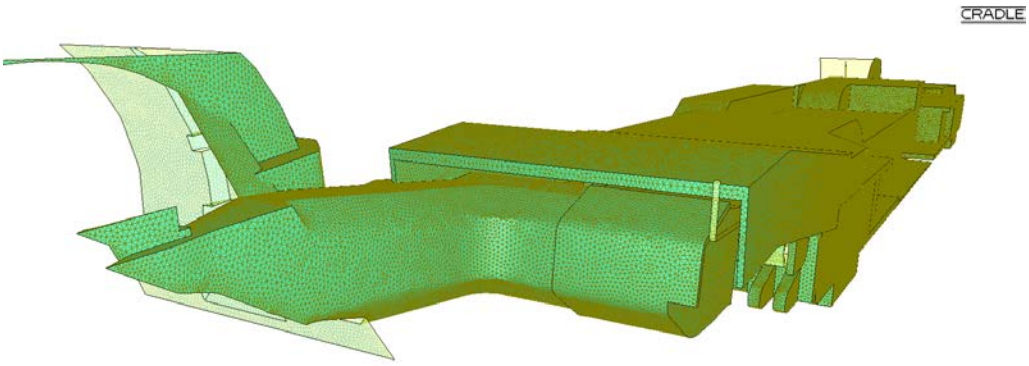


Figure 4.11 Refined mesh close to the inlet of the scrubber.

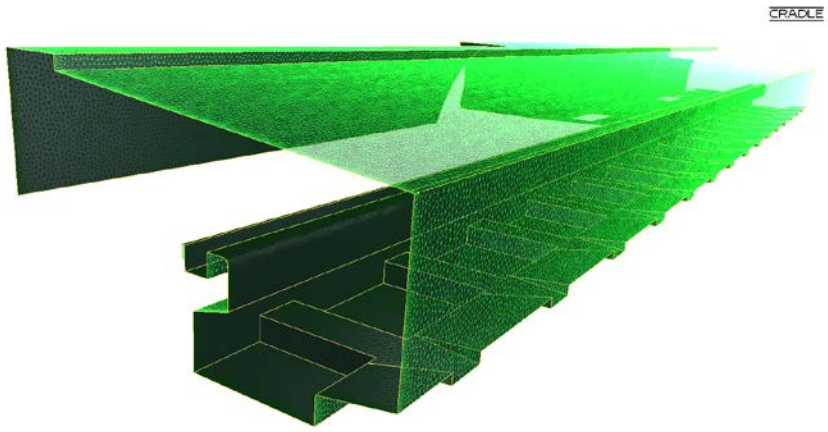


Figure 4.12 Mesh on all other walls including the coal face and the support surfaces.

The volume mesh projects from the surface and encompasses the entire flow volume. The figure 4.13 shows the three prism layers, accounting for the shearing forces.

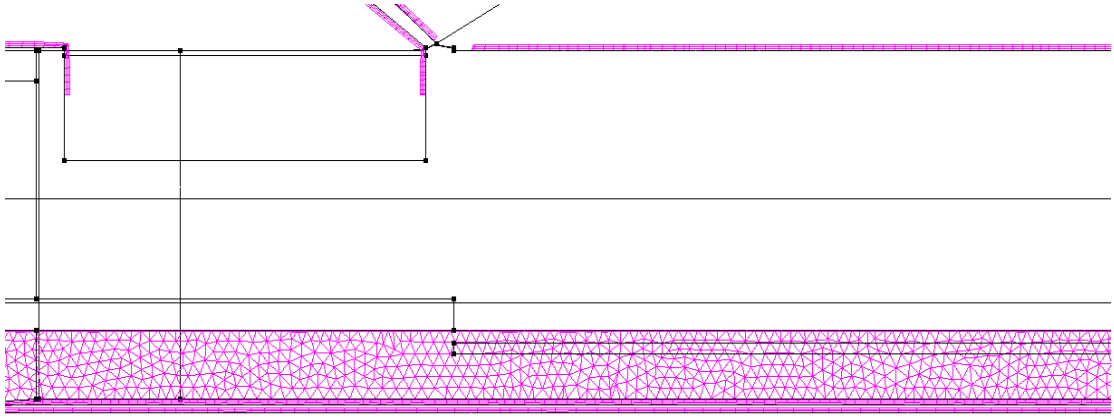

Figure 4.13 Mesh on a plane parallel to the ventilation airflow direction, three prism layers can be seen on the surface as well.

**Mesh Quality**

It is usually difficult to ascertain the quality of a good mesh just by a visual inspection. Percentage of prism layer insertion, smoothness and low skewness are usually are good parameters. A good mesh should be able to capture all the entire domain of a flow. Poor meshes almost always result in inaccurate solutions or poor convergence since they do not apply the fluid parameters accurately to all the elements. Hexahedral meshes usually will yield more accurate solutions.

There is no standard method of mesh generation with the right number of elements applicable to all scenarios. A definite pattern of increase in cell size towards the volume of flow and away from the surfaces is a good meshing practice. This reduces the number of elements wherever possible without affecting the accuracy. Figure 4.14 depicts one such pattern.

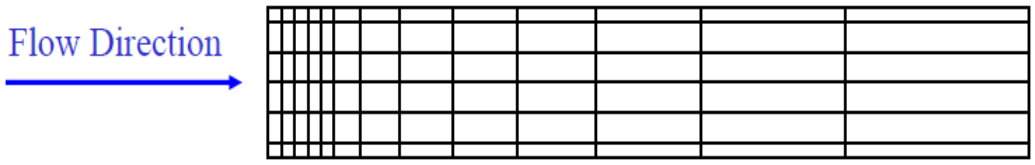


Figure 4.14 Growth of cell size for a good mesh (Source: Andre Bakker, Applied CFD).

### 4.3 Setting up the CFD Model for Dust Capture

Various elements of the geometry were registered as discussed in the previous section for modeling the dust capture. *Face_Inlet* was imparted volumetric flow rates (11.0 $m^3/s$ and 13.2 $m^3/s$) corresponding to an incoming airflow speeds of 2.50 m/sec (500 fpm) and 3.00 m/sec (600 fpm) respectively. The *Face_Outlet* was assigned a static pressure of 0 Pa. The *Belt* was assigned a translation speed of 1.80 m/sec (360 fpm). The drums have been assumed to rotate at 45 rotations per minute, similar to the speeds at the cooperating mine. The walls had been assigned a log-law wall condition and suitable roughness assigned to them. Volumetric flow rates, varying from 3.0 $m^3/s$ to 6.0 $m^3/s$ were assigned, in increments of 0.6 $m^3/s$. Identical volumetric flow rate as discharge was assigned for each scenario at the discharge of the scrubber.

Each steady simulation was run for convergence, thereby establishing a definite flow field. Transient state simulation was then set up. Two-hundred and fifty dust particles were assumed to be massless and point entities. They were assumed to be released at time, $t = 0.0$ from the *Coal_Face*. These particles were then allowed to travel under the influence of airflows. The particles which hit the inlet of the scrubber were assumed to be captured and killed by the scrubber. Particles hitting the walls elsewhere were also assumed to be killed.

Simulations were run for 20.0 seconds at very small time steps. Number of particles captured out of 250 dust particles indicate the capture efficiency.

All these parameters were fed into the analysis conditions which was then saved as a condition (*.s) file. This file was then used for running the simulation and solving the specific scenario. This will be discussed in later sections.

### 4.4 Solving

The solver of SC/Tetra software was used to run the specific scenario of face and scrubber airflows. The solver uses the mesh (*.pre) and condition (*.s) file to run the CFD simulations.

Steady state simulations are being run for convergence or 4,000 cycles, whichever comes earlier. Most of the steady state simulations converged well within 500 cycles. A convergence was considered when the monitors of parameters became constant with respect to the cycles, or otherwise when the graphs of convergence monitors became flat or showed minimal fluctuation. Figure 4.15 shows one such monitor where magnitude of velocity attains a constant value. Converge of steady state simulations can be assumed to have been attained by a careful visual inspection if the model set up for simulation is very complex even after initial simplifications.

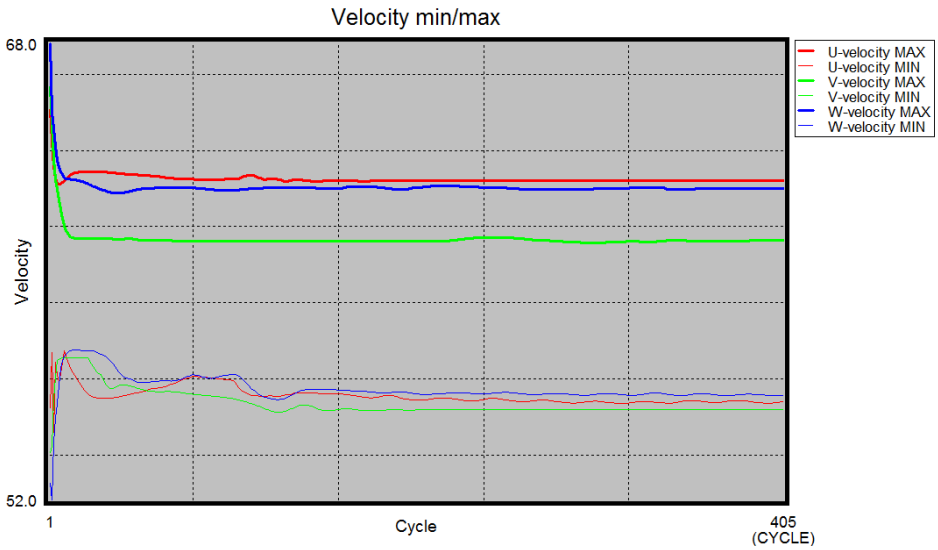


Figure 4.15 Monitors of velocity with respect to iterations for a steady state simulation.

Similarly, transient state simulations are run for 20 seconds of 'physical time'. A low Courant number helps calculations proceed in very small times steps. The number of cycles of calculations are expected to exceed 40,000.

### 4.5 Grid Independence Study

A computational mesh should be capable of explaining a process. A good CFD analysis should be able to come up with results that show that the process can best be described by the physical phenomenon including the boundary conditions and not on the mesh size, number or fineness. A good computational mesh should be fine enough to be able to capture the majority of fluid flows precisely in the entire flow domain. Refining the mesh further may not improve the results significantly; however, will certainly result in much more computational time, efforts, and costs.

Grid independence was carried out using grids for the simulations with increasing number of elements. The following points should be taken care of:

(i) Residuals must be lower than $10^{-4}$ or $10^{-5}$, depending on the problem set up.

(ii) Monitors for different parameters should reach a steady state. If the monitors oscillate around a median point widely, a refined mesh would be required. The imbalances less than 1% can sometimes be assumed to have led to a converged solution.

Plotting the values of monitors against the number of mesh elements is usually the best method to check for grid independence study. If the monitors have their values steady over different mesh sizes, the mesh with lowest number of elements would suffice for the particular set up.

CFD simulations were generated for a multiple number of mesh elements ranging between 1.11 million and 8.12 million elements, and most of them resulted in close values. Further, mesh with elements numbering 1.12 million, 1.60 million, 3.20 million and 8.12 million were chosen to compare the results.

Steady state simulations were generated for all of them. Magnitude of velocity was considered to be a good parameter to establish the mesh independence. Figure 4.16 shows

the contours of velocity through a plane parallel to the coal floor and 1.23 m above it for meshes containing 1.60 million, 3.20 million, and 8.12 million elements for a scrubber flow of 4.8 $m^3/s$ and a face flow of 11.0 $m^3/s$.

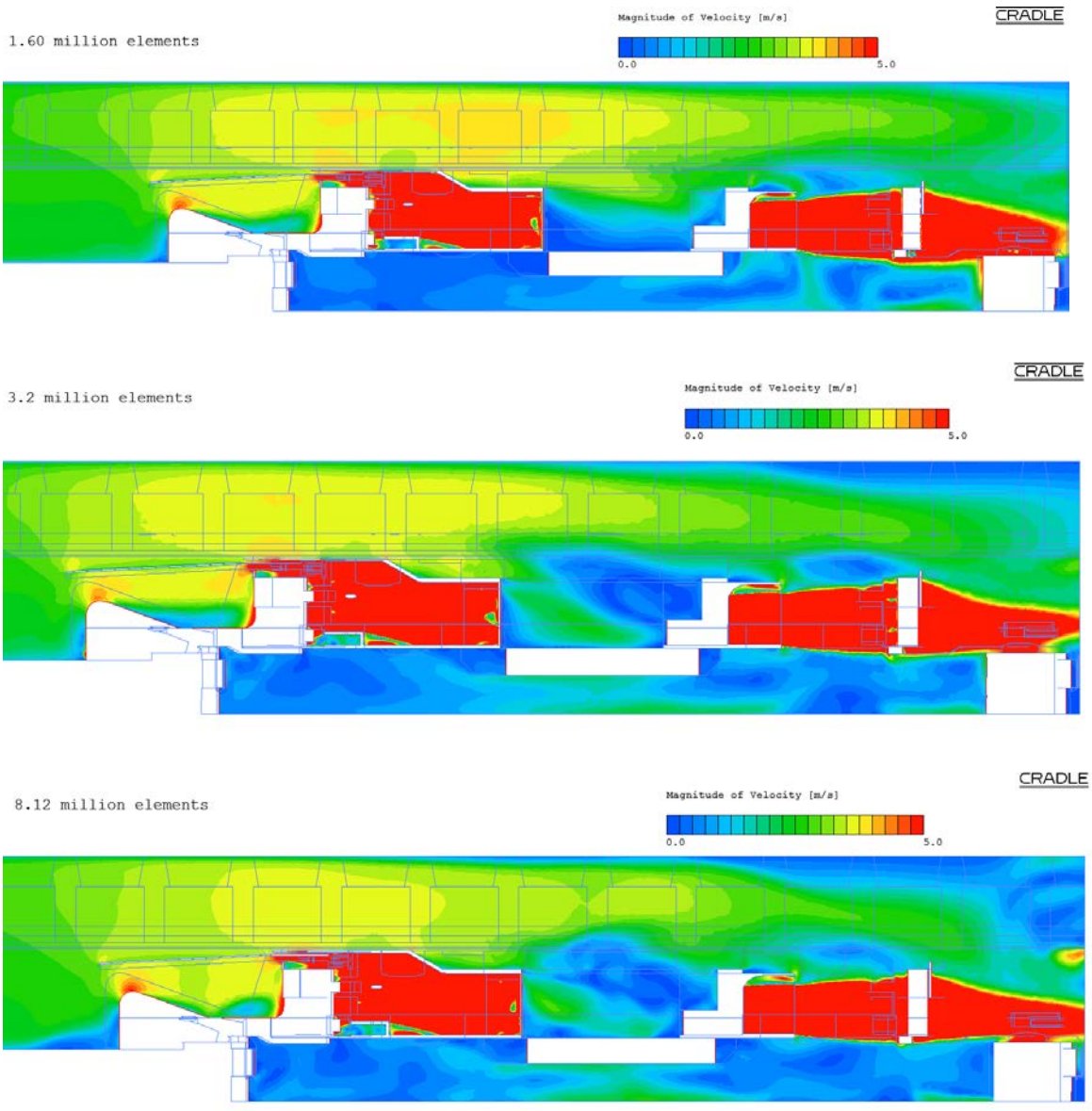


Figure 4.16 Contours of velocity on a given plane for three meshes, with increasing mesh element number.

However, since the flow domain has many zones of high gradients in measurable parameters like pressure and velocity, a scalar integration of the parameter over the entire surface may not yield any meaningful results. Therefore, three circles, 0.0254 m (1 in.) in diameter, were generated on the walkway. Figure 4.17 shows one such circle with absolute

coordinates (16, 1, -4.75). Two other circles were chosen at a distance of 8 m from this circle towards the headgate and tailgate. The scalar integration of magnitudes of velocities in the circles attained a constant value at 3.2 million elements. This establishes mesh independence.

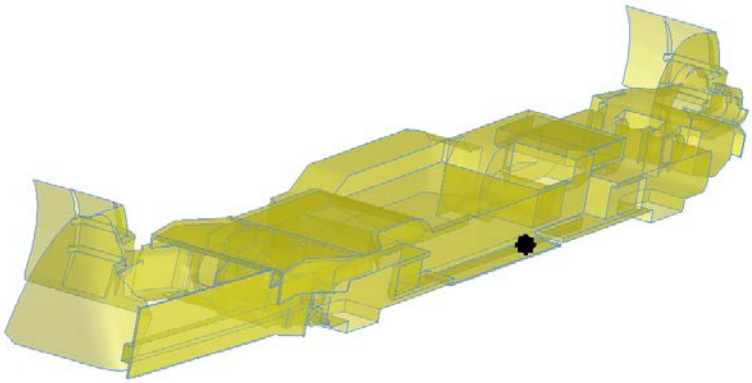

Figure 4.17 Location of one of three circles to establish mesh independence.

Furthermore, transient state simulations for a face airflow of 11.0 $m^3/s$ and a scrubber flow of 4.2 $m^3/s$ were run for all of these elements. Figure 4.18 shows the capture with respect to time for different mesh numbers.

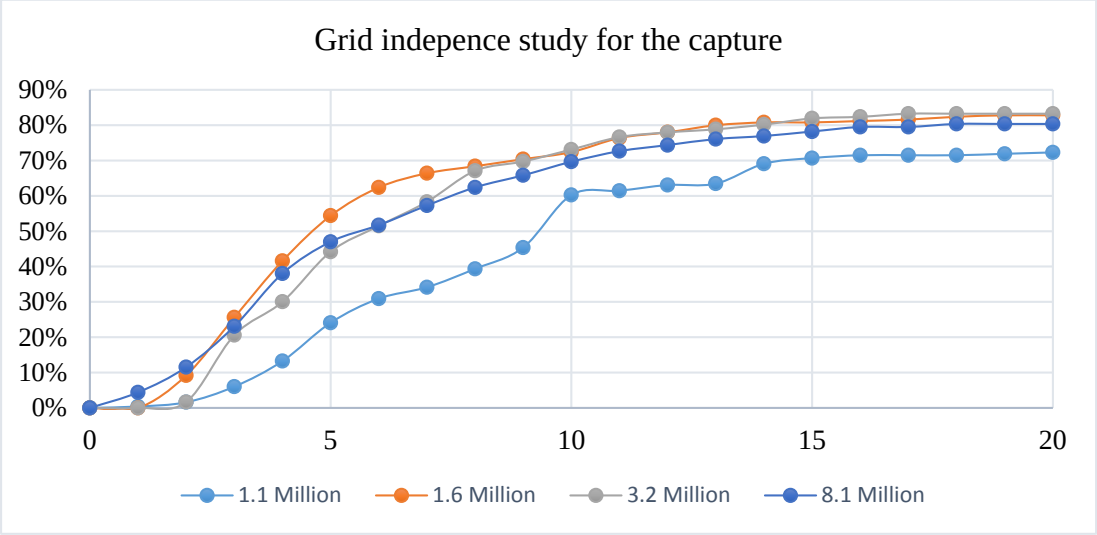


Figure 4.18 The chart showing capture vs time for different grid number.

The results become independent of mesh number at approximately 3.2 million elements. Considering the complexity of the geometry in question and similar trend line of the capture, grid independence can be assumed to have been established.

### 4.6 Supercomputing Facility

As the number of mesh elements increases, computational time increases drastically. A workstation would not have been substantially powerful to run thousands of cycles for each set of boundary conditions and could have taken an enormous time to run. University of Kentucky has high performance computing (HPC) facility, which can be used to run the CFD simulations if the problem demands excessive computing resources. Moving onto the HPC for running simulations drastically reduces the computational time, compared even to a workstation with an i7 processor, running 32 GB RAM.

The high performance computing facility at the Department of Mining Engineering, University of Kentucky was used to run the simulations. It has 45 cores, 128 GB of RAM and 8 TB of storage space and runs on the Linux operating system.

Transfer of files between the workstation and the HPC requires two client applications- WinSCP and Putty. WinSCP is an open source SCP client for Windows. It is primarily used to transfer files to and fro between local and remote computers. Figure 4.19 depicts one such instance with displays of remote and local computers put adjacent to each other. The ***.pre file, which stores the geometry as well as the mesh and ***.s file, which stores the conditions for a particular simulation are transferred via WinSCP to the HPC.

Putty serves as the command prompt and is the platform where execution is seen.

A typical command to run a scenario on SC-Tetra V11 and on 32 nodes is:

[username@mining-hpc]$ sct11 –lfilename <filename>.l <filename>.s 32;

To keep a check on current values of parameters of interest, monitoring the log files is a good approach. The putty interface shows the log files as the simulations run. Figure 4.20 shows an instance of simulations.

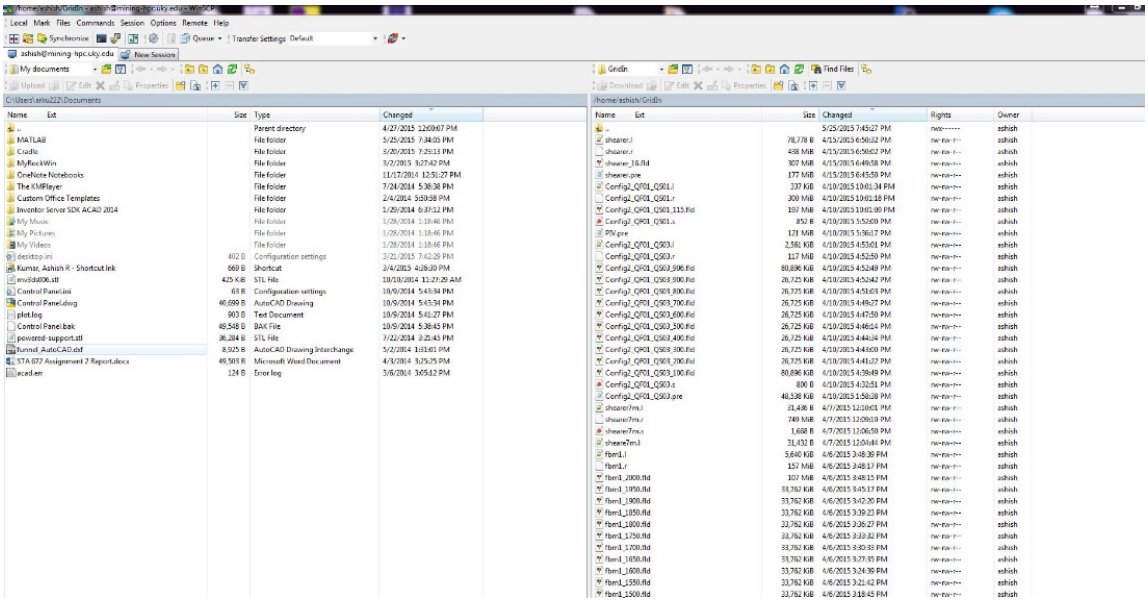

Figure 4.19 WinSCP screen, showing the local and remote computers.

```
</SECTION>
<SECTION Name="STEADY STATE CHECK">
=== STEADY STATE CHECK ===
  U...  3.01e-04   V...  1.05e-04   W...  1.45e-04   P...  1.48e-04
  TK..  1.43e-04   TE..* 6.83e-06
</SECTION>
<SECTION Name="BOUNDARY FLUX">
=== BOUNDARY FLUX ===
  REGION                  AREA       MASS FLUX     VOLUME FLUX
  Face-Inlet             4.78163         24.1200         20.0000
  Face-Outlet            6.81952        -24.1200        -20.0000
  Scrubber-Inlet        0.754223        -3.61800        -3.00000
  Scrubber-Outlet       0.178580         3.61800         3.00000
  TOTAL:                 12.5340     8.57580e-07     7.11095e-07
</SECTION>
<SECTION Name="FIELD EXTREMA">
=== FIELD EXTREMA ===
  VAR        MAX/MIN             X             Y             Z (    NODE)
  U           17.7987       19.8949       1.22081      -6.23668 ( 2084789)
             -15.0260       14.2968       1.07577      -5.50384 (  208967)
  V           8.11287       21.8389       1.20977      -6.11847 ( 2270107)
             -15.6594       21.8070      0.855951      -6.06163 ( 2158254)
  W           15.7516       11.7785       1.40682      -6.37595 (  566469)
             -14.4794       14.0289       1.09363      -5.72513 (  233025)
  P           155.884       21.8384       1.15886      -6.09850 ( 2247533)
             -257.589       14.0205       1.16849      -6.50449 (  188986)
  TK          10.7367       24.1910      0.531406      -6.16554 ( 2522360)
         1.00000e-09       8.20555       2.04014      -6.90001 (  341421)
  TE          9275.19       24.1910      0.531406      -6.16554 ( 2522360)
         1.00000e-09       8.20555       2.04014      -6.90001 (  341421)
  EVS       0.0720617       25.4182      0.694232      -4.10597 ( 2466447)
         1.08540e-10       10.5344       1.36131      -6.65075 (  565542)
</SECTION>
<SECTION Name="YPLUS MIN-MAX">
=== YPLUS MIN-MAX ===
          NODE       YPLUS        DIST     TAUWALL        TURK        TEPS
  MAX  2522438     2196.49   0.0473820    0.596740    0.487037     2.94681
  MIN   566184     0.00000     0.00000     0.00000 1.00000e-09 1.00000e-09
          NODE           X           Y           Z
       2522438     24.1188    0.529848    -6.19506
        566184     11.8135     1.41016    -6.65075
</SECTION>
```

Figure 4.20 Screenshot displaying the current scenario during a certain cycle of calculations.

The *.fld files are saved after completing the requisite number of cycles according to the task requirements. Transient state simulations need to have the filed files saved at closely spaced intervals. The *.l (log) files are also saved and monitored according to the task at hand. Any of these files can be downloaded onto the workstation.

### 4.7 Turbulence Models

A turbulence model is a procedure to numerically solve the mean flow equations and the effect turbulence has on the mean flow. Turbulence modeling is an extremely resource consuming procedure, since finer details of flows need to be captured. For common engineering applications, it is not required to know the fine details of turbulence. A certain percentage of energy is assumed to have dissipated without having to model how it was lost.

Turbulence models are chosen based on their applicability. A turbulence model should be versatile, accurate, simple to handle and economical to run. Extreme ends on the velocity scale calls for specific turbulence models. These models are based on “Boussinesq Hypothesis” which postulates that the momentum transfer brought about by the eddy currents in a turbulent flow can be modelled with eddy viscosity. All of these models have their distinct characteristics and associated advantages and disadvantages.

Classical turbulence models are based on Reynolds averaged Naviers-Stokes (RANS) equations. These mostly differ in terms of the number of additional partial differential equations being solved. A two equation Standard κ-EPS is the most preferred turbulence model due to its robustness and well documented literature for common day to day and industrial applications. Table 4.4 compares the models for strengths and weaknesses.

Table 4.4 Applicability of common turbulence models (Source: Cradle CFD, Lecture 10-Applied CFD by Andre Bakker).

| Model | Advantages | Disadvantages |
|---|---|---|
| Standard κ-EPS | Robust, proven, good literature and data, economical, fairly accurate, good convergence and least computationally intensive. | Average results for complex flow patterns, including swirls and turbulences.<br>Poor results for swirling and unconfined flows.<br>Valid only for fully turbulent flows.<br>Poor results for complex flows with high gradients. |
| RNG-(Re-Normalization Group) κ-EPS | Better results than standard κ-EPS and can handle separating and swirling flows.<br>Good predictions for high streamlined flows and wall heat and mass transfer. | Not very good with viscous flows because of isotropic eddy viscosity assumption.<br>Average predictions for round jets. |
| MP (Modified Production) κ-EPS | Compensates for formation near the stagnation point in the Standard κ-EPS model. | Poor results for modeling complex flows. |
| Realizable κ-EPS | Better results than standard κ-EPS and can handle separating and swirling flows.<br>Handles the round jet anomaly well. | Not very good with viscous flows because of isotropic eddy viscosity assumption. |
| SST κ-OMG | Good predictions for low Reynold's number.<br>Strength lies in efficient modeling of adverse pressure gradients and separating flows also. | Not very efficient for modeling flows under stagnation or high acceleration. |
| Spalart-Allmaras one equation | Excellent for flows attached to the wall, or mild recirculation and separation.<br>Used widely in aviation. | Weak for flows that are separated widely.<br>Specific usage only. |
| LKE κ- κL-OMG | Works well in the zones of strong acceleration or deceleration, especially for turbomachinery. | Diminishing popularity competing with other models having built in limiters.<br>Switching off turbulence production outside of the boundary layers affects heat transfer and skin-friction. |

**Standard κ-EPS model**

The standard κ-EPS model is most commonly used in solving engineering problems. It is a simple model and fairly robust with respect to general flow problems. This model solves for two variables, κ, being the turbulent kinetic energy and EPS, which is the dissipation rate of kinetic energy. κ-EPS model normally exhibits a good convergence rate and low memory allocation, making it faster compared to other models. The model can be expressed by the following equations:

For the turbulent kinetic energy,

$$\frac{\partial}{\partial t}(\rho k) + \frac{\partial}{\partial x_i}(\rho k u_i) = \frac{\partial}{\partial x_j}\left[\left(\mu + \frac{\mu_t}{\sigma_k}\right)\frac{\partial k}{\partial x_j}\right] + P_k + P_b - \rho\epsilon - Y_M + S_k$$

For the dissipation of kinetic energy,

$$\frac{\partial}{\partial t}(\rho\epsilon) + \frac{\partial}{\partial x_i}(\rho\epsilon u_i) = \frac{\partial}{\partial x_j}\left[\left(\mu + \frac{\mu_t}{\sigma_\epsilon}\right)\frac{\partial \epsilon}{\partial x_j}\right] + C_{1\epsilon}\frac{\epsilon}{k}\left(P_k + C_{3\epsilon}P_b\right) - C_{2\epsilon}\rho\frac{\epsilon^2}{k} + S_\epsilon$$

where, turbulent viscosity is modelled as

$$\mu_t = \rho C_\mu \frac{k^2}{\epsilon}$$

Production of Kinetic Energy is expressed by the equation,

$$P_k = -\rho\overline{u_i' u_j'}\frac{\partial u_j}{\partial x_i}$$

$$P_k = \mu_t S^2$$

Where S represents the magnitude of the mean rate of strain tensor and is given by,

$$S \equiv \sqrt{2S_{ij}S_{ij}}.$$

In order to include the effect of buoyancy on the flow, an additional factor $P_b$ is introduced, where

$$P_b = \beta g_i \frac{\mu_t}{\mathrm{Pr}_t}\frac{\partial T}{\partial x_i}$$

$P_r$ represents the turbulent Prandtl number and is defined by

$$Pr = \frac{\mu C_p}{k}$$

To include the expansion under thermal stresses, the coefficient of thermal expansion, ß has been included and is defined by

$$\beta = -\frac{1}{\rho}\left(\frac{\partial \rho}{\partial T}\right)_p$$

This model does not work well for high gradients or curvature in flows. κ-EPS is also not useful for jet flows. It is preferred not to use this model when the effect of water jets on capture efficiency of a flooded bed is being modelled and similar cases.

The modeling of airflow on a longwall panel offers intense turbulent flows including swirling motions as well as sharp gradients in velocity and pressure. The standard κ-EPS model was expected to yield acceptable results. However, a comparison of the output with other turbulence models was deemed necessary. Therefore, in order to validate the applicability of the standard κ-EPS model, modeling for a face airflow of 11.0 $m^3/s$ and a scrubber flow of 5.4 $m^3/s$ was done across seven RANS models. Table 4.5 shows the range of velocities and pressures on a plane parallel to the coal floor.

The closeness of results obtained on each simulation showed that the standard κ-EPS model would suffice. This model was therefore used for further steady as well as transient state simulations. Figures 77-83 show the velocity contours and vectors on identical planes across all these models. A close examinations of the models also show resemblance of patterns.

Table 4.5 Range of velocities and pressures for the flow on the longwall panel under different scenarios and obtained from different turbulence models.

| Model | Flow at the Face ($m^3/s$) | Flow through Scrubber ($m^3/s$) | Cycles for Steady State Convergence (Number) | Range of Velocities (m/sec) | Range of Pressures (Pa) |
|---|---|---|---|---|---|
| Standard κ-EPS | 11.0 | 5.4 | 327 | 28.482 | 965.745 |
| | 13.2 | 5.4 | 4000 | 28.392 | 960.296 |
| RNG- κ-EPS | 11.0 | 5.4 | 390 | 28.579 | 960.214 |
| | 13.2 | 5.4 | 4000 | 28.466 | 962.040 |
| MP κ-EPS | 11.0 | 5.4 | 242 | 28.647 | 976.193 |
| | 13.2 | 5.4 | 390 | 28.604 | 968.852 |
| Realizable κ-EPS | 11.0 | 5.4 | 190 | 28.438 | 985.619 |
| | 13.2 | 5.4 | 252 | 28.366 | 975.986 |
| SST κ-OMG | 11.0 | 5.4 | 443 | 28.676 | 986.629 |
| | 13.2 | 5.4 | 735 | 28.630 | 977.708 |
| Spalart-Allmaras one equation | 11.0 | 5.4 | 399 | 28.789 | 991.680 |
| | 13.2 | 5.4 | 4000 | 28.693 | 983.107 |
| LKE κ- κL-OMG | 11.0 | 5.4 | 242 | 28.647 | 976.193 |
| | 13.2 | 5.4 | 390 | 28.604 | 968.852 |

### 4.8 Typical Steady State Post-processing

Field files are saved periodically for steady state analysis. Saving the field files at regular intervals also help monitor the pattern for flow field before reaching a steady state. Y+ values are monitored carefully for mesh quality for each simulation.

Typical contours of velocity obtained as a part of post processing for face flow of 11 $m^3/s$ and scrubber flow of 4.2 $m^3/s$ follow in figures 4.21, 4.22 and 4.23.

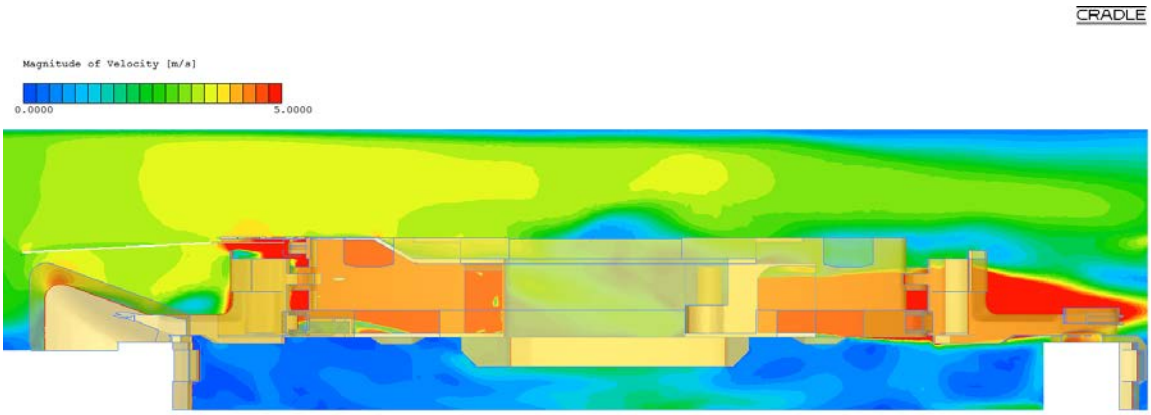


Figure 4.21 Velocity contours on a plane through the inlet and discharge of the scrubber and parallel to the coal floor for a face airflow of 11 $m^3/s$, scrubber flow of 4.2 $m^3/s$.

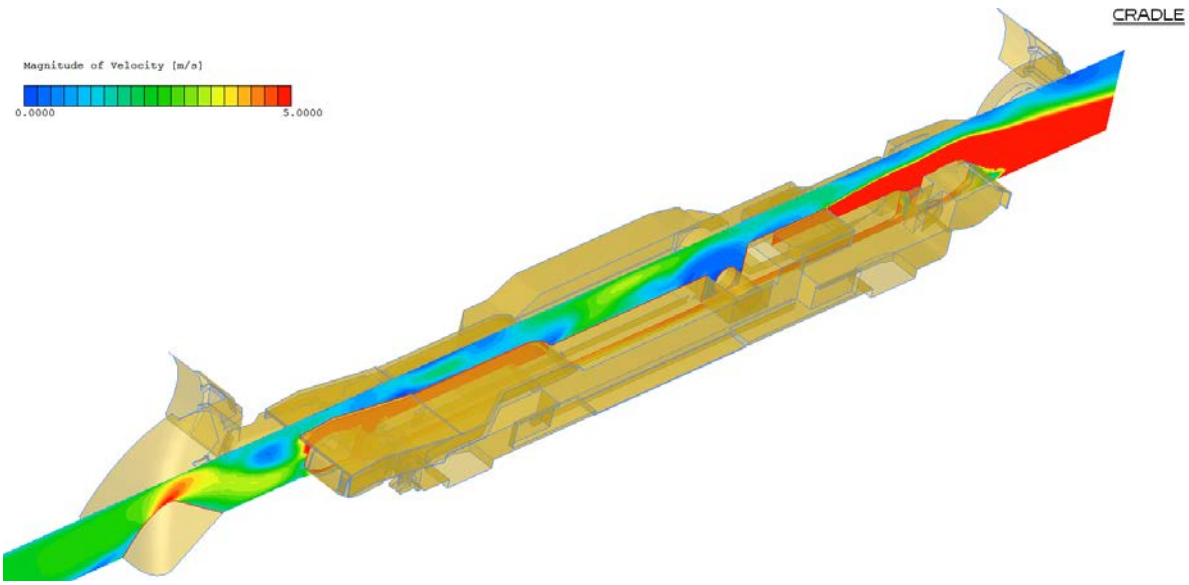


Figure 4.22 Velocity contours on a plane parallel to the coal face and though the scrubber for a face airflow of 11 $m^3/s$ and scrubber flow of 4.2 $m^3/s$.

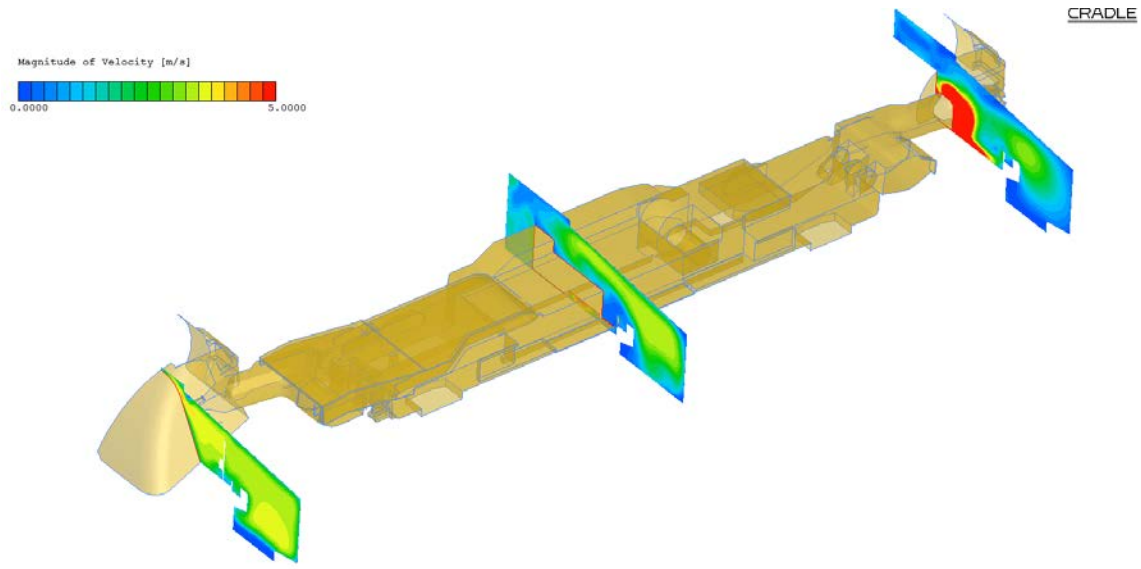


Figure 4.23 Velocity contours on three planes perpendicular to general airflow at the face for a face airflow of 11 $m^3/s$ and scrubber flow of 4.2 $m^3/s$.

### 4.9 Transient State Modeling

Transient state simulations capture the variation of physical properties with respect to space and time. This is the method of logging the changing states or magnitudes of certain parameters.

Tracking of dust particles and their capture with respect to time is a part of transient analysis. The dust particles are assumed to be massless. Dust particles are also assumed to be generated at time, $t$ = 0.0 seconds at the coal face close to the leading shearer drum. CFD simulations are generated to capture the location of the dust particles under varying face flows as well as scrubber flows. The dust particles which hit the *Scrubber_Inlet* are killed and captured by the scrubber. Captures are expected to have reached a steady value within 15.0 seconds and therefore particles are monitored for 20.0 seconds after generation.

For carrying out a transient state analysis, usually a time step is chosen so as to be able to capture the phenomena in question precisely. The Courant number defines the time step of calculations. Figure 4.24 describes the elemental calculation of the Courant number.

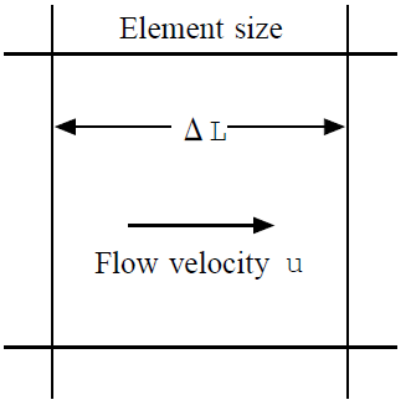


Figure 4.24 Computation of Courant number.

Time step is calculated using the equation, $\Delta t = \Delta L/u \times C$

Where, $\Delta L$ = Element size [m]

u = Flow velocity [m/sec]

C = Courant number.

The Courant number is usually kept below 10 for all the transient state simulations. Since the number of mesh elements often runs into millions and the geometry of the flow does not have any symmetries, fluid particles may move through two or more cells at each time step. Inaccuracy arising out of the Courant number is therefore ruled out.

In order to ensure that convergence is not affected, $\Delta L$ has been kept very low by refining the octree and generating a fine mesh. A time step ($\Delta t$) of the order of $10^{-4}$ - $10^{-5}$ seconds is usually assumed. This calls for approximately 30,000-50,000 cycles or more for capturing transient states for 20 seconds of time.

A converged solution is achieved at the end of every cycle of calculations. If the solution does not converge, reliability of simulations is lost and the calculations can diverge very fast. The time step is relative and depends on the process. For a CFD analysis of heat produced in a fast neutralization reaction needs to be very slow. Slow diffusion reaction may have a large time step since a noticeable change in parameters may not occur very fast in the defined time step.

Cradle CFD has an excellent module for transient state analysis. However, mesh adaptation analysis of scenarios in transient analysis is very time consuming. It is therefore, extremely important to have a steady state solution converged and mesh adaptation analysis carried out before using the *.r (restart) files and the *.fld (field) files to start calculations towards transient state simulations. The *.fld files are often saved periodically based on the time elapsed rather than the cycle of calculations since the actual physical time is of utmost interest.

The restart file is saved after steady state is achieved and is used an input for transient state analysis. Transient state analysis commences after the steady state analysis is completed. Transient state analysis is also carried out for the same face airflows and six scrubber airflows. Table 4.6 shows the flows which are changed for each set of iterations.

Table 4.6 Different face airflows and scrubber airflows for CFD simulation.

| Airflow | Flows | Quantity |
|---|---|---|
| Face airflow | QF 01 | 11.0 $m^3/s$ (23,298 cfm) |
| | QF 02 | 13.2 $m^3/s$ (27,958 cfm) |
| Scrubber airflow | QS 01 | 3.0 $m^3/s$ (6,354 cfm) |
| | QS 02 | 3.6 $m^3/s$ (7,625 cfm) |
| | QS 03 | 4.2 $m^3/s$ (8,896 cfm) |
| | QS 04 | 4.8 $m^3/s$ (10,166 cfm) |
| | QS 05 | 5.4 $m^3/s$ (11,437 cfm) |
| | QS 06 | 6.0 $m^3/s$ (12,708 cfm) |

Figure 4.25 shows the positions of dust particles with respect to time for a face airflow of 11.0 $m^3/s$ and scrubber flow of 4.2 $m^3/s$.

0.5 s

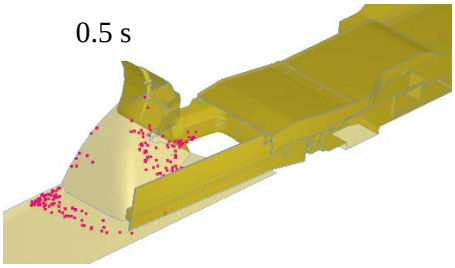

1.0 s

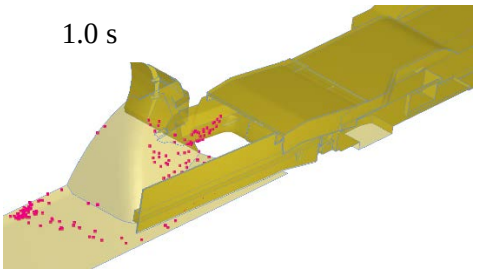

1.5 s

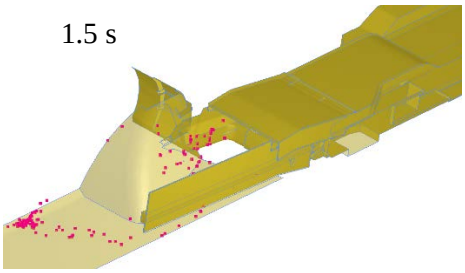

2.0 s

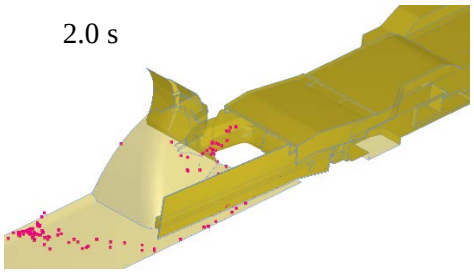

2.5 s

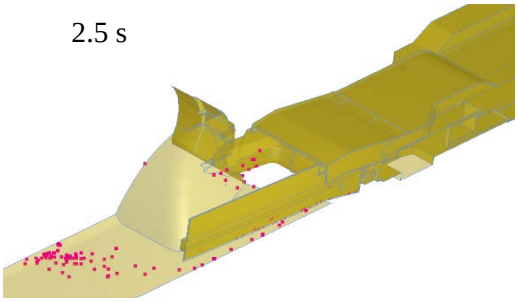

3.0 s

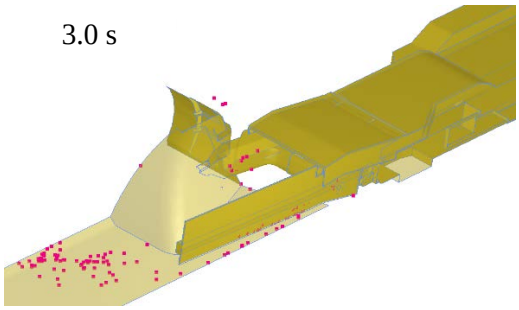

3.5 s

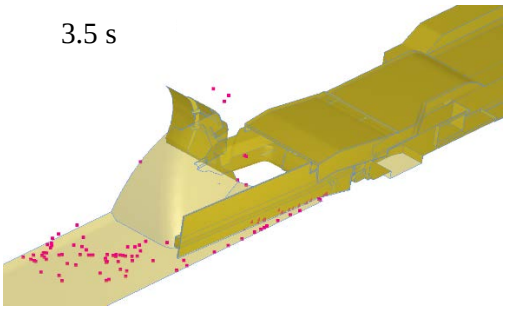

4.0 s

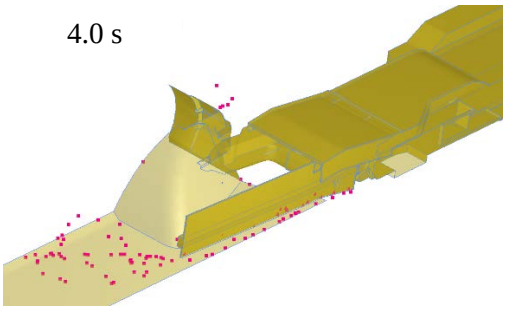

4.5 s

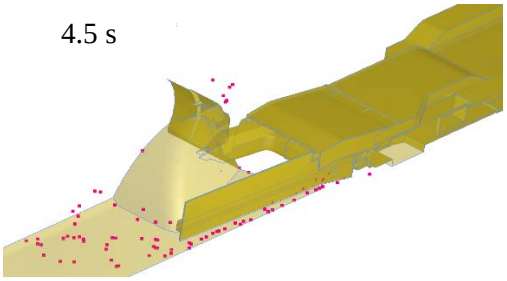

5.0 s

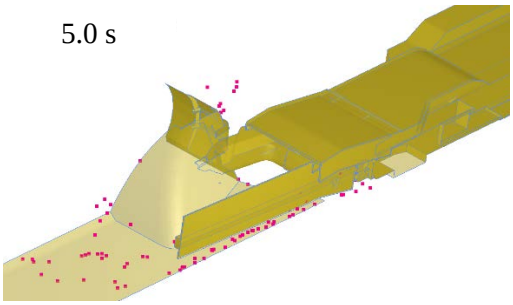

5.5 s

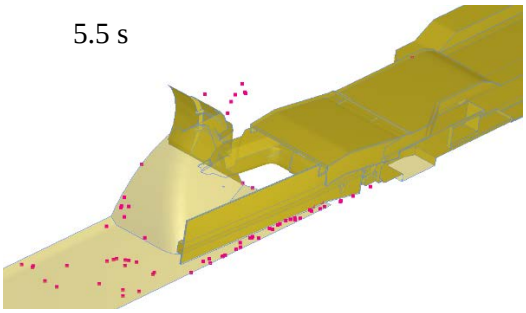

6.0 s

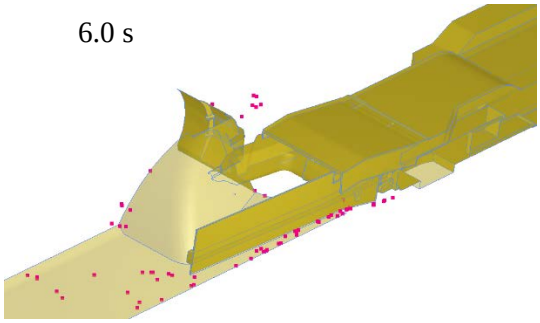

6.5 s

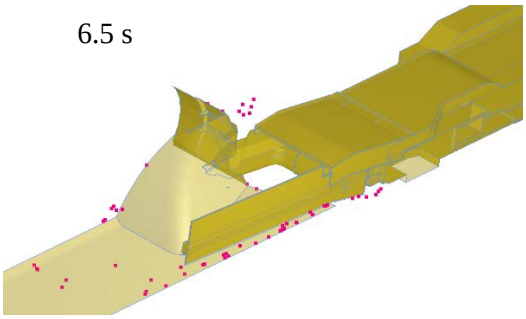

7.0 s

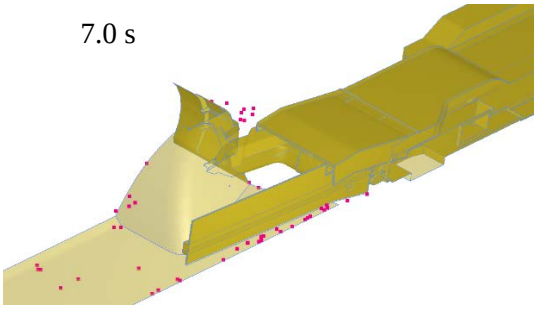

7.5 s

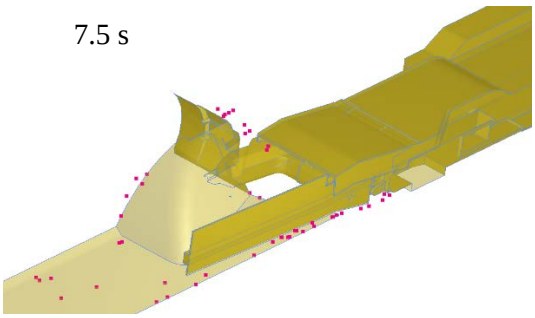

8.0 s

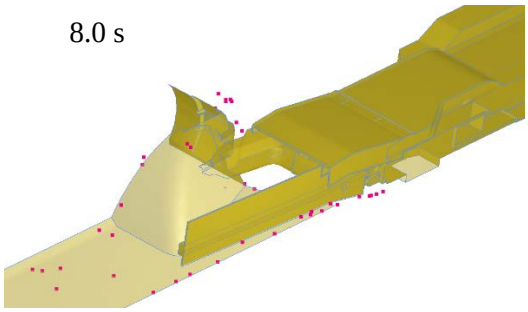

8.5 s

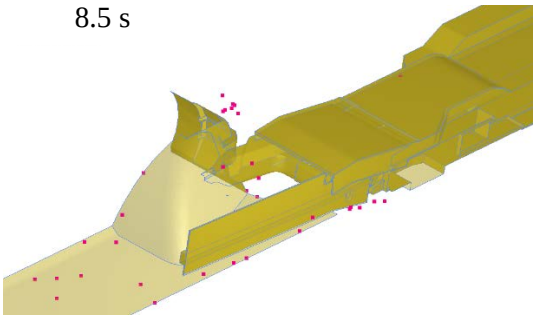

9.0 s

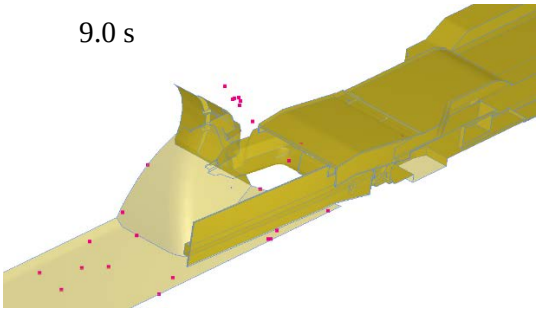

9.5 s

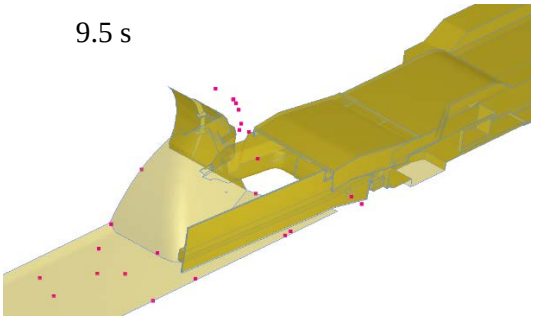

10.0 s

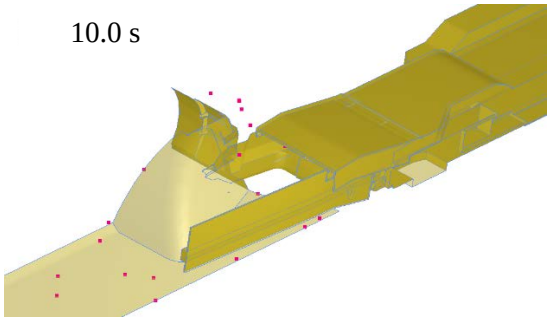

10.5 s

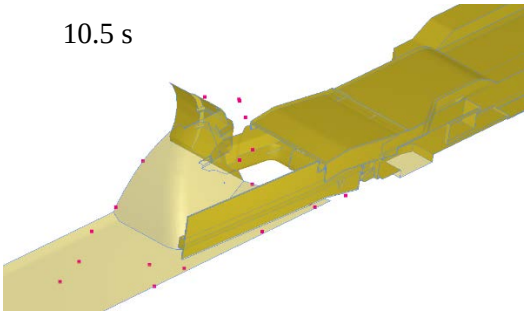

11.0 s

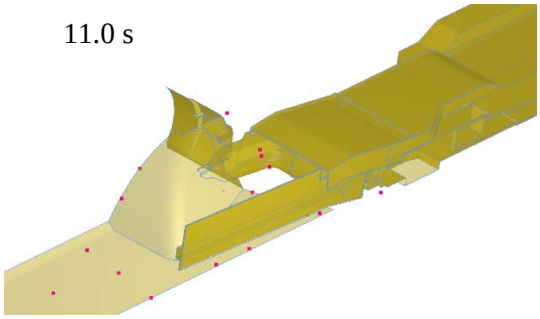

12.0 s

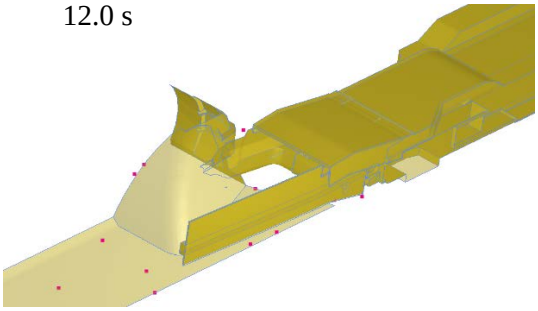

13.0 s

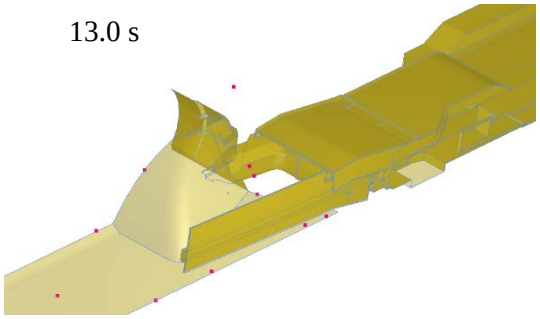

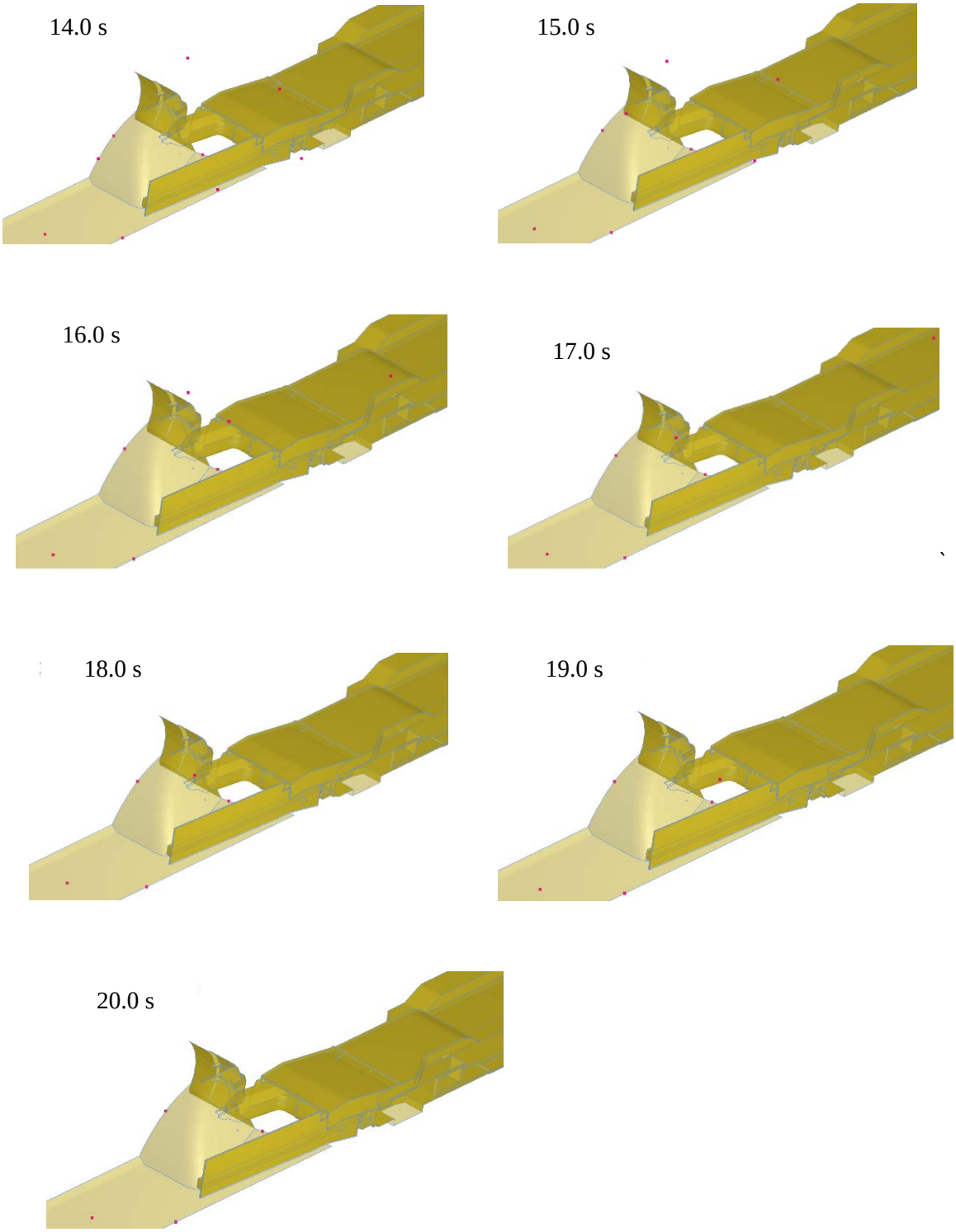


Figure 4.25 Screenshots representing the dust particles (in pink color) close to the active longwall face with respect to time between 0-20.0 seconds.

The cumulative captures with respect to time have been plotted for two different airflows at the face and six different flows through the dust scrubber. Figures 4.26 and 4.27 show the plots of captures for the flows.

The capture of dust particles tends to reach a steady state after a few seconds. It is also worth noting that increasing the flow through the scrubber increases the capture efficiency, and the reason can be attributed to more quantity of air being processed as well as more turbulence being generated.

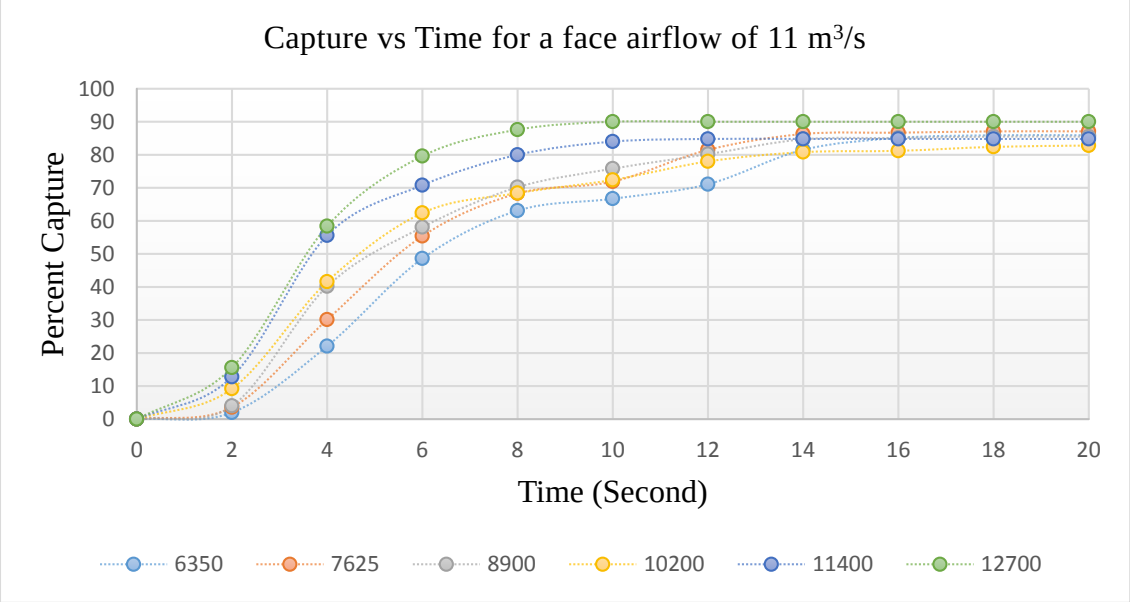


Figure 4.26 Capture vs Time for different airflows through the scrubber at a face flow of 11 $m^3/s$.

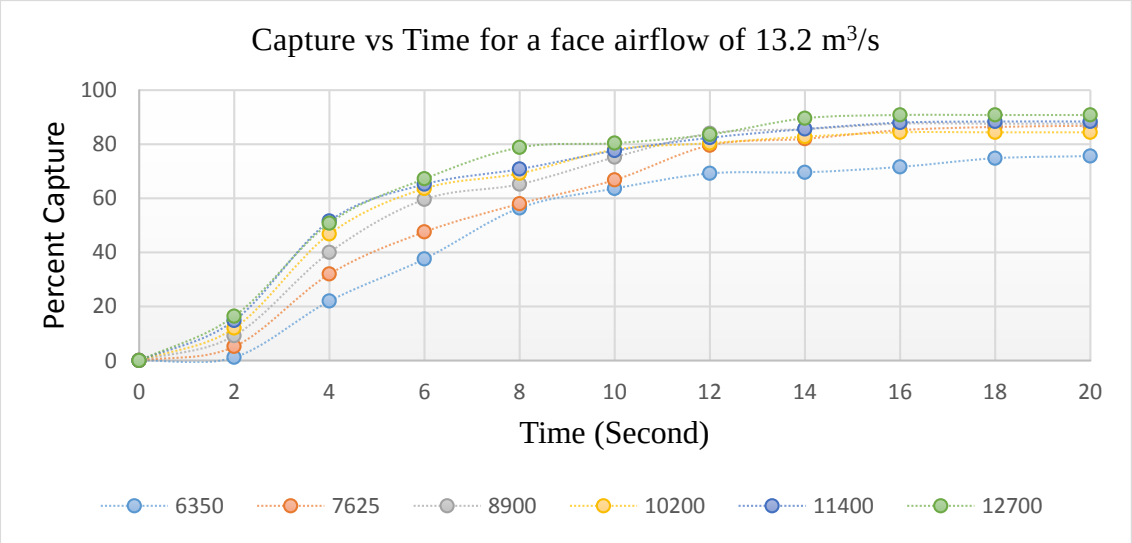


Figure 4.27 Capture vs Time for different airflows through the scrubber at a face flow of 13.2 $m^3/s$.

### 4.10 Conclusions

CFD models yielded high capture percentages for dust particles generated from the headgate drum. The capture percent typically ranges between 75-90 % for flows from 3.0 $m^3/s$ to 6.0 $m^3/s$ through the scrubber. With the increase in airflow through the flooded bed dust scrubber, capture generally increases progressively. This is because a higher percentage of air is now being captured and cleaned by the scrubber. Table 4.7 summarizes the final captures at the end of 20.0 seconds under two face airflows and six scrubber flows.

Table 4.7 Capture efficiency by the flooded bed dust scrubber for two face airflows and six scrubber flows.

| Sl. No. | Capture efficiency | | | | | |
|---|---|---|---|---|---|---|
| Face flow | Scrubber flow ($m^3/s$) | | | | | |
| ($m^3/s$) | 3.0 | 3.6 | 4.2 | 4.8 | 5.4 | 6.0 |
| 11.0 | 75.7 | 85.1 | 81.7 | 80.3 | 90.4 | 88.3 |
| 13.2 | 74.6 | 80.9 | 83.9 | 88.8 | 90.8 | 88.0 |

An examination of the contour profiles of the velocity magnitudes on parallel planes just ahead of the scrubber inlet show well-developed uniformly spaced contours. This shows that there is no turbulent mixing of dust particles with the incoming airflow. This aids in

better capture. Similarly, the airflow is discharged parallel to the coal floor, thereby resulting in no additional generation of dust particles. Furthermore, redirecting air towards the scrubber inlet using additional arrangements is expected to result in higher captures. Chapter five discusses the validation of the conceived model using tracer gas experiments and further CFD modeling.

# 5 Full Scale Mockup and Scale Modeling

## 5.1 Full Scale Model Building

In order to accurately predict the performance of the scrubber on the longwall panel, it was decided to build a full scale model of the JOY 7LS shearer along with the scrubber in the mine ventilation laboratory at the Department of Mining Engineering, University of Kentucky. The completed model will be shipped to the National Institute for Occupational Health and Safety (NIOSH) at Pittsburgh, Pennsylvania where experiments have been planned to test the effectiveness of the scrubber.

The first drawing of the shearer, provided by the cooperating mine, included all the fine details of the shearer. The drawing needed to be slightly modified to tweak the complex features which were not expected to make any significant difference to the airflow around the shearer or performance of the flooded bed dust scrubber. It was decided to use the 80/20 aluminum extrusions for constructing the skeleton of the mockup. Theses extrusions are manufactured by Industrial Erector Set ®. The 80/20 components can withstand enormous loads in the longitudinal direction, as shown in Tables 5.1, 5.2 and 5.3. Figures 5.1, 5.2 and 5.3 show the isometric views of the bars. Specific dimensions of the 80/20 extrusions were chosen based on the expected beam forces. One-quarter inch thick PVC plastic sheets were used to construct the outer surface of the shearer mockup by bolting them onto the aluminum extrusions.

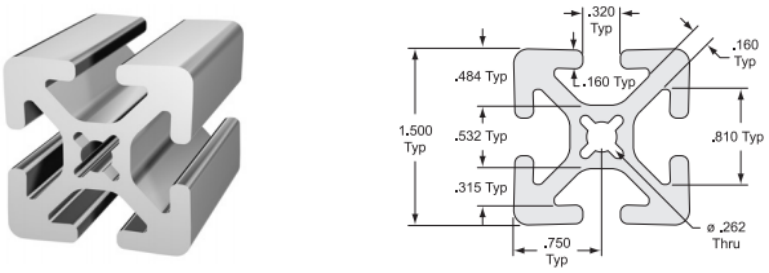


Figure 5.1 Cross section of the 1515 series T-slotted profile 80/20 erector set.

Table 5.1 Specifications of the 1515 series 80/20 erector set.

| Parameter | Description/ value |
|---|---|
| Material/ Finish | Clear anodized |
| Linear mass distribution | 1.98 kg/m (1.33 lbs/ft.) |
| Cross Section | 7.45 $cm^2$ (1.15 $in^2$) |

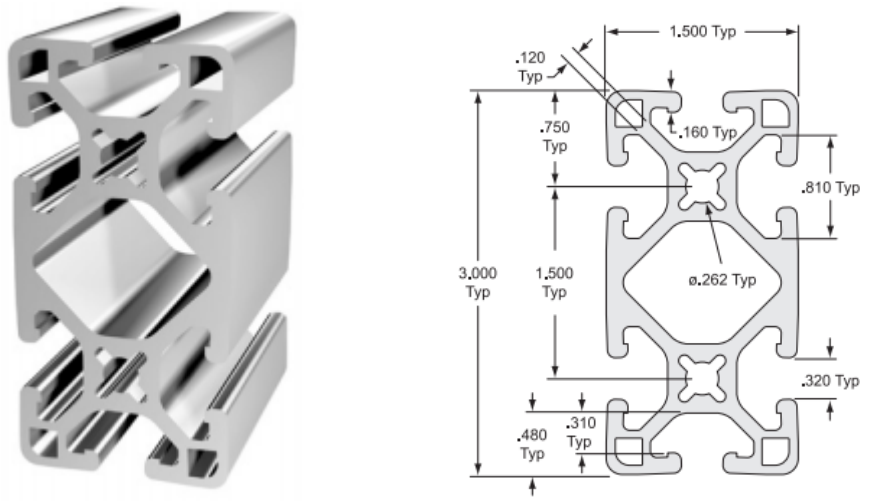


Figure 5.2 Cross section of the 1530 series T-slotted profile 80/20 erector set.

Table 5.2 Specifications of the 1515 series 80/20 erector set.

| Parameter | Description/ value |
|---|---|
| Material/ Finish | Clear anodized |
| Linear mass distribution | 1.98 kg/m (2.39 lbs./ft) |
| Cross Section | 13.22 $cm^2$ (2.05 $in^2$) |

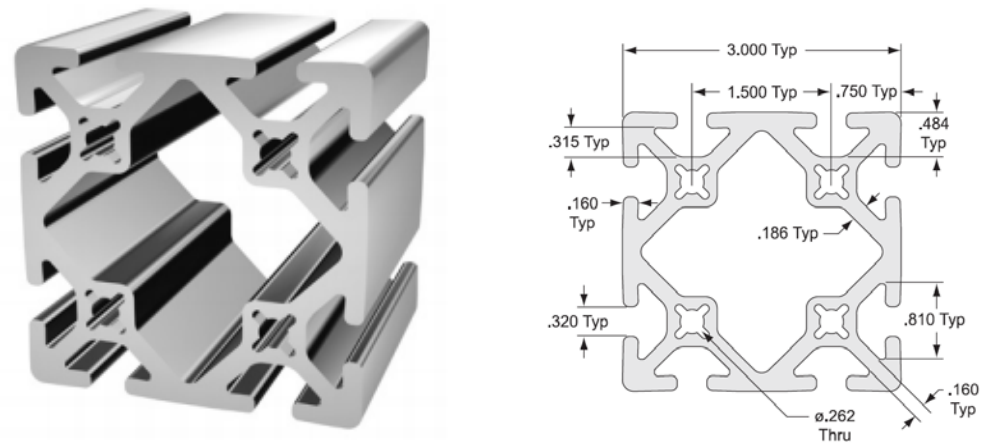


Figure 5.3 Cross section of the 3030 series 80/20 erector set.

Table 5.3 Cross section of the 1530 series T-series profile 80/20 erector set, used to support the fan housing.

| Parameter | Description/ value |
|---|---|
| Material/ finish | Clear anodized |
| Linear mass distribution | 5.70 kg/m (3.83 lbs/ft). |
| Cross section | 21.22 $cm^2$ (3.29 $in^2$) |

Various combination of 80/20 were used to build the skeleton of the shearer. T-nuts coupled with different connectors were used to join the 80/20 erector bars. Figure 5.4 shows the skeleton of one of the ranging arms.

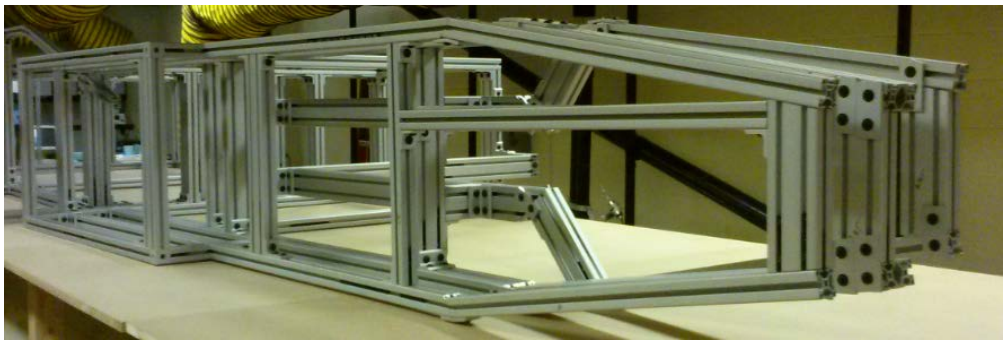

Figure 5.4 80/20 erector sets used to build the ranging arm of the shearer.

As previously stated, one-quarter inch thick PVC plastic sheets were used to build the external surface of the shearer, which is of critical importance with respect to airflow. Figure 5.5 shows the PVC plastic attached to the outer skin of the shearer. Figure 5.6 shows the hinged arrangement for connecting the ranging arm with the drive compartment. A 186.4 W (0.25 hp) motor is used to drive the shearer drum by means of belt-pulley system. The motor is rated at a speed of 47 rotations per minute, which closely matches that of the actual shearer. Figure 5.7 shows the motor.

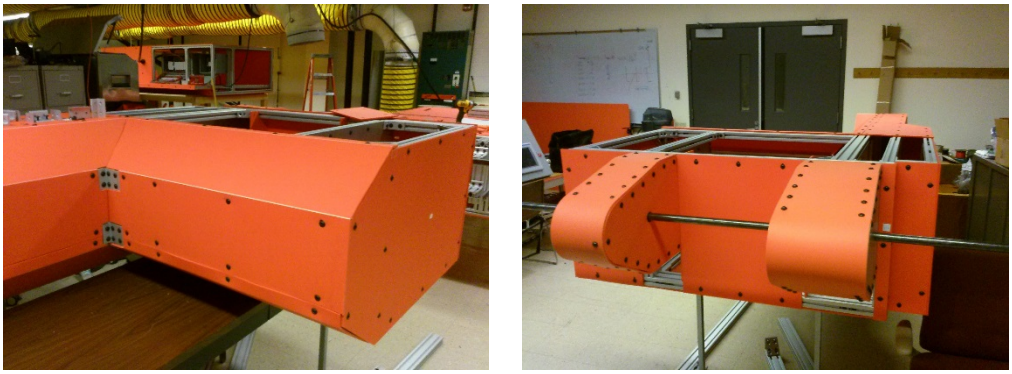

Figure 5.5 A quarter inch thick PVC sheets being out to generate the outer skin of the shearer.

Figure 5.6 Testing the coupling of the ranging arm as well as the drive unit of the shearer.

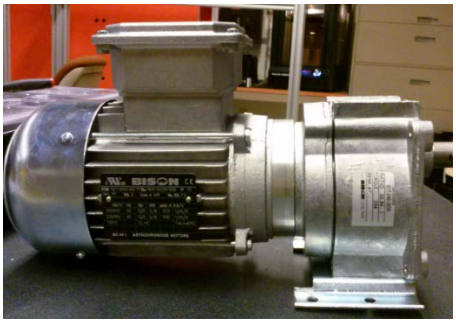


Figure 5.7 A 0.25 hp motor used to rotate the drum.

Ball valves, as shown in figure 5.8, are used for controlling the water flows to the cutter drum and the flooded bed scrubber. The valves allow for various water flow rates, and their effects on scrubber efficiency will be analyzed during the experimentation at NIOSH. The scrubber valve is connected to a 2.54 cm (1 in.) supply line, while the cutter drum valve is connected to a 3.81 cm (1 ½ in.) supply line.


Figure 5.8 Ball valves used for supplying water to sprays on the shearer drum and impingement screen.

The control compartmentof the full-scale mockup houses the electrical controls and monitoring equipment. Figure 5.9 shows a portion of the control compartment where the three-phase 480 Vac power enters the mockup. The shearer-drum motor starter and a 24 Vdc power supply are shown in figure 5.10, along with the variable frequency drive (VFD) that supplies the 50 hp fan motor.


Figure 5.9 The central panel housing the control units on the full scale model.


Figure 5.10 Allen Bradley power supply and variable frequency drive.

The programmable logic controller, shown in figure 5.11, is used to control various components, such as the VFD, cutter-drum motor, and water valves. It also makes decisions based on information received from the various sensors. The human machine interface for the PLC is also shown in figure 5.11.

These together, provide for necessary controls to vary the parameters and run experiments to investigate the performance of the scrubber package.

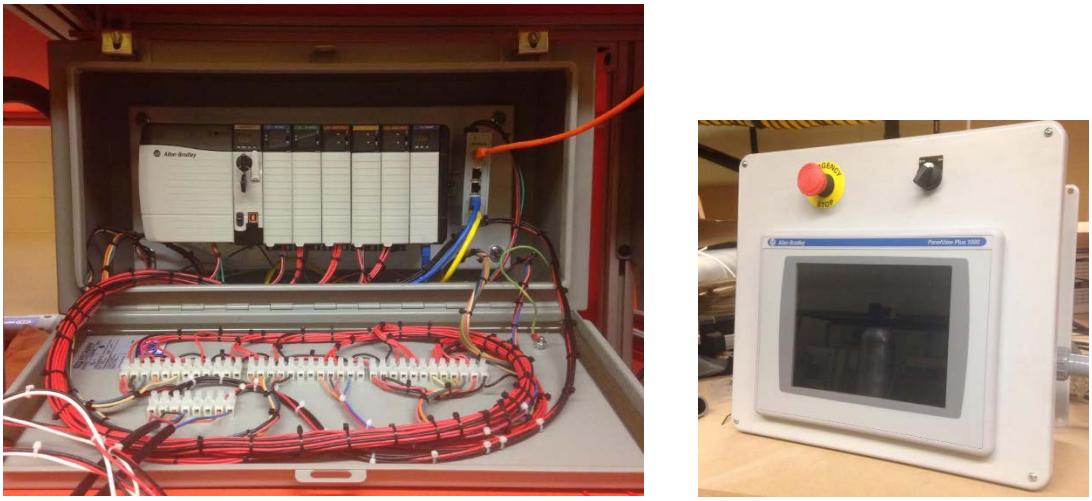

Figure 5.11 Programmable logic controllers to monitor vital parameters on the shearer, a HMI connected to the controls using an umbilical cord displays the parameters.

### 5.2 Tracer gas experiments on the 1:20 scaled model

Scale modeling is a methodology of replicating a physical phenomenon or a process at a different convenient size or 'characteristic length'. It is based on making well thought out assumptions and applying scaling laws for different scaled lengths. Usually, a constant ratio is obtained for each set of scaling laws. Scaling down the model further calls for other laws derived from diffusion and so on. Well designed scaled models can help understand mechanisms which control the full scale and often expensive real life models as well as ascertain the numerical model predictions with a high degree of certainty.

Geometrical and dynamical similarity are the two common scaling approaches. While the geometrical similarity deals with different length scales, dynamical similarity works on momentum and energy for motion as well as chemical reactions and force fields based on a problem at hand. Figure 5.12 presents a flowchart showing the progressive decisions during the course of scale modeling.

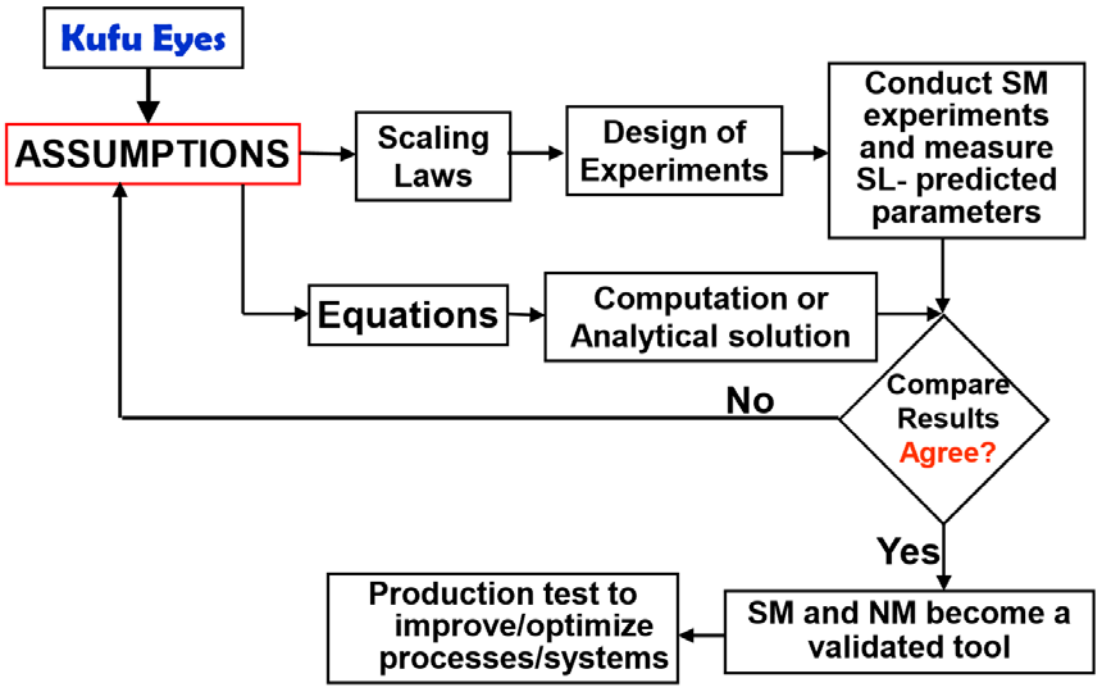


Figure 5.12 The process of scale modeling explained (Source: Scale Models in Engineering, Third Edition, Emori, Saito, Sekimto).

A convenient size to handle experiments like particle image velocimetry (PIV) as well as tracer gas analysis calls for a small size replica of the longwall panel. Researchers at the

Department of Mining Engineering, University of Kentucky decided to generate a 1:20 scaled model, using a 3D printer, of the same set up as the CFD models. Figure 5.13 shows the 1:20 printed scaled model. Figure 5.14 shows two views of the experimental set up in a wind tunnel.

Figure 5.13 The 1:20 scaled model generated using a 3D printer.

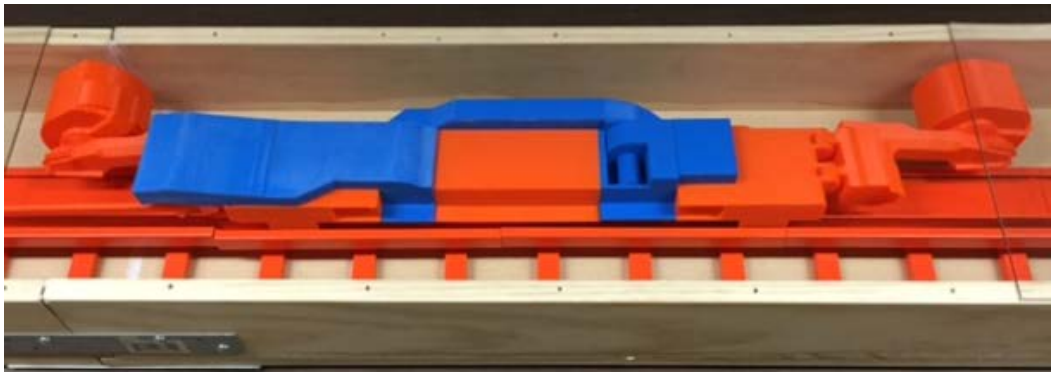

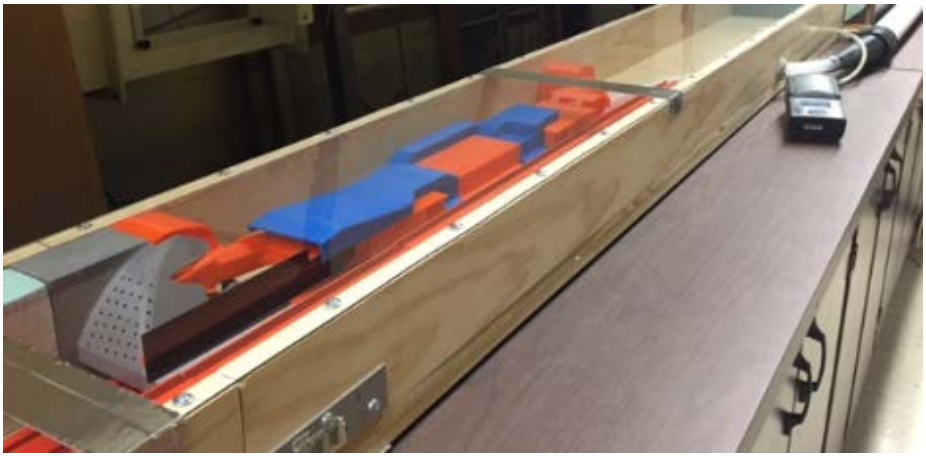

Figure 5.14 Experimental set up to measure the capture efficiency on the 1:20 scaled model.

In a simple experimental set up, a shop vacuum cleaner served as an alternative to the centrifugal fan used in the actual prototype. A thermos anemometer was used to monitor the speed of air flowing along the coal face. The speeds were kept similar to values encountered at the specific mine under study.

Carbon dioxide gas was used as a tracer and to simulate the dust particles on the panel. Holes on the 'coal lump' close to the leading drum released carbon dioxide onto the panel and was being sucked by the 'scrubber' in question. A gas monitor placed downstream measured the concentrations before and after the 'scrubber' was tuned on. Good capture efficiencies reiterated the usefulness of the design of the inlet extending close to the rotating drums.

The experiment was controlled carefully by sealing off the 1:20 scaled longwall panel. The $CO_2$ readings prevailing at that point of time in the atmosphere were subtracted from the readings to get an accurate representation of the concentrations and hence the capture efficiencies. The undergraduate researchers reported significant capture of the 'dust particles' by the scrubber. Tables 5.4 and 5.5 show the capture efficiencies on two successive trails.

Table 5.4 Trial 1 of experiment of capture of tracer gas by the 1:20 scaled model of scrubber.

| Scrubber OFF | | | Scrubber ON | | | |
|---|---|---|---|---|---|---|
| Air Velocity | | | Air Velocity | | | Capture |
| m/sec | fpm | CO2 Content (%) | m/sec | fpm | $CO_2$ Content (%) | Efficiency (%) |
| 2.06 | 405 | 0.60 | 2.06 | 406 | 0.08 | 94.55 |
| 2.32 | 456 | 0.52 | 2.34 | 460 | 0.11 | 87.23 |
| 2.54 | 500 | 0.52 | 2.57 | 505 | 0.11 | 87.23 |
| 2.82 | 555 | 0.47 | 2.79 | 550 | 0.14 | 78.57 |
| 3.07 | 605 | 0.41 | 3.05 | 600 | 0.14 | 75.00 |

Table 5.5 Trial 2 of experiment of capture of tracer gas by the 1:20 scaled model of scrubber.

| Scrubber OFF | | | Scrubber ON | | | |
|---|---|---|---|---|---|---|
| Air Velocity | | $CO_2$ | Air Velocity | | $CO_2$ | Capture |
| m/sec | fpm | Content (%) | m/sec | fpm | Content (%) | Efficiency (%) |
| 2.05 | 403 | 0.69 | 2.06 | 405 | 0.08 | 95.31 |
| 2.29 | 451 | 0.60 | 2.32 | 457 | 0.11 | 89.09 |
| 2.54 | 500 | 0.52 | 2.55 | 501 | 0.11 | 87.23 |
| 2.79 | 549 | 0.47 | 2.82 | 555 | 0.14 | 78.57 |
| 3.03 | 596 | 0.41 | 3.07 | 605 | 0.14 | 75.00 |

### 5.3 CFD Modeling of Tracer Gas Experiments on the 1:20 Scaled Model

CFD models were generated for all the scenarios run in the tracer gas experiments. The same geometrical model as that of the longwall face as discussed in the proceeding chapters was used to simulate the airflow on the 1:20 scaled model. Octree was generated, along with a volume and surface mesh following the same process as discussed in previous chapters. An incoming velocity was imparted to the inlet which was developed by the vane axial flow fan in the tunnel. Similarly, the flow through the scrubber kept constant at 0.0151 $m^3/s$ (32 cfm) throughout the experiment which was brought about by the shop vacuum cleaner. Wall conditions were applied onto all the surfaces. Roughness of surfaces were considered for all the simulations. Table 5.6 shows the analysis conditions for the steady and transient state simulations.

Table 5.6 Analysis conditions for steady and transient state simulations.

| Parameter | Description / value |
|---|---|
| Analysis type | Turbulent flow for steady and transient states. |
| Turbulence model | Standard k-EPS. |
| Time step | Of the order of $10^{-5}$ seconds or a low Courant number. |
| Working fluid | Incompressible air at 20° C. |
| Boundary conditions | Face- Inlet: Velocity specified<br>Face-Outlet : Static pressure<br>Scrubber-Inlet/Outlet : Volumetric flow rate<br>Belt/Coal-Floor/Coal-Roof/Coal-Face/Cable-Tray: Wall conditions |
| Particle tracking | 500 massless marker particles release once at time, *t=0.0* second. |
| Solver settings | Convergence criterion- Average threshold residual : 0.0001 |
| Output control | Field (*.fld) files saved every stipulated intervals. |

Figure 5.15 shows the surface mesh file generated for the CFD simulation of the scaled model.

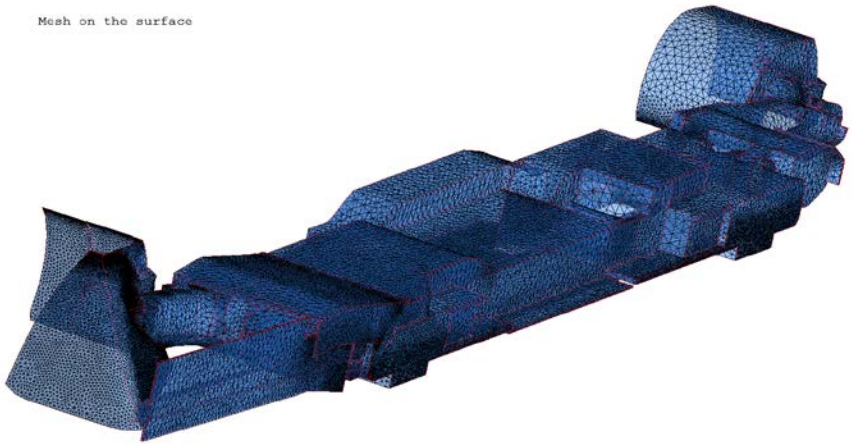


Figure 5.15 A computational mesh on the surface.

Steady state simulations were run for convergence to establish a definite flow field. Figure 5.16 shows the contours of velocity on three parallel planes and perpendicular to the general airflow on the scaled model. Figure 5.17 shows the velocity vectors on a plane parallel to the floor.

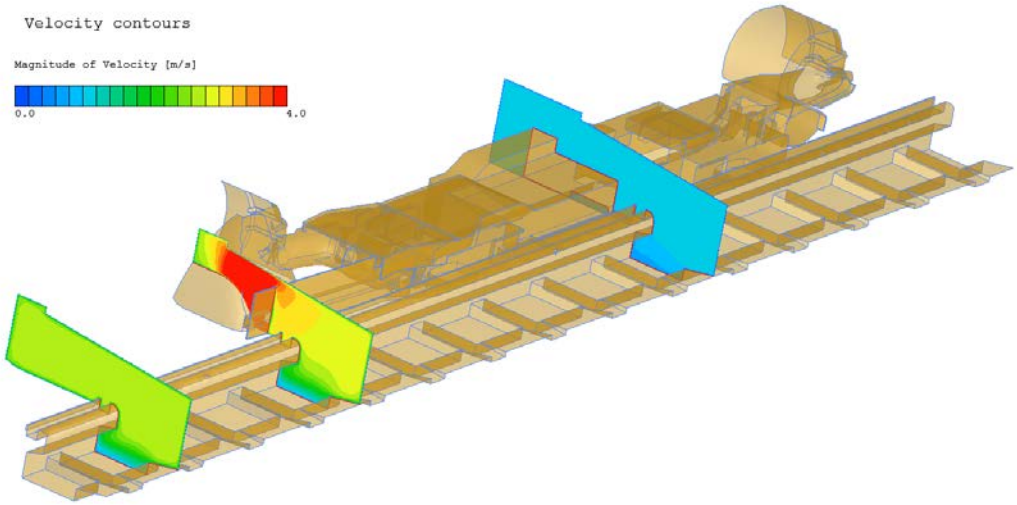


Figure 5.16 Contours of magnitude of velocity before the inlet, on the coal lump and downstream of the inlet.

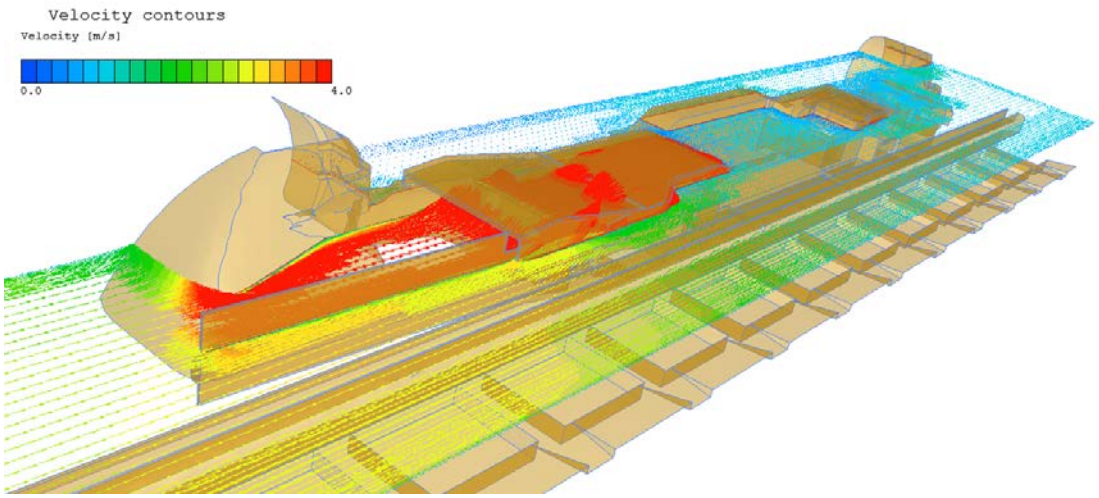


Figure 5.17 Velocity vectors on a plane parallel to the coal floor.

The mesh (*.pre), field (*.fld) and restart (*.r) files were used to run a set of transient state simulations. Five hundred dust particles were released from the active part of the coal face to simulate the release of dust. A sufficiently low time step, on the order of 10 microseconds, was considered corresponding to a low Courant number. Dust particles were

assumed to be captured if they hit the inlet of the scrubber. Capture efficiencies were observed to reach a stable value by the end of 0.3 second. Table 5.7 compares the capture efficiencies observed for five different airflow velocities at the inlet of the tunnel for a constant flow through the scrubber on the tracer gas experiments against the CFD models.

Table 5.7 Capture efficiencies indicated by CFD models and tracer gas experiments.

| Incoming airflow velocity at the face (fpm) | Average capture on tracer gas experiments (%) | Capture indicated by CFD models (%) |
|---|---|---|
| 405 | 94.93 | 92.20 |
| 456 | 88.16 | 91.78 |
| 500 | 87.23 | 87.60 |
| 555 | 78.57 | 77.60 |
| 605 | 75.00 | 75.20 |

Although true scaling laws have not been established for the 1:20 scale model, the captures are in close agreement with each other. Further, captures indicate the usefulness of design of the proposed flooded bed dust scrubber in general.

# 6 Conclusions & Future Work

## 6.1 Results

The primary objective of this thesis was to investigate the applicability of a highly efficient flooded bed dust scrubber to a specific longwall. The project's success would further promulgate the applicability to general longwall set up. A detailed study was carried out on the existing dust control methods currently under application, particularly in the US.

The following results were obtained and are have been found to be promising:

1. Capture efficiencies of 74.6 – 90.8 % of the dust generated from the headgate drum of the shearer were obtained from the CFD results. Assuming almost half of the dust on the longwall panel is generated on the panel by the shearer, an appreciable reduction in dust concentration can be brought about on implementation of the designed flooded bed dust scrubber.
2. The inlet of the scrubber should extend close to the cutting drum as far as possible to be able to capture most of the dust particles. The inlet also needs to be maintain the continuity of airflow with the ranging arm in any position. Further, the inlet needs to maintain a prescribed clearance from the canopies. An articulated inlet has been found useful to address these operational issues. Course grizzly bars can be used to arrest big coal chunks from getting into the scrubber inlet.
3. Lack of sufficient space above the main body of the shearer led the researchers to add additional modules to house the screen and fan. A centrifugal fan was preferred over a vane axial flow fan also because it brought about the desired changes in airflow direction.
4. In order to survive the vastly punishing environment of the active longwall panel, the proposed dust scrubber has been conceived as an integral part of the shearer itself. Survivability of the scrubber can be improved vastly by incorporating the scrubber into the main body of the shearer itself, rather than designing it as an external attachment.

## 6.2 Future Work

The thesis discusses the application of Flooded Bed Dust Scrubbers in detail under certain assumptions. However, further work can attempted as a continuation of the research:

(i) This project looks at the optimum location and efficiency of the dust scrubbers close to the leading drum. However, in bidirectional cutting the shearer also encounters anti-tropal ventilation. Simulating both the drums rotating is expected to yield a different capture efficiency. Designing the inlet to capture the dust generated at the trailing drum may be interesting.

(ii) The dust is assumed to be generated out of a large heap of coal that gets accumulated in front of the leading drum cutting in one direction. Other sources of dust generation can also be included in the model. A part of those dust particles can also be captured theoretically by the dust scrubber by if the particles get trapped in the velocity field lines running towards the scrubber inlet. This can also be used to gauge the effectiveness of the dust scrubber towards capturing the dust particles generated elsewhere as well. A study can be carried out on dust samples obtained from the coal mine ($mg/m^3$) and inserted as an input to the CFD models and results verified.

(iii) A detailed study on the water sprays can be carried out with CFD model as well as experimental observations. Effects to different orientations, flow rates and type can be studied and all parameters optimized.

(iv) Discharge of the scrubber may be modeled to minimize the shock loses. Well established flow fields is expected to improve the performance of the fan.

(v) The gob has been assumed to be perfectly tight. In other words, there is no movement of air into or out of the gob. However, the gob does ‘breathe’ and results in to-and-fro movement of the air. CFD simulations accounting for leakage of air into the gob is one area that can be looked into.

**Appendix**

A typical condition file used to generate the model representing steady state scenario for a face airflow volume of 11.0 $m^3/s$ and a scrubber inflow of 4.2 $m^3/s$ for steady state simulations is shown below.

```
SDAT
SC/Tetra
  11   0   0
PREI    Config2.pre
RO      Config2_QF01_QS01.r
POST    Config2_QF01_QS01
/
   1   1   0

   0   1
CHKL
               1              1              0              1
0
CYCS
       1   4000
EQUA
1101
FLUX
%CNAM Flux_1
  -1   7   0   0   0   0
              11   0
Face-Inlet
/
%CNAM Flux_2
  -4   0   1   0   0   0
               0
Face-Outlet
/
%CNAM Flux_3
  -1   7   0   0   0   0
             -4.2   0
Scrubber-Inlet
/
%CNAM Flux_4
  -1   7   0   0   0   0
```

```
              4.2   0
Scrubber-Outlet
/
/
PROP
%CNAM air(incompressible/20C)
   1   1            1.206        1.83e-005              1007
0.0256   0
/
WL02
%CNAM Wl02_1
   0   0
%CNAM Wl02_2
   0   2
           0.02             0.4             8.5
%CNAM Wl02_3
   1   0
           -1.8               0               0
%CNAM Wl02_4
   2   0
         4.71239              0            8.5           1.32
0               0               0               1
/
   1
Shearer
/
   2
Walls
/
   3
Belt
/
   4
Coal
/
/
GOGO
```

The steady state simulations attain convergence at the end of 577 cycle of calculations. A typical condition file used to generate the transient state scenarios for a face airflow flow volume of 11.0 $m^3/s$ and a scrubber inflow of 4.2 $m^3/s$ is shown below.

```
SDAT
SC/Tetra
  11   0   0
PREI    Config2.pre
RI      Config2_QF01_QS01.r
RO      Config2_Dust_QF01_QS01.r
POST    Config2_Dust_QF01_QS01
/
   1   1   0

   0   1
CHKL
               1              1              0              1
0
CYCL

       578    40000            0.05       1               10

EQUA

1101

FLUX

%CNAM Flux_1

  -1   7   0   0   0   0

              11   0

Face-Inlet

/

%CNAM Flux_2

  -4   0   1   0   0   0

               0
```

```
Face-Outlet
/
%CNAM Flux_3
  -1   7   0   0   0   0
              -4.2   0
Scrubber-Inlet
/
%CNAM Flux_4
  -1   7   0   0   0   0
               4.2   0
Scrubber-Outlet
/
/
GFIL
              -1   1
               1
GWLN
   0
PCLB
Face-Outlet
Scrubber-Inlet
/
PCLC
```

```
Face-Outlet
Scrubber-Inlet
/
PCLD
STRT               -1
STRD              -10
REGN    1
TSUM    1
TSUP    2
CSUP    1
/
PCLE
   1   0
Coal             250
               0               0   0   0   0   0
/
PROP
%CNAM air(incompressible/20C)
   1    1            1.206        1.83e-005             1007
0.0256   0
/
STOP
              20
```

```
WL02
%CNAM Wl02_1
   0   0
%CNAM Wl02_2
   0   2
           0.02              0.4              8.5
%CNAM Wl02_3
   1   0
           -1.8                0                0
%CNAM Wl02_4
   2   0
         4.71239              0            8.5           1.32
0               0               0               1
/
   1
Shearer
/
   2
Walls
/
   3
Belt
/
```

```
   4
Coal
/
/
WPUT
   0
ZGWV
   0
GOGO
```

## Bibliography

Balusu, R, S Chaudari, T Harvey, and T Ren. 2005. An Investigation of Air and Dust Flow Patterns around the Shearer. Eight International Mine Ventilation Congress. Brisbane, Queensland. 135-142.

Belle-GK; Ramani-RV; Colinet-JF. 2000. Evaluation of Two-Phase Spray System for Airborne Dust Control in a Longwall Gallery. Proceedings of 12th International Conference on Coal Research, Sandton, Republic of South Africa, Sep 12-15, 2000 Wash, DC International Conference on Coal Research.113-119.

Bhaskar. 1987. Spatial and Temporal Behavior of Dust in Mines: Theoretical and Experimental Studies.

Breslin, John A., and Anthony J. Strazisar. 1976. Dust control studies using scale models of coal mine entries and mining machines. Report of Investigation, Washington: United States Department of the Interior, Bureau of Mines.

Bureau of Mines, United States Department of the Interior. 1981. Reoriented Shearer Water Sprays Move Dust toward Face. Technology News.

Bureau of Mines, United States Department of the Interior. 1986. Research on water proportioning for dust control on longwalls. Washington DC.

Bureau of Mines, United States Department of the Interior. 1987. Shearer mounted dust collector; Evaluation of ventilated cutting drums. Spokane, WA.

Centres for Disease Control and Prevention, National Institute for Occupational Safety and Health. 2010. Best practices for dust control in coal mining. IC 9517, Pittsburgh, Spokane.: Department of Health and Human Services.

Cheng, L, and P P Zukovich. 1973. Respirable dust adhering to run-of-face bituminous coals. RI 7765, NTIS No. PB 221-883., Pittsburgh, PA: U.S. Department of the Interior, Bureau of Mines.

Colinet J.F., Spencer E.R. & Jankowski R. A., 1997. Status of dust control technology on US longwalls. In: Ramani RV, ed. Proceedings of the Sixth International Mine Ventilation

Congress, Littleton, CO: Society for Mining, Metallurgy, and Exploration, Inc., pp. 345-351.

Colinet, J. F., Rider, J. P., & Thimons, E. D. 2006. Controlling respirable dust in underground coal mines in the United States. The 21st World Mining Congress. 231–238.

Colinet-JF; Spencer-ER; Jankowski-RA. 1997. Status of Dust Control Technology on U.S. Longwalls. In: Proceedings of the 6th International Mine Ventilation Congress, Ramani RV, ed., Chapter 55. Society for Mining, Metallurgy, and Exploration, Inc.: Littleton, CO. 345-351.

Divers, E.F., and J. Kelly R.A. Jankowski. 1987. Ventilated drum controls longwall dust and methane. Third U.S. Mine Ventilation Symposium. 85-89.

Donaldson Company Inc. 1980. Dust control on longwall shearer. Final Report, Minneapolis, Minnesota: Bureau of Mines, United States Department of the Interior.

Du, J. J. L., Appelman, G., & Oberholzer, J. W. 1978. Assessment of on-board scrubbers for use on continuous miners in South African collieries. In 7th US Mine Ventilation Symposium.

Ghosh, T., Rezaee, M., Honaker, R.Q., and Saito, K. 2014. Scale and Numerical Modeling of an Air Density-Based Separator, In: Progress in Scale Modeling, Vol II, Ed. Saito, K., Ito, A., Nakamura, Y., and Kuwana, K., ISBN: 978-3-319-10308-2, Springer, pp. 225-239.

Gillies, A. D. S. 1982. Studies in Improvements to Coal Face Ventilation with Mining Machine Mounted Dust Scrubber Systems. SME-AIME Annual Meeting, Dallas.

Goodman, G.V.R. 2000. Using water sprays to improve performance of a flooded bed dust scrubber. Applied Occupational and Environmental Hygiene, 15(7), 550–560.

Heerden, J. Van, & Sullivan, P. 1993. The Application of CFD for Evaluation of Dust Suppression and Auxiliary Ventilating Systems Used with Continuous Miners. 6th US Mine Ventilation Symposium; 293-297.

J Grigal, D., & McAndrew, W. J. 1979. Flooded Bed Scrubber for Machine Mounted Coal Mine Applications. Minnesota.

J.Kelly, T.Muldoon, W. S. 1982. Shearer Mounted Dust Collector. Waltham, MA.

Jankowski RA, Daniel JH, Kissell FN .1987. Longwall dust control: An overview of progress in recent years. In: Proceedings of the 22nd International Conference of Safety in Mines Research Institutes (Beijing, China, Nov. 2-6, 1987), pp. 737-747.

Jankowski  Jankowski, R. A., J. A. Organiscak, and N. I. Jayaraman. 1990. Dust sources and controls on high tonnage longwall faces. SME Annual Meeting. Salt Lake City.

Jayaraman, Natesa I., and Dennis Grigal. 1977. Dust Control on a Longwall Face with a Shearer-Mounted Dust Collector. Report of Investigation, RI 8248, Washington: United States Department of the Interior, Bureau of Mines.

Jon C Volkwein, T. S. W. 1989. Impact of Water Sprays on Scrubber Ventilation Effectiveness.

Kelly JS, Jankowski RA 1984. Evaluation of homotropal ventilation for longwall dust control. In: Proceedings of the Coal Mine Dust Conference (Morgantown, WV, Oct. 8-10), pp. 92-100.

Kissell, Fred N. 2003. Handbook for Dust Control in Mining. Information Circular 9465, Pittsburgh, PA: Centres for Disease Control and Prevention, National Institute for Occupational Safety and Health.

Kollipara, V. K., & Chugh, Y. P. 2011. CFD modeling of dust dispersion in mine airways. SME Annual Meeting. Denver, CO.

Kollipara, V. K., Chugh, Y. P., & Southern, D. D. R. 2012. A CFD analysis of airflow patterns in face area for Continuous Miners making a right turn cut. In SME Annual Meeting. Seattle, WA.

Ludlow, J., and Wilson, R.J. 1982. Deep cutting: Key to dust free longwalling, Coal Mining and Processing, Vol. 19, No. 8, August, pp. 40-43.

Miller, G. 2004. Drum scrubber design and selection. MetPlant. Perth, WA. 529-539.

Moloney, K. W., Lowndes, I. S., Stokes, M. R., & Hargrave, G. 1997. Studies on Alternative Methods of Ventilation Using Computational Fluid Dynamics (CFD), Scale

and Full Scale Gallery Tests. 6th International Mine Ventilation Congress - May 17-22, 1997, 497-503.

Mondal, K., Bariar, B., Relangi, D. D., & Kollipara, V. K. 2012. Coal Dust Wettability: It's role in dust control and its determination. SME Annual Meeting. Seattle, WA.

MSHA. 1999. Practical Ways to Reduce Exposure to Coal Dust in Longwall Mining-A Toolbox.

Novak, Thomas, and William Chad Wedding. January 2015. "Scrubbed clean." World Coal.

Oberholzer, J. W., & Meyer, C. F. 1995. The Evaluation of Heading Ventilation Systems Through the Use of Computer Simulations. 7th US Mine Ventilation Symposium, 485-490.

Organiscak, J. A., & Pollock, D. E. 2005. Development of a low pressure water-powered spot scrubber for mining applications. SME Annual Meeting, Salt Lake City.

Organiscak, J., and T. Beck. October, 2010. Continuous miner spray considerations for optimizing scrubber performance in exhaust ventilation systems. Mining Engineering, 41-46.

P. Rider, James, and Jay F. Colinet. 2011. Benchmarking longwall dust control technology and practices. Mining Engineering Journal. 74-80.

Prostanski, Dariusz. 2013. Use of air and water spraying system for improving dust control in mines. Journal of Sustainable Mining 29-34.

Rao, B. Srinivasa, and N.I. Aziz, R.N. Singh E.Y. Baafi. 1993. Three dimensional Numerical Modeling of Air Velocities and Dust Control Techniques in a Longwall Face. 6th US Mine Ventilation Symposium. Salt Lake City. 287-292.

Ren, T. X., & Balusu, R. June 2007. ACARP Project C14036 Dust control technology development for longwall faces – Shearer Scrubber Development.

Rider, J. P., & Colinet, J. F. 2011. Benchmarking Longwall Dust Control Technology and Practices. Mining Engineering Journal, 63, 74–80.

Ruggieri SK, Jankowski RA .1983. Fundamental approaches to longwall dust control. In: Proceedings of the Symposium on Control of Respirable Dust (Beckley, WV, Oct. 4-8, 1983).

S.K. Ruggieri, and R.A. Jankowski. 1983. Fundamentals of longwall dust control. Symposium on Control on Control of Respirable Dust. Beckley, WV.

Samanta, Arindam, Ragula Bhaskar, and Rouming Gong. 1993. Studies on the use of scrubber in continuous miner faces. 6th US Mine Ventilation Symposium. Salt Lake City. 51-56.

T.F.Tomb, R. O. 1992. Evaluation of respitable dust control on longwall mining operations. . SME Transactions, (pp. 1874-1878).

Taylor, C. D., & Jankowski, R. A. 1982. How the Six Cleanest US Longwalls Stay in Compliance. Proceedings of the 1st Mine Ventilation Symposium, 67–69.

Taylor, C.D., P. D. Kovscek, and E. D. Thimons. 1986. Dust Control on Longwall Shearers Using Water-Jet-Assisted Cutting. Information Circular 9077, Bureau of Mines, United States Department of the Interior.

Thimsons, E. December 2011. Respirable Dust Control. Coal News, 23.

US Department of the Interior, Bureau of Mines 1987. Shearer Mounted Dust Collector, Evaluation of Ventilated Cutting Drums. Spokane, WA: US Bureau of Mines.

Wala, A. M., Vytla, S., Huang, G., & Taylor, C. D. 2008. Study on the effects of scrubber operation on the face ventilation. In Proceedings of the 12th US/North American Mine Ventilation Symposium 12 th US/North American Mine Ventilation Symposium (pp. 281–286).

Wirch, Steve, and Robert Jankowski. 1995. Shearer-mounted scrubbers, are they viable and cost effective? Edited by Andrew Wala, 7th US Mine Ventilation Symposium. 319-325.

# VITA

Ashish Ranjan Kumar was born in Daltonganj, India. He attended MKDAV Public School and Delhi Public School, Bokaro Steel City for high school education. He subsequently went to the Indian School of Mines and earned a Bachelor's of Technology degree with a mining engineering major with a first class honors.

He accepted a full time position with Reliance Power Limited. He was transferred to Sasan Power Limited which was developing an integrated 6000 MW power plant fed by a captive coal mine. He was soon promoted to the position of assistant manager-mining engineering and worked across various departments including planning, cost control, project management and mine information systems. Prior to joining the University of Kentucky, he had worked for three years in the coal mine and played vital role in many firsts.